ETH
Eidgenössische Technische Hochschule Zürich
Swiss Federal Institute of Technology Zurich

Seminar for Applied Mathematics SAM

Applications of Chebyshev polynomials and Toeplitz theory to topological metamaterials

H. Ammari and S. Barandun and P. Liu

Research Report No. 2024-29
September 2024

Seminar für Angewandte Mathematik
Eidgenössische Technische Hochschule
CH-8092 Zürich
Switzerland

Funding SNF: 200021-200307

Applications of Chebyshev polynomials and Toeplitz theory to topological metamaterials

Habib Ammari, Silvio Barandun, and Ping Liu

Abstract. We survey the use of Chebyshev polynomials and Toeplitz theory for studying topological metamaterials. We consider both Hermitian and non-Hermitian systems of subwavelength resonators and provide a mathematical framework to explain some spectacular properties of metamaterials.

Keywords. Topological metamaterials, nonreciprocal metamaterials, topological interface modes, non-Hermitian skin effect, tunable localisation, generalised Brillouin zone, Chebyshev polynomials, Toeplitz theory.

AMS Subject classifications. 35B34, 47B28, 35P25, 35C20, 81Q12, 15A18, 15B05.

Contents

1. Introduction 2

Part I. Theoretical foundations 3
2. Chebyshev polynomials and Toeplitz theory 3
2.1. Chebyshev polynomials 3
2.2. Toeplitz matrices and operators 4
2.3. Spectra of tridiagonal Toeplitz matrices with perturbations 6
2.4. Spectra of tridiagonal 2-Toeplitz matrices with perturbations 7
2.5. Tridiagonal k-Toeplitz operators and matrices and their spectra 10
3. One-dimensional subwavelength systems 13
3.1. Hermitian case 14
3.2. Non-reciprocal case 15

Part II. Applications 17
4. Topological interface modes 17
4.1. Dimer chains with a geometric defect 18
4.2. Perturbed tridiagonal 2-Toeplitz matrices 19
4.3. Asymptotic spectral gap and localised interface modes 20
4.4. Existence, uniqueness, and convergence of the eigenvalue in the gap 21
4.5. Stability analysis 23
5. Non-Hermitian skin effect 25
5.1. The skin effect in monomer systems of subwavlength resonators 25
5.2. Non-Hermitian skin effect in dimer systems of subwavelength resonators 27
5.3. Stability of the skin effect 29
5.4. Topological origin of the skin effect 34
5.5. Non-Hermitian interface modes between opposing signs of the gauge potential 36
6. Tunable localisation in parity-time symmetric systems 38
6.1. Properties of the generalised gauge capacitance matrix 40
6.2. Eigenvalue of the generalised gauge capacitance matrix 42
6.3. Eigenvectors of the generalised gauge capacitance matrix 44

7. Generalised Brillouin zone for non-reciprocal problems 48
7.1. Physical systems and their mathematical models 48
7.2. Floquet–Bloch theory in the Hermitian case 48
7.3. The non-reciprocal case 49
7.4. k-Toeplitz operators and the generalised Brillouin zone 50
7.5. Three spectral limits 52
Appendix A. Capacitance matrix 55
Acknowledgements 57
Code Availability 57
Conflict of interest 57
References 58

1. Introduction

Subwavelength resonators are materials with high-contrast material parameters and size much smaller than the operating wavelength. They are typical building blocks for large, complex structures, known as metamaterials [37]. These microstructures can exhibit a variety of exotic and useful properties, such as robust localisation and transport properties at subwavelength scales. The starting point for their mathematical analysis is that, in the subwavelength regime, their eigenfrequencies and eigenmodes are described using a capacitance matrix formalism. This discrete formulation can be applied to a wide variety of settings, including both finite- and infinite-sized models and both Hermitian and non-Hermitian systems; see [9, 10] and the references therein.

In this survey, we specifically consider one dimensional metamaterials consisting of subwavelength resonators, which allows for more explicit formulations and applications not only in the field of metamaterials, but also in condensed matter physics due to its analogies with quantum mechanical phenomena. This is due to the fact that, in contrast to higher dimensional cases, interactions between the subwavelength resonators in one dimension only imply the nearest neighbours. Thus, the capacitance matrix formalism in one dimension is analogous to the tight-binding approximation for quantum systems, while in three dimensions some correspondence holds only for dilute resonators [13].

We consider both Hermitian systems of subwavelength resonators where the material parameters are real positive and non-Hermitian ones. In subwavelength wave physics, non-Hermiticity can be obtained via either a reciprocal mechanism by adding gain and loss inside the resonators [46], or via a non-reciprocal one by introducing a directional damping term, which is motivated by an imaginary gauge potential [65]. On the one hand, introducing gain and loss inside the resonators, represented by the imaginary parts of complex-valued material parameters, can create exceptional points. An exceptional point is a point in parameter space at which two or more eigenmodes coalesce [11, 15, 35, 46]. On the other hand, for systems that are non-Hermitian due to non-reciprocity, the wave propagation is usually amplified in one direction and attenuated in the other. This inherent unidirectional dynamics is related to the non-Hermitian skin effect, which leads to the accumulation of modes at one edge of the structure [34, 55, 65].

Our aim here is to highlight the powerful mathematical tools used for studying systems of subwavelength resonators in one dimension which are based on Chebyshev polynomials and Toeplitz theory. We use these mathematical tools to (i) characterise quantitatively the localised (topologically protected) interface modes in systems of finitely many resonators, (ii) study the skin effect in a system of finitely many subwavelength resonators with a non-Hermitian imaginary gauge potential and prove the condensation of bulk eigenmodes at one of the edges of the system, (iii) prove that all but two eigenmodes of a system of subwavelength resonators equipped with two kinds of non-Hermiticity — an imaginary gauge potential and on-site gain and loss–pass through exceptional points and decouple, and (iv)

introduce the notion of generalised Brillouin zone to account for the unidirectional spatial decay of the eigenmodes in non-reciprocal systems and obtain correct spectral convergence properties of finite to corresponding infinite systems.

The survey is organised as follows. In Section 2, we first recall monotonicity properties of Chebyshev polynomials. Then, we characterise the spectra of tridiagonal Toeplitz matrices with perturbations in the diagonal corners and show that their associated eigenvectors exhibit exponential decay. These matrices are crucial in the study of the one-dimensional monomer systems of subwavelength resonators [1, 6, 9, 27]. Finally, we consider tridiagonal k-Toeplitz matrices and illustrate the connection between the winding number of the eigenvalues of the symbol function and the exponential decay of the associated eigenvectors. In Section 3, we consider one-dimensional systems of subwavelength resonators as our main physical reference. This choice follows the rigorous derivation from first principles of the governing mathematical model: the capacitance matrix. We discuss both the Hermitian and the non-reciprocal cases. In Section 4, we prove the existence of a spectral gap for defectless finite dimer structures and provide a direct relationship between eigenvalues being within the spectral gap and the localisation of their associated eigenmodes. Then, we show the existence and uniqueness of an eigenvalue in the gap in the defect structure, proving the existence of a unique localised interface mode. Our method, based on Chebyshev polynomials, is the first to characterise quantitatively the localised interface modes in systems of finitely many resonators. Section 5 is devoted to the mathematical foundations of the non-Hermitian skin effect in systems of subwavelength resonators where a gauge potential is added inside the resonators to break Hermiticity. We prove the condensation of the eigenmodes at one edge of the structure and show the robustness of such effect with respect to random imperfections in the system. It is worth emphasising that the effect of adding this gauge potential only inside the subwavelength resonators would be negligible without exciting the structure's subwavelength eigenfrequencies. In Section 6, we study the interplay of an imaginary gauge potential and on-site gain and loss. By tuning the gain-to-loss ratio, we prove that a system of subwavelength resonators changes from a phase with unbroken parity-time symmetry to a phase with broken parity-time symmetry. At the macroscopic level, this is observed as a transition from symmetrical eigenmodes to condensated eigenmodes at one edge of the structure. In Section 7, we show how the spectral properties of a finite structure are associated with those of the corresponding semi-infinitely or infinitely periodic lattices and give explicit characterisations of how to extend the Floquet–Bloch theory in the Hermitian case to non-reciprocal settings. Finally, in the appendix we outline for completness the derivation of the capacitance matrix approximation to the eigenfrequencies and eigenmodes of a system of subwavelength resonators.

Part I. Theoretical foundations

2. Chebyshev polynomials and Toeplitz theory

2.1. Chebyshev polynomials

Chebyshev polynomials are two sequences of polynomials related to the cosine and sine functions, denoted respectively by $T_n(x)$ and $U_n(x)$. In particular, the Chebyshev polynomials of the first kind are obtained from the recurrence relation

$$\begin{aligned} T_0(x) &= 1, \\ T_1(x) &= x, \\ T_{n+1}(x) &= 2xT_n(x) - T_{n-1}(x), \end{aligned} \tag{2.1}$$

and the Chebyshev polynomials of the second kind are obtained from the recurrence relation

$$\begin{aligned} U_0(x) &= 1, \\ U_1(x) &= 2x, \\ U_{n+1}(x) &= 2xU_n(x) - U_{n-1}(x). \end{aligned} \tag{2.2}$$

A Chebyshev polynomial of either kind with degree n has n different simple roots, called Chebyshev roots, in the interval $[-1,1]$. The roots of $T_n(x)$ are

$$x_k = \cos\left(\frac{\pi(k+1/2)}{n}\right), \quad 0 \leqslant k \leqslant n-1,$$

and the roots of $U_n(x)$ are

$$x_k = \cos\left(\frac{k\pi}{n+1}\right), \quad 1 \leqslant k \leqslant n. \tag{2.3}$$

It is also well-known that for $-1 \leqslant x \leqslant 1$ and any $n \geqslant 0$, we have the upper bounds

$$|T_n(x)| \leq |T_n(1)| = 1, \quad |U_n(x)| \leq |U_n(1)| = n+1. \tag{2.4}$$

Although both $T_n(x)$ and $U_n(x)$ are highly oscillating in the interval $[-1,1]$, they have some monotonicity properties outside $[-1,1]$.

PROPOSITION 2.1. *Let $n \in \mathbb{N}$. Then,*

(i) $T_{2n+1}(x)$ is strictly increasing for $x \in (-\infty,-1) \cup (1,+\infty)$. $T_{2n}(x)$ is strictly increasing for $x \in (1,+\infty)$ and strictly decreasing for $x \in (-\infty,-1)$.

(ii) $U_{2n+1}(x)$ is strictly increasing for $x \in (-\infty,-1) \cup (1,+\infty)$. $U_{2n}(x)$ is strictly increasing for $x \in (1,+\infty)$ and strictly decreasing for $x \in (-\infty,-1)$.

(iii) $\frac{U_{n-1}(x)}{U_n(x)}$ is strictly decreasing for $x \in (-\infty,-1) \cup (1,+\infty)$.

A proof of item (iii) of Proposition 2.1 can be found in [3, Lemma 5.2].

We show in Figure 2.1 the behaviour of the Chebyshev polynomials of first and second kinds and illustrate the opposite behaviors of $T_n(x)$ and $U_n(x)$ for x inside and outside the interval $[-1,1]$. We will see in the subsequent sections that the two different outside and inside behaviors correspond to the skin effect and interface modes, respectively.

2.2. Toeplitz matrices and operators

Consider a complex valued function $f : \mathbb{T}^1 \to \mathbb{C}$ on the unit circle $\mathbb{T}^1$ represented by its Fourier series

$$f(z) = \sum_{k\in\mathbb{Z}} a_k z^k. \tag{2.5}$$

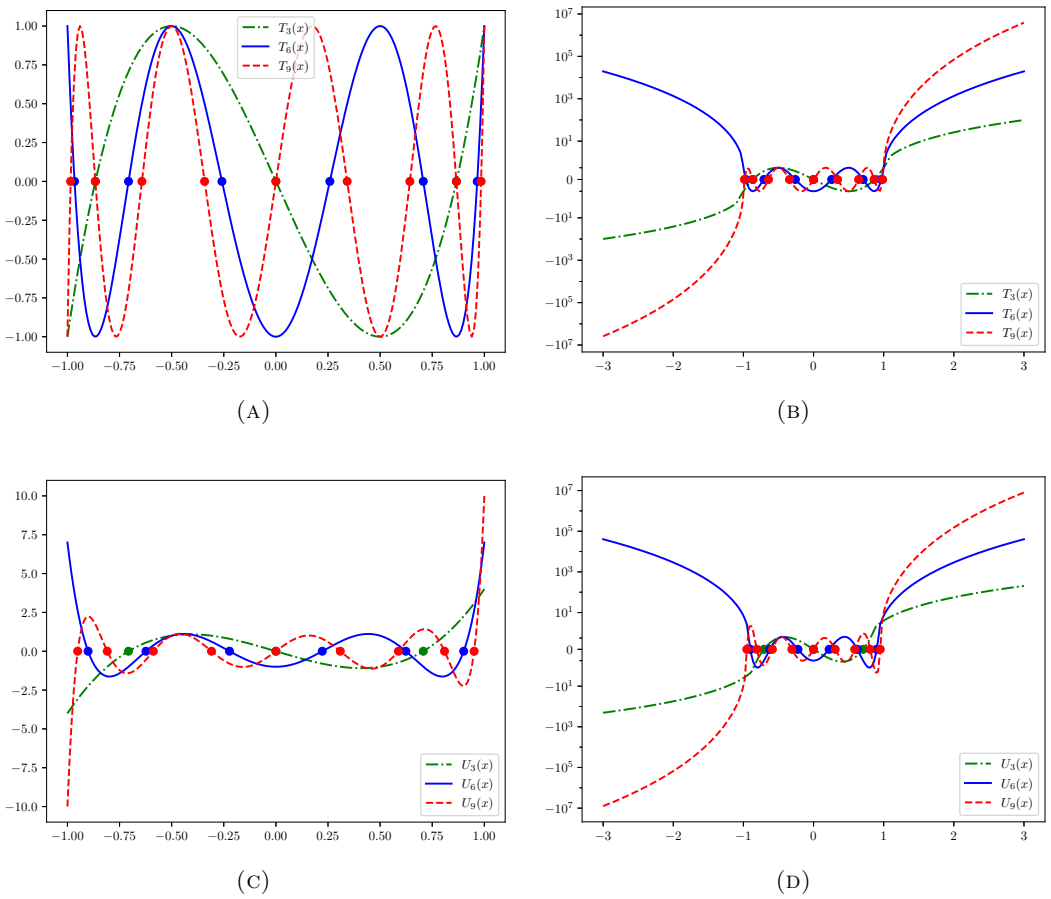
The $m \times m$ *Toeplitz matrix* associated to f is the matrix whose entries are constant along diagonals and are given by the Fourier coefficients of f:

$$T_m(f) = \begin{pmatrix} a_0 & a_{-1} & & \cdots & a_{1-m} \\ a_1 & a_0 & & & \vdots \\ & \ddots & \ddots & \ddots & \\ \vdots & & & a_0 & a_{-1} \\ a_{m-1} & \cdots & & a_1 & a_0 \end{pmatrix}.$$

A semi-infinite matrix of the same form is known as the *Toeplitz operator* associated to f and is denoted by $T(f)$ while a (bi-)infinite matrix of the same form is known as the *Laurent operator* associated to f and is denoted by $L(f)$. In all three cases, we call f the *symbol* associated to the matrix or the operator. Moreover, the Toeplitz operators (matrices) with $a_j = 0, j > l$ are called l-semibanded Toeplitz operators (matrices). The Toeplitz operators (matrices) with $a_j = 0, |j| > l$ are called l-banded Toeplitz operators (matrices).

We assume that the symbol function $f : \mathbb{T}^1 \to \mathbb{C}$ is L^2-integrable and continuous. This represents a certain loss of generality, but will be more than sufficient for the applications we are interested in.

The Toeplitz operator associated to f as above is an operator on $\ell^2(\mathbb{N})$, where $\ell^2(\mathbb{N})$ is the set of square summable sequences. Similarly, the Laurent operator acts on $\ell^2(\mathbb{Z})$. Note that the assumption that f is continuous is sufficient to ensure that $T(f)$ is bounded. Often



(A) (B)

(C) (D)

FIGURE 2.1. The Chebyshev polynomials of first (Figures 2.1a and 2.1b) and second (Figures 2.1c and 2.1d) kinds on a narrow interval (Figures 2.1a and 2.1c) where one observes the oscillating behaviour and on a wide interval (Figures 2.1b and 2.1d) where the monotone behaviour is visible (note the symmetrical log y-axis).

we shall fix f and consider the family of Toeplitz matrices $\{T_m(f)\}$ of increasing dimensions obtained as $m \times m$ finite sections of the infinite matrix $T(f)$.

Given a point $\lambda \in \mathbb{C} \backslash f(\mathbb{T}^1)$, we define the *winding number of the symbol* f, $\mathrm{wind}(f, \lambda)$, to be the winding number of f about λ in the usual positive (counterclockwise) sense, that is,

$$\mathrm{wind}(f, \lambda) \coloneqq \frac{1}{2\pi \mathbf{i}} \int_{f(\mathbb{T}^1)} (\xi - \lambda)^{-1} \, \mathrm{d}\xi.$$

If $\lambda \in f(\mathbb{T}^1)$, then $\mathrm{wind}(f, \lambda)$ is undefined.

The spectrum of the Toeplitz operator $T(f)$,

$$\sigma(T(f)) \coloneqq \{\lambda \in \mathbb{C} : (T(f) - \lambda) \text{ is not invertible}\},$$

is given by its symbol f [54, 61]. In particular, the following proposition holds.

PROPOSITION 2.2. *Let $T(f)$ be a Toeplitz operator with continuous symbol f. Then $\sigma(T(f))$ is equal to $f(\mathbb{T}^1)$ together with all the points λ enclosed by this curve with nonzero winding number* $\mathrm{wind}(f, \lambda)$. *In particular, for l-banded or l-semibanded Toeplitz operators $T(f)$, if* $\mathrm{wind}(f, \lambda) < 0$, *then there exists an eigenvector $\boldsymbol{x} \in \ell^2$ of $T(f)$ associated to λ and some*

$\rho < 1$ *such that*

$$\frac{|\boldsymbol{x}_j|}{\max_i |\boldsymbol{x}_i|} \leq C j^{l-1} \rho^{j-1}, \quad j \geq 1, \tag{2.6}$$

where $C > 0$ *is a constant depending only on* λ *and* f.

Remark that Proposition 2.2 characterises eigenvectors whose eigenvalues satisfy

$$\mathrm{wind}(f, \lambda) < 0.$$

Similar characterisation can formally be done with eigenvalues with $\mathrm{wind}(f, \lambda) > 0$, but the corresponding eigenvectors would not be square summable.

For Toeplitz matrices, similar results can be derived. We will need the concept of pseudospectrum.

Definition 2.3. Let $\varepsilon > 0$ and M be a matrix or an operator on a normed space. Then we denote by $\sigma_\varepsilon(M)$ the ε-pseudospectrum of M defined by

$$\sigma_\varepsilon(M) := \{\lambda \in \mathbb{C} : \|(M - \lambda)^{-1}\| > \varepsilon^{-1}\}.$$

Any value λ with $\|(M - \lambda)^{-1}\| > \varepsilon^{-1}$ is called ε-pseudoeigenvalue.

The topic of pseudoeigenvalues is extensively discussed in [61]. We recall from there the following result.

Lemma 2.4. *Let* M *be an operator with enough regularity (*e.g.*, a matrix) and* $\varepsilon > 0$. *Then, the* ε*-pseudospectrum of* M *is defined equivalently as the set of* $z \in \mathbb{C}$*:*

(i) $\|(M - \lambda)^{-1}\| > \varepsilon^{-1}$*;*
(ii) $z \in \sigma(M + E)$ *for some* E *with* $\|E\| < \varepsilon$*;*
(iii) $\sigma \in \sigma(M)$ *or* $\|(z - M)u\| < \varepsilon$ *for some* u *with* $\|u\| = 1$.

A vector u as in item (iii) is called an ε-pseudoeigenvector to z.

Let the tridiagonal Toeplitz matrix $T_N(f)$ be the finite, truncated, counterpart of $T(f)$ of size $N \times N$. Then the following proposition holds.

Proposition 2.5. *Consider a symbol* f *of a banded or semi-banded Toeplitz matrix. Let* $\lambda \in \mathbb{C}$ *be such that* $\mathrm{wind}(f, \lambda) \neq 0$. *Then there exists* $M > 1$ *so that, for* N *sufficiently large,* λ *is an* M^{-N}*-pseudoeigenvalue,*

$$\|(T_N(f) - \lambda)^{-1}\| \geq M^N,$$

with an exponentially localised pseudoeigenvector v *such that*

$$\frac{|v^{(j)}|}{\max_j |v^{(j)}|} \leq \begin{cases} M^{-j} & \text{if } \mathrm{wind}(f, \lambda) < 0, \\ M^{j-N} & \text{if } \mathrm{wind}(f, \lambda) > 0. \end{cases}$$

2.3. Spectra of tridiagonal Toeplitz matrices with perturbations

In this section, we characterise the spectra of tridiagonal Toeplitz matrices with perturbations in the diagonal corners and show that their associated eigenvectors exhibit exponential decay.

We denote by $T_m^{(a,b)}$ the tridiagonal Toeplitz matrix of order m with perturbations (a, b) in the diagonal corners, that is,

$$T_m^{(a,b)} = \begin{pmatrix} \alpha + a & \beta & & & & \\ \eta & \alpha & \beta & & & \\ & \eta & \alpha & \beta & & \\ & & \ddots & \ddots & \ddots & \\ & & & \eta & \alpha & \beta \\ & & & & \eta & \alpha + b \end{pmatrix}. \tag{2.7}$$

The tridiagonal Toeplitz matrix is thus $T_m^{(0,0)}$. Its spectrum is given as follows.

Lemma 2.6 (Eigenvalues and eigenvectors of tridiagonal Toeplitz matrices). *The eigenvalues of $T_m^{(0,0)}$ are given by*

$$\lambda_k = \alpha + 2\sqrt{\eta\beta}\cos\left(\frac{k}{m+1}\pi\right), \quad 1 \leq k \leq m,$$

and the corresponding eigenvectors are

$$\boldsymbol{v}_k^{(i)} = \left(\frac{\eta}{\beta}\right)^{\frac{1}{2}} \sin\left(\frac{ik}{m+1}\pi\right), \quad 1 \leq k \leq m \text{ and } 1 \leq i \leq m,$$

where $\boldsymbol{v}_k^{(i)}$ is the i^{th} coefficient of the k^{th} eigenvector.

The spectral theory of the Toeplitz matrices with perturbations in the diagonal corners, *i.e.*, $T_m^{(a,b)}$, is also well understood, as the following result [67, Theorem 3.1] shows.

Lemma 2.7. *Suppose that $\eta\beta \neq 0, a = \eta, b = \beta, \alpha + \beta + \eta = 0$ and let λ be an eigenvalue of $T_m^{(a,b)}$. Then, either $\lambda = \lambda_1 := 0$ and the corresponding eigenvector is $\boldsymbol{v}_1 = \mathbf{1} = (1, \ldots, 1)^\top$, where $\top$ denotes the transpose, or*

$$\lambda = \lambda_k := \alpha + 2\sqrt{\eta\beta}\cos\left(\frac{\pi}{m}(k-1)\right), \quad 2 \leq k \leq m,$$

and the corresponding eigenvector $\boldsymbol{v_k} = (\boldsymbol{v}_k^{(1)}, \ldots, \boldsymbol{v}_k^{(m)})^\top$ is given by

$$\boldsymbol{v}_k^{(j)} = \left(\frac{\eta}{\beta}\right)^{\frac{j-1}{2}} \left(a\sin\left(\frac{j(k-1)\pi}{m}\right) - \eta\sqrt{\frac{\eta}{\beta}}\sin\left(\frac{(j-1)(k-1)\pi}{m}\right)\right)$$

for $2 \leq k \leq m$ and $1 \leq j \leq m$.

2.4. Spectra of tridiagonal 2-Toeplitz matrices with perturbations

In this section, we generalise the results obtained in the previous section and characterise the spectra of tridiagonal 2-Toeplitz matrices with perturbations in the diagonal corners.

Let $A_{2m+1}^{(a,b)}$ be the tridiagonal 2-Toeplitz matrix of order $2m+1$ with perturbations (a, b) in the diagonal corners, that is,

$$A_{2m+1}^{(a,b)} = \begin{pmatrix} \alpha_1 + a & \beta_1 & & & & & \\ \eta_1 & \alpha_2 & \beta_2 & & & & \\ & \eta_2 & \alpha_1 & \beta_1 & & & \\ & & \eta_1 & \alpha_2 & \ddots & & \\ & & & \ddots & \ddots & \ddots & \\ & & & & \eta_1 & \alpha_2 & \beta_2 \\ & & & & & \eta_2 & \alpha_1 + b \end{pmatrix}. \tag{2.8}$$

Here, $\beta_i, \eta_i, \alpha_i$, $i = 1, 2$ and a, b are in $\mathbb{R}$. Denote furthermore by $A_{2m}^{(a,b)}$ the tridiagonal 2-Toeplitz matrix of order $2m$ with perturbations (a, b) in the diagonal corners, that is,

$$A_{2m}^{(a,b)} = \begin{pmatrix} \alpha_1 + a & \beta_1 & & & & & \\ \eta_1 & \alpha_2 & \beta_2 & & & & \\ & \eta_2 & \alpha_1 & \beta_1 & & & \\ & & \eta_1 & \alpha_2 & \ddots & & \\ & & & \ddots & \ddots & \ddots & \\ & & & & \eta_2 & \alpha_1 & \beta_1 \\ & & & & & \eta_1 & \alpha_2 + b \end{pmatrix}. \tag{2.9}$$

We assume throughout that the off-diagonal elements in (2.8) and (2.9) are nonzero and satisfy the following condition:

$$\eta_i\beta_i > 0, \quad i = 1, 2.$$

We first consider the eigenvalues of $A_{2m+1}^{(0,0)}$ and $A_{2m}^{(0,0)}$ and define the polynomials

$$P_m^*(x) = \left(\sqrt{\eta_1\beta_1\eta_2\beta_2}\right)^m U_m\left(\frac{(x-\alpha_1)(x-\alpha_2)-\eta_1\beta_1-\eta_2\beta_2}{2\sqrt{\eta_1\beta_1\eta_2\beta_2}}\right), \tag{2.10}$$

where U_m is the Chebyshev polynomial of the second kind defined in (2.2). It is well-known (see [21, 33, 43]) that the characteristic polynomials of the 2-Toeplitz matrices $A_{2m+1}^{(0,0)}, A_{2m}^{(0,0)}$ are respectively

$$\chi_{A_{2m+1}^{(0,0)}}(x) = (x-\alpha_1)\,P_m^*(x)$$

and

$$\chi_{A_{2m}^{(0,0)}}(x) = P_m^*(x) + \eta_2\beta_2 P_{m-1}^*(x).$$

More generally, it can be shown that the characteristic polynomials of $A_{2m+1}^{(a,b)}, A_{2m}^{(a,b)}$ are respectively

$$\chi_{A_{2m+1}^{(a,b)}}(x) = (x-\alpha_1-a-b)\,P_m^*(x) + (ab(x-\alpha_2) - a\eta_1\beta_1 - b\eta_2\beta_2)\,P_{m-1}^*(x)$$

and

$$\chi_{A_{2m}^{(a,b)}}(x) = P_m^*(x) + (a(\alpha_2-x) + b(\alpha_1-x) + ab + \eta_2\beta_2)\,P_{m-1}^*(x) + ab\eta_1\beta_1 P_{m-2}^*(x).$$

In particular, for the case when $\alpha_1=\alpha_2=\alpha, \eta_j=\beta_j, j=1,2$, the characteristic polynomials of $A_{2m+1}^{(a,b)}$ and $A_{2m}^{(a,b)}$ are respectively

$$\chi_{A_{2m+1}^{(a,b)}}(x) = (x-\alpha-a-b)\,P_m^*(x) + \left(ab(x-\alpha) - a\beta_1^2 - b\beta_2^2\right)P_{m-1}^*(x) \tag{2.11}$$

and

$$\chi_{A_{2m}^{(a,b)}}(x) = P_m^*(x) + \left((a+b)(\alpha-x) + ab + \beta_2^2\right)P_{m-1}^*(x) + ab\beta_1^2 P_{m-2}^*(x) \tag{2.12}$$

for the corresponding $P_m^*(x)$'s.

We now present a detailed characterisation of the eigenvalues of $A_{2m+1}^{(a,b)}$ and $A_{2m}^{(a,b)}$. All the following results in this section and their justification can be found in the authors' paper [6].

Theorem 2.8. *Let m be large enough. The eigenvalues λ_r's of $A_{2m+1}^{(a,b)}$ are all real numbers. Except for at most 11 eigenvalues, we can reindex the λ_r's to have*

$$\lambda_3^l < \lambda_4^l < \cdots < \lambda_{m-3}^l \le \min\{\alpha_1,\alpha_2\} \le \max\{\alpha_1,\alpha_2\} \le \lambda_{m-3}^r < \cdots < \lambda_4^r < \lambda_3^r.$$

In particular, for $k=3,\cdots,m-3$,

$$\cos\left(\frac{k\pi}{m}\right) \le \min\left\{y\left(\lambda_k^l\right), y\left(\lambda_k^r\right)\right\} \le \max\left\{y\left(\lambda_k^l\right), y\left(\lambda_k^r\right)\right\} \le \cos\left(\frac{(k-2)\pi}{m}\right) \tag{2.13}$$

with

$$y(x) = \frac{(x-\alpha_1)(x-\alpha_2)-\eta_1\beta_1-\eta_2\beta_2}{2\sqrt{\eta_1\beta_1\eta_2\beta_2}}. \tag{2.14}$$

Theorem 2.9. *Let m be large enough. The eigenvalues $\{\lambda_r\}$ of $A_{2m}^{(a,b)}$ are all real numbers. Except for at most 12 eigenvalues, we can reindex the λ_r's to have*

$$\lambda_3^l < \lambda_4^l < \cdots < \lambda_{m-4}^l \le \min\{\alpha_1,\alpha_2\} \le \max\{\alpha_1,\alpha_2\} \le \lambda_{m-4}^r < \cdots < \lambda_4^r < \lambda_3^r.$$

In particular, for $k=3,\cdots,m-4$,

$$\cos\left(\frac{(k+1)\pi}{m}\right) \le \min\left\{y\left(\lambda_k^l\right), y\left(\lambda_k^r\right)\right\} \le \max\left\{y\left(\lambda_k^l\right), y\left(\lambda_k^r\right)\right\} \le \cos\left(\frac{(k-2)\pi}{m}\right) \tag{2.15}$$

with $y(x)$ being defined by (2.14).

We next present explicit formulas for the eigenvectors of tridiagonal 2-Toeplitz matrices with perturbations on the diagonal corners, that is the matrices $A_{2m+1}^{(a,b)}$ and $A_{2m}^{(a,b)}$, through a direct construction. We start by introducing the following two families of polynomials.

Definition 2.10. We define the two families of polynomials $q_k^{(\xi_p,\xi_q)}, p_k^{(\xi_p,\xi_q)}$ by

$$q_0^{(\xi_p,\xi_q)}(\nu) = \xi_q, \qquad p_0^{\xi_p,\xi_p}(\nu) = \xi_p,$$

and the recurrence formulas

$$q_k^{(\xi_p,\xi_q)}(\nu) = \nu p_{k-1}^{(\xi_p,\xi_q)}(\nu) - q_{k-1}^{(\xi_p,\xi_q)}(\nu), \tag{2.16}$$

$$p_k^{(\xi_p,\xi_q)}(\nu) = q_k^{(\xi_p,\xi_q)}(\nu) - \zeta p_{k-1}^{(\xi_p,\xi_q)}(\nu), \tag{2.17}$$

where

$$\zeta = \frac{\eta_2\beta_2}{\eta_1\beta_1}. \tag{2.18}$$

The recurrence formulas (2.16) and (2.17) can be simplified as follows.

Proposition 2.11. *If $p_k^{(\xi_p,\xi_q)}(\nu)$ and $q_k^{(\xi_p,\xi_q)}(\nu)$ satisfy (2.16) and (2.17) respectively, then*

$$p_{k+1}^{(\xi_p,\xi_q)}(\nu) = [\nu - (1+\zeta)]p_k^{(\xi_p,\xi_q)}(\nu) - \zeta p_{k-1}^{(\xi_p,\xi_q)}(\nu) \tag{2.19}$$

and

$$q_{k+1}^{(\xi_p,\xi_q)}(\nu) = [\nu - (1+\zeta)]q_k^{(\xi_p,\xi_q)}(\nu) - \zeta q_{k-1}^{(\xi_p,\xi_q)}(\nu) \tag{2.20}$$

with

$$\begin{aligned} p_0^{(\xi_p,\xi_q)}(\nu) &= \xi_p, \quad p_1^{(\xi_p,\xi_q)}(\nu) = (\nu-\zeta)\,\xi_p - \xi_q, \\ q_0^{(\xi_p,\xi_q)}(\nu) &= \xi_q, \quad q_1^{(\xi_p,\xi_q)}(\nu) = \nu\xi_p - \xi_q, \end{aligned} \tag{2.21}$$

where ζ is defined in (2.18).

For later use of the Chebyshev polynomials, we further normalise the polynomials $p_k^{(\xi_p,\xi_q)}(\nu), q_k^{(\xi_p,\xi_q)}(\nu)$. This can be achieved by setting

$$\mu = \frac{\nu - \left(1+\beta^2\right)}{2\beta} \tag{2.22}$$

with

$$\beta^2 = \frac{\beta_2\eta_2}{\beta_1\eta_1},$$

and

$$\widehat{p}_k^{(\xi_p,\xi_q)}(\mu) = \frac{1}{\beta^k}p_k^{(\xi_p,\xi_q)}\left(1+2\beta\mu+\beta^2\right), \ \widehat{q}_k^{(\xi_p,\xi_q)}(\mu) = \frac{1}{\beta^k}q_k^{(\xi_p,\xi_q)}\left(1+2\beta\mu+\beta^2\right). \tag{2.23}$$

Thus, from (2.19) and (2.20), we respectively get

$$\widehat{p}_{k+1}^{(\xi_p,\xi_q)}(\mu) = 2\mu\widehat{p}_k^{(\xi_p,\xi_q)}(\mu) - \widehat{p}_{k-1}^{(\xi_p,\xi_q)}(\mu), \tag{2.24}$$

and

$$\widehat{q}_{k+1}^{(\xi_p,\xi_q)}(\mu) = 2\mu\widehat{q}_k^{(\xi_p,\xi_q)}(\mu) - \widehat{q}_{k-1}^{(\xi_p,\xi_q)}(\mu). \tag{2.25}$$

Equations (2.24) and (2.25) are the Chebyshev three point recurrence formula. Also, from (2.21), the initial polynomials are given by

$$\begin{aligned} \widehat{p}_0^{(\xi_p,\xi_q)}(\mu) &= \xi_p, \quad \widehat{p}_1^{(\xi_p,\xi_q)}(\mu) = 2\mu\xi_p + \frac{\xi_p-\xi_q}{\beta}, \\ \widehat{q}_0^{(\xi_p,\xi_q)}(\mu) &= \xi_q, \quad \widehat{q}_1^{(\xi_p,\xi_q)}(\mu) = (2\mu+\beta)\xi_p + \frac{\xi_p-\xi_q}{\beta}. \end{aligned} \tag{2.26}$$

Now, we characterise the eigenvectors of $A_{2m+1}^{(a,b)}$ and $A_{2m}^{(a,b)}$ by the "Chebyshev like" polynomials introduced above.

Theorem 2.12. *The eigenvector of $A_{2m+1}^{(a,b)}$ in (2.8) associated with the eigenvalue λ_r is given by*

$$\begin{aligned}\boldsymbol{x} = \Bigg(& \widehat{q}_0^{(\xi_p,\xi_q)}(\mu_r), -\frac{1}{\beta_1}(\alpha_1-\lambda_r)\widehat{p}_0^{(\xi_p,\xi_q)}(\mu_r), s\widehat{q}_1^{(\xi_p,\xi_q)}(\mu_r), -\frac{1}{\beta_1}s(\alpha_1-\lambda_r)\widehat{p}_1^{(\xi_p,\xi_q)}(\mu_r), \\ & \ldots, -\frac{1}{\beta_1}s^{m-1}(\alpha_1-\lambda_r)\widehat{p}_{m-1}^{(\xi_p,\xi_q)}(\mu_r), s^m\widehat{q}_m^{(\xi_p,\xi_q)}(\mu_r)\Bigg)^\top,\end{aligned} \tag{2.27}$$

where $\widehat{q}_k^{(\xi_p,\xi_q)}, \widehat{p}_k^{(\xi_p,\xi_q)}$ are defined as in (2.23) with

$$\xi_q = (\alpha_1 - \lambda_r), \xi_p = (\alpha_1 + a - \lambda_r),$$

and s, μ_r are respectively given by

$$s = \sqrt{\frac{\eta_1\eta_2}{\beta_1\beta_2}}, \quad \mu_r = \frac{(\alpha_1-\lambda_r)(\alpha_2-\lambda_r) - (\eta_1\beta_1+\eta_2\beta_2)}{2\sqrt{\eta_1\beta_1\eta_2\beta_2}}. \tag{2.28}$$

The eigenvector of $A_{2m}^{(a,b)}$ in (2.9) associated with the eigenvalue λ_r is given by the first $2m$ elements of $\boldsymbol{x}$ in (2.27).

Remark 2.13. By (2.26), in Theorem 2.12, the initial values of $\widehat{p}_k^{(\xi_p,\xi_q)}(\mu_r)$ and $\widehat{q}_k^{(\xi_p,\xi_q)}(\mu_r)$ are

$$\begin{aligned} &\widehat{p}_0^{(\xi_p,\xi_q)}(\mu_r) = (\alpha_1-\lambda_r), && \widehat{p}_1^{(\xi_p,\xi_q)}(\mu_r) = 2\mu_r(\alpha_1-\lambda_r) - \frac{a}{\beta}, \\ &\widehat{q}_0^{(\xi_p,\xi_q)}(\mu_r) = (\alpha_1+a-\lambda_r), && \widehat{q}_1^{(\xi_p,\xi_q)}(\mu_r) = (2\mu_r+\beta)(\alpha_1-\lambda_r) - \frac{a}{\beta}. \end{aligned} \tag{2.29}$$

2.5. Tridiagonal k-Toeplitz operators and matrices and their spectra

In Section 2.3, we have analysed the spectrum of tridiagonal Toeplitz matrices. Then we have generalised our results in Section 2.4 to tridiagonal 2-Toeplitz matrices with an extensive complexity overhead. It is natural to ask how the spectrum of a general tridiagonal k-Toeplitz operator looks like and this will be done in this section where we will also show that their associated eigenvectors exhibit exponential decay. The tools are, once more, different from those in the previous two cases. We refer the reader to [33] for the spectral theory of tridiagonal 2-Toeplitz matrices (without any perturbation) and to [20] and the references therein for further results on the eigenvalues of tridiagonal k-Toeplitz.

Note that tridiagonal k-Toeplitz operators and their associated truncated operators (*i.e.*, matrices) are crucial in the study of the one-dimensional polymer systems of subwavelength resonators [1, 6, 9, 27]. A k-Toeplitz operator is a semi-infinite matrix of the following kind:

$$T(f) = A = \begin{pmatrix} \alpha_1 & \beta_1 & 0 & & & & & \\ \eta_1 & \alpha_2 & \beta_2 & \ddots & & & & \\ 0 & \ddots & \ddots & \ddots & \ddots & & & \\ & \ddots & \eta_{k-2} & \alpha_{k-1} & \beta_{k-1} & \ddots & & \\ & & \ddots & \eta_{k-1} & \alpha_k & \beta_k & \ddots & \\ & & & \ddots & \eta_k & \alpha_1 & \beta_1 & \ddots \\ & & & & \ddots & \ddots & \ddots & \ddots \end{pmatrix}, \tag{2.30}$$

where $\alpha_i, \beta_i, \eta_i \in \mathbb{C}$ for $i \in \mathbb{N}$ and $A_{ij} = 0$ if $|i-j| > 1$ for $i, j \in \mathbb{N}$. A bi-infinite matrix of the same form is called a tridiagonal k-Laurent operator. We consider that these two operators act on sequences of square integrable numbers.

Recall, furthermore, that the tridiagonal k-Toeplitz operator A presented in (2.30) can be reformulated as a tridiagonal block Toeplitz operator, where the blocks repeat in a 1-periodic

way:

$$A = \begin{pmatrix} A_0 & A_{-1} & \\ A_1 & A_0 & \ddots \\ & \ddots & \ddots \end{pmatrix}, \tag{2.31}$$

with

$$A_0 = \begin{pmatrix} \alpha_1 & \beta_1 & 0 & \cdots & 0 \\ \eta_1 & \alpha_2 & \beta_2 & \ddots & \vdots \\ 0 & \ddots & \ddots & \ddots & 0 \\ \vdots & \ddots & \eta_{k-2} & \alpha_{k-1} & \beta_{k-1} \\ 0 & \cdots & 0 & \eta_{k-1} & \alpha_k \end{pmatrix}, A_{-1} = \begin{pmatrix} 0 & \cdots & \cdots & 0 \\ \vdots & \ddots & & \vdots \\ 0 & & \ddots & \vdots \\ \beta_k & 0 & \cdots & 0 \end{pmatrix}, A_1 = \begin{pmatrix} 0 & \cdots & 0 & \eta_k \\ \vdots & \ddots & & 0 \\ \vdots & & \ddots & \vdots \\ 0 & \cdots & \cdots & 0 \end{pmatrix}.$$

In this case, the symbol of A in (2.30) is

$$\begin{aligned} f : \mathbb{T}^1 &\to \mathbb{C}^{k\times k} \\ z &\mapsto A_{-1}z^{-1} + A_0 + A_1 z, \end{aligned} \tag{2.32}$$

or explicitly

$$f(z) = \begin{pmatrix} \alpha_1 & \beta_1 & 0 & \dots & 0 & \eta_k z \\ \eta_1 & \alpha_2 & \beta_2 & 0 & \dots & 0 \\ 0 & \eta_2 & \alpha_3 & \beta_3 & \ddots & \vdots \\ \vdots & \ddots & \ddots & \ddots & \ddots & 0 \\ 0 & \dots & 0 & \eta_{k-2} & \alpha_{k-1} & \beta_{k-1} \\ \beta_k z^{-1} & 0 & \dots & 0 & \eta_{k-1} & \alpha_k \end{pmatrix}. \tag{2.33}$$

Further, let now $n, k \geq 1$ and define the projections

$$\begin{aligned} P_n : \ell^2(\mathbb{N}, \mathbb{C}) &\to \ell^2(\mathbb{N}, \mathbb{C}) \\ (x_1, x_2, \dots) &\mapsto (x_1, \dots x_n, 0, 0, \dots). \end{aligned} \tag{2.34}$$

Then, the *k-Toeplitz matrix* of order mk for $m \in \mathbb{N}$ associated to the symbol $f \in L^\infty(\mathbb{T}^1, \mathbb{C}^{k\times k})$ is given by

$$T_{m\times k}(f) \coloneqq P_{mk} T(f) P_{mk},$$

and can be identified as an $mk \times mk$ matrix. The spectra of tridiagonal k-Toeplitz matrices is not well understood yet. For the results of the pseudospectra of tridiagonal k-Toeplitz matrices, we refer the reader to [5, Section 3].

Now, we start to introduce the spectra of the operator $T(f)$. We denote by $\sigma, \sigma_{\text{ess}}$ the spectrum and the essential spectrum of the operator, respectively. We define

$$\sigma_{\det}(f) = \{\lambda \in \mathbb{C} : \det(f(z) - \lambda) = 0,\ \exists z \in \mathbb{T}^1\}. \tag{2.35}$$

We first have the following result characterising the essential spectrum of $T(f)$.

Proposition 2.14. *The operator $T(f)$ in (2.30) is Fredholm if and only if* $\det(f)$ *has no zeros on $\mathbb{T}^1$. Furthermore, the essential spectrum of $T(f)$ is given by*

$$\sigma_{\text{ess}}(T(f)) = \sigma_{\det}(f).$$

Next, we provide a full characterisation of $\sigma(T(f))$. Before stating the result, we first define

$$\sigma_{\text{wind}}(f) \coloneqq \{\lambda \in \mathbb{C} \setminus \sigma_{\det}(f) : \text{wind}(\det(f - \lambda), 0) \neq 0\}. \tag{2.36}$$

By [5, Lemma A.1],

$$\det(f(z) - \lambda) = (-1)^{k+1} \left(\prod_{i=1}^{k} \eta_i \right) z + (-1)^{k+1} \left(\prod_{i=1}^{k} \beta_i \right) z^{-1} + g(\lambda)$$

with $g(\lambda)$ being given by [5, (A.2)]. This yields

$$\sigma_{\mathrm{wind}}(f) = \left\{ \lambda \in \mathbb{C} \setminus \sigma_{\mathrm{det}}(f) : \mathrm{wind}\left((-1)^{k+1} \left((\prod_{i=1}^{k} \eta_i) z + (\prod_{i=1}^{k} \beta_i) z^{-1} \right), -g(\lambda) \right) \neq 0 \right\}. \tag{2.37}$$

Furthermore, since

$$\det(f(z) - \lambda) = \prod_{j=1}^{k} (\lambda_j(z) - \lambda),$$

where $\lambda_j(z), 1 \leq j \leq k$, are the eigenvalues of the matrix $f(z)$, we obtain that

$$\sigma_{\mathrm{wind}}(f) = \left\{ \lambda \in \mathbb{C} \setminus \sigma_{\mathrm{det}}(f) : \sum_{j=1}^{k} \mathrm{wind}(\lambda_j(\mathbb{T}) - \lambda, 0) \neq 0 \right\},$$

or equivalently,

$$\sigma_{\mathrm{wind}}(f) = \left\{ \lambda \in \mathbb{C} \setminus \sigma_{\mathrm{det}}(f) : \sum_{j=1}^{k} \mathrm{wind}(\lambda_j(\mathbb{T}), \lambda) \neq 0 \right\}. \tag{2.38}$$

In (2.38) and in the rest of the text, eigenvalues traces are considered to be concatenated if their endings match.

We now state the following result on the spectrum of the operator $T(f)$. We refer to [5] for its proof.

Theorem 2.15. *Let $f \in \mathbb{C}^{k\times k}(\mathbb{T}^1)$ be the symbol of a tridiagonal k-Toeplitz operator $T(f)$. Denote by B_0 the leading $(k-1)\times(k-1)$ principal minor of A_0. It holds that*

$$\sigma_{\mathrm{det}}(f) \cup \sigma_{\mathrm{wind}}(f) \subset \sigma(T(f)) \subset \sigma_{\mathrm{det}}(f) \cup \sigma_{\mathrm{wind}}(f) \cup \sigma(B_0),$$

where $\sigma_{\mathrm{det}}(f), \sigma_{\mathrm{wind}}(f)$ are given by (2.35) and (2.38), respectively.

Note that this characterisation is optimal. It cannot be made more precise, as it cannot be guaranteed that an eigenvalue λ of B_0 with $\mathrm{wind}(\det(f-\lambda),0) = 0$ is also an eigenvalue of $T(f)$; see the example given in [5].

Now that we have characterised the spectra of tridiagonal k-Toeplitz operators, we venture onwards to explore their eigenvectors. In particular, we have the following theorem from [5] showing that the eigenvectors exhibit exponential decay.

Theorem 2.16. *Suppose $\Pi_{j=1}^{k}\eta_j \neq 0$ and $\Pi_{j=1}^{k}\beta_j \neq 0$. Let $f(z) \in \mathbb{C}^{k\times k}$ be the symbol (2.33) and let $\lambda \in \mathbb{C}\setminus\sigma_{\mathrm{ess}}(T(f))$. If $\sum_{j=1}^{k} \mathrm{wind}(\lambda_j, \lambda) < 0$ for λ_j being the eigenvalues of $f(z)$, then there exists an eigenvector $\boldsymbol{x} \in \ell^2$ of $T(f)$ associated to λ and some $\rho < 1$ such that*

$$\frac{|\boldsymbol{x}_j|}{\max_i |\boldsymbol{x}_i|} \leq C_1 \lceil j/k \rceil \rho^{\lceil j/k \rceil - 1}, \quad j \geq 1, \tag{2.39}$$

where $C_1 > 0$ is a constant depending only on $\lambda, \alpha_p, \beta_p, \eta_p$ for $1 \leq p \leq k$.

Last, we introduce a condition for the symbol f to be collapsed. We call a symbol f *collapsed* if for all $\lambda \in \mathbb{C}$ it holds that $\mathrm{wind}(\det(f-\lambda),0) = 0$. This corresponds to the fact that the curves traced out by the eigenvalues of the symbol $\mathbb{T}^1 \ni z \mapsto \sigma(f(z))$ do not generate winding regions. Relating this to Proposition 2.2 and its k-Toeplitz analogue, there is no exponential behaviour of the eigenvectors of a collapsed symbol.

In the tridiagonal setting this is easy to identify; see [7].

LEMMA 2.17. *Let $T(f)$ be a symmetric or Hermitian tridiagonal k-Toeplitz operator. Then the symbol $f(z)$ is collapsed.*

3. One-dimensional subwavelength systems

We consider a one-dimensional chain of N disjoint subwavelength resonators $D_i \coloneqq (x_i^{\mathsf{L}}, x_i^{\mathsf{R}})$, where $(x_i^{\mathsf{L},\mathsf{R}})_{1\leq i\leq N} \subset \mathbb{R}$ are the $2N$ extremities satisfying $x_i^{\mathsf{L}} < x_i^{\mathsf{R}} < x_{i+1}^{\mathsf{L}}$ for any $1 \leq i \leq N$. We fix the coordinates such that $x_1^{\mathsf{L}} = 0$. We also denote by $\ell_i = x_i^{\mathsf{R}} - x_i^{\mathsf{L}}$ the length of the i^{th} resonators, and by $s_i = x_{i+1}^{\mathsf{L}} - x_i^{\mathsf{R}}$ the spacing between the i^{th} and $(i+1)^{\text{th}}$ resonator. The system is illustrated in Figure 3.1. We will use

$$D \coloneqq \bigcup_{i=1}^{N} (x_i^{\mathsf{L}}, x_i^{\mathsf{R}})$$

to symbolise the set of subwavelength resonators.

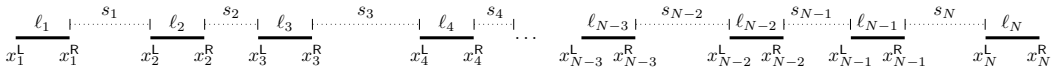


FIGURE 3.1. A chain of N subwavelength resonators, with lengths $(\ell_i)_{1\leq i\leq N}$ and spacings $(s_i)_{1\leq i\leq N-1}$.

As a scalar wave field $u(t,x)$ propagates in a heterogeneous medium, it satisfies the following one-dimensional wave equation:

$$\frac{1}{\kappa(x)}\frac{\partial^2}{\partial t^2}u(t,x) - \frac{\partial}{\partial x}\left(\frac{1}{\rho(x)}\frac{\partial}{\partial x}u(t,x)\right) = 0, \qquad (t,x) \in \mathbb{R}\times\mathbb{R}\,.$$

The parameters $\kappa(x)$ and $\rho(x)$ are the material parameters of the medium. We consider piecewise constant material parameters

$$\kappa(x) = \begin{cases} \kappa_b & x \in D, \\ \kappa & x \in \mathbb{R}\setminus D, \end{cases} \quad \text{and} \quad \rho(x) = \begin{cases} \rho_b & x \in D, \\ \rho & x \in \mathbb{R}\setminus D, \end{cases}$$

where the constants $\rho_b, \rho, \kappa, \kappa_b \in \mathbb{R}_{>0}$. The wave speeds inside the resonators D and inside the background medium $\mathbb{R}\setminus D$, are denoted respectively by v_b and v, the wave numbers respectively by k_b and k, and the contrast between the densities of the resonators and the background medium by δ:

$$v_b \coloneqq \sqrt{\frac{\kappa_b}{\rho_b}}, \qquad v \coloneqq \sqrt{\frac{\kappa}{\rho}}, \qquad k_b \coloneqq \frac{\omega}{v_b}, \qquad k \coloneqq \frac{\omega}{v}, \qquad \delta \coloneqq \frac{\rho_b}{\rho}. \tag{3.1}$$

Up to using a Fourier decomposition in time, we can assume that the total wave field $u(t,x)$ is time-harmonic:

$$u(t,x) = \Re(e^{-\mathbf{i}\omega t}u(x)),$$

for a function $u(x)$ which solves the one-dimensional Helmholtz equation:

$$-\frac{\omega^2}{\kappa(x)}u(x) - \frac{\mathrm{d}}{\mathrm{d}x}\left(\frac{1}{\rho(x)}\frac{\mathrm{d}}{\mathrm{d}x}u(x)\right) = 0, \qquad x \in \mathbb{R}\,. \tag{3.2}$$

In these circumstances of piecewise constant material parameters, the wave problem determined by (3.2) can be rewritten as the following system of coupled one-dimensional Helmholtz equations:

$$\begin{cases} u''(x) + \dfrac{\omega^2}{v_b^2} u(x) = 0, & x \in D, \\ u''(x) + \dfrac{\omega^2}{v^2} u(x) = 0, & x \in \mathbb{R} \setminus D, \\ u|_{\mathsf{R}}(x_i^{\mathsf{L},\mathsf{R}}) - u|_{\mathsf{L}}(x_i^{\mathsf{L},\mathsf{R}}) = 0, & \text{for all } 1 \le i \le N, \\ \left.\dfrac{\mathrm{d}u}{\mathrm{d}x}\right|_{\mathsf{R}} (x_i^{\mathsf{L}}) = \delta \left.\dfrac{\mathrm{d}u}{\mathrm{d}x}\right|_{\mathsf{L}} (x_i^{\mathsf{L}}), & \text{for all } 1 \le i \le N, \\ \delta \left.\dfrac{\mathrm{d}u}{\mathrm{d}x}\right|_{\mathsf{R}} (x_i^{\mathsf{R}}) = \left.\dfrac{\mathrm{d}u}{\mathrm{d}x}\right|_{\mathsf{L}} (x_i^{\mathsf{R}}), & \text{for all } 1 \le i \le N, \\ \dfrac{\mathrm{d}u}{\mathrm{d}\,|x|}(x) - \mathbf{i}ku(x) = 0, & x \in (-\infty, x_1^{\mathsf{L}}) \cup (x_N^{\mathsf{R}}, \infty), \end{cases} \tag{3.3}$$

where, for a one-dimensional function w, we denote by

$$w|_{\mathsf{L}}(x) \coloneqq \lim_{\substack{s \to 0 \\ s>0}} w(x-s) \quad \text{and} \quad w|_{\mathsf{R}}(x) \coloneqq \lim_{\substack{s \to 0 \\ s>0}} w(x+s)$$

if the limits exist.

We are interested in the subwavelength eigenfrequencies $\omega \in \mathbb{C}$ such that (3.3) has a nontrivial solution. We will perform an asymptotic analysis in a high-contrast limit, given by $\delta \to 0$. We will look for the subwavelength modes within this regime, which we characterise by requiring that $\omega \to 0$ as $\delta \to 0$. This limit will recover subwavelength resonances, while keeping the size of the resonators fixed.

In all what follows we will denote by $H^1(D)$ the usual Sobolev spaces of complex-valued functions on D.

Definition 3.1 (Subwavelength eigenfrequency). A (complex) frequency $\omega(\delta) \in \mathbb{C}$, with nonnegative real part, satisfying

$$\omega(\delta) \to 0 \quad \text{as} \quad \delta \to 0 \tag{3.4}$$

and such that (3.3) admits a nonzero solution $u(\omega, \delta) \in H^1(D)$ for $\omega = \omega(\delta)$ is called a *subwavelength eigenfrequency*. The solution $u(\omega, \delta)$ is called a *subwavelength eigenmode*.

We can immediately see that $\omega = 0$ is a trivial solution to (3.3) corresponding to an eigenmode which is constant across all the resonators. In what follows, we will restrict attention to other solutions of (3.3).

3.1. Hermitian case

In the high-contrast, low-frequency scattering problems, recent work has shown that capacitance matrices can be used to provide asymptotic characterisations of the resonant modes [9]. Capacitance matrices were first introduced to describe many-body electrostatic systems by Maxwell [45], and have recently enjoyed a resurgence in subwavelength physics. In particular, for one-dimensional models like the one considered here, a capacitance matrix formulation has proven to be very effective in both efficiently solving the problem as well as providing valuable insights in the solution [2, 28].

For a system as in Figure 3.1, we define the *capacitance matrix* C as

$$C_{i,j} \coloneqq -\int_{\partial D_i} \frac{\partial V_j}{\partial \nu} \,\mathrm{d}x \qquad \text{with} \qquad \begin{cases} -\dfrac{\mathrm{d}^2}{\mathrm{d}x^2} V_i = 0 \quad \text{in } \mathbb{R} \setminus D, \\ V_i(x_j^{\mathsf{L},\mathsf{R}}) = \delta_{i,j}, \\ V_i(x) = \mathcal{O}(1) \quad \text{for } |x| \to +\infty, \end{cases} \tag{3.5}$$

where $\delta_{i,j}$ is the Kronecker delta and ν the outward pointing normal. Then, it is easy to see that

$$C_{i,j} = -\frac{1}{s_{j-1}}\delta_{i,j-1} + \left(\frac{1}{s_{j-1}} + \frac{1}{s_j}\right)\delta_{i,j} - \frac{1}{s_j}\delta_{i,j+1}, \quad 1 \leq i,j \leq N \tag{3.6}$$

with the convention that $\frac{1}{s_j} = 0$ for $j < 1$ and $j > N$. The capacitance matrix has thus the following tridiagonal form:

$$\begin{pmatrix} s_1^{-1} & -s_1^{-1} & & & & & \\ -s_1^{-1} & s_1^{-1}+s_2^{-1} & -s_2^{-1} & & & & \\ & -s_2^{-1} & \ddots & \ddots & & & \\ & & \ddots & \ddots & \ddots & & \\ & & & \ddots & \ddots & -s_{N-2}^{-1} & \\ & & & & -s_{N-2}^{-1} & s_{N-2}^{-1}+s_{N-1}^{-1} & s_{N-1}^{-1} \\ & & & & & -s_{N-1}^{-1} & s_{N-1}^{-1} \end{pmatrix}. \tag{3.7}$$

The main findings of [28] are the following.

Proposition 3.2. *The scattering problem* (3.3) *admits exactly N subwavelength resonant frequencies as $\delta \to 0$, namely*

$$\omega_i = v_b\sqrt{\delta\lambda_i} + \mathcal{O}(\delta),$$

where $(\lambda_i)_{1\leq i\leq N}$ are the eigenvalues of the eigenvalue problem

$$V^2 C\boldsymbol{a}_i = \lambda_i L\boldsymbol{a}_i, \qquad 1 \leq i \leq N, \tag{3.8}$$

where $L \coloneqq \operatorname{diag}(\ell_1,\dots,\ell_N)$ and $V \coloneqq \operatorname{diag}(v_1,\dots,v_N)$. Furthermore, let u_i be a subwavelength eigenmode corresponding to ω_i and let $\boldsymbol{a}_i$ be the corresponding eigenvector of C. Then

$$u_i(x) = \sum_j \boldsymbol{a}_i^{(j)} V_j(x) + \mathcal{O}(\delta),$$

where V_j is defined by (3.5) *and $\boldsymbol{a}_i^{(j)}$ denotes the j^{th} entry of the eigenvector $\boldsymbol{a}_i$.*

Note that the choice of the N "physical" resonant frequencies between $\pm\omega_i$ for $1 \leqslant i \leqslant N$ occurs thought the radiation condition. Moreover, the study of Hermitian subwavelength systems is thus entirely governed at the leading order in δ by the linear eigenvalue problem (3.8).

3.2. Non-reciprocal case

Hermitian systems are a first step, but a much richer physics is observed for non-Hermitian systems. In this subsection, we study one subset of them: non-reciprocal systems. To this end, we consider the following variation of (3.2):

$$-\frac{\omega^2}{\kappa(x)}u(x) - \gamma(x)\frac{\mathrm{d}}{\mathrm{d}x}u(x) - \frac{\mathrm{d}}{\mathrm{d}x}\left(\frac{1}{\rho(x)}\frac{\mathrm{d}}{\mathrm{d}x}u(x)\right) = 0, \qquad x \in \mathbb{R}, \tag{3.9}$$

for a piecewise constant coefficient

$$\gamma(x) = \begin{cases} \gamma, & x \in D, \\ 0, & x \in \mathbb{R}\setminus D. \end{cases}$$

This new parameter γ extends the usual scalar wave equation to a generalised Strum–Liouville equation via the introduction of an imaginary gauge potential [65]. Alternatively, one may think about (3.9) as a damped wave equation where the damping acts in the space variable instead of the time variable.

In these circumstances of piecewise constant material parameters, the wave problem determined by (3.9) can be rewritten as the following system of coupled one-dimensional equations:

$$\begin{cases} u''(x)+\gamma u'(x)+\dfrac{\omega^2}{v_b^2}u(x)=0, & x\in D,\\ u''(x)+\dfrac{\omega^2}{v^2}u(x)=0, & x\in\mathbb{R}\setminus D,\\ u|_{\mathsf{R}}(x_i^{\mathsf{L},\mathsf{R}})-u|_{\mathsf{L}}(x_i^{\mathsf{L},\mathsf{R}})=0, & \text{for all } 1\le i\le N,\\ \dfrac{\mathrm{d}u}{\mathrm{d}x}\Big|_{\mathsf{R}}(x_i^{\mathsf{L}})=\delta\,\dfrac{\mathrm{d}u}{\mathrm{d}x}\Big|_{\mathsf{L}}(x_i^{\mathsf{L}}), & \text{for all } 1\le i\le N,\\ \delta\,\dfrac{\mathrm{d}u}{\mathrm{d}x}\Big|_{\mathsf{R}}(x_i^{\mathsf{R}})=\dfrac{\mathrm{d}u}{\mathrm{d}x}\Big|_{\mathsf{L}}(x_i^{\mathsf{R}}), & \text{for all } 1\le i\le N,\\ \dfrac{\mathrm{d}u}{\mathrm{d}|x|}(x)-\mathbf{i}ku(x)=0, & x\in(-\infty,x_1^{\mathsf{L}})\cup(x_N^{\mathsf{R}},\infty). \end{cases} \tag{3.10}$$

We seek a similar capacitance matrix formulation for the case of subwavelength resonators with an imaginary gauge potential.

In the case of systems of Hermitian subwavelength resonators (*i.e.*, when $\gamma=0$), the entries of the capacitance matrix are defined by (3.5). For non-reciprocal systems the formulation is different.

Definition 3.3 (Gauge capacitance matrix). For $\gamma\in\mathbb{R}\setminus\{0\}$, we define the *gauge capacitance matrix* $C^\gamma\in\mathbb{R}^{N\times N}$ by

$$C^\gamma_{i,j}:=-\frac{|D_i|}{\int_{D_i}e^{\gamma x}\,\mathrm{d}x}\int_{\partial D_i}e^{\gamma x}\frac{\partial V_j(x)}{\partial\nu}\,\mathrm{d}\sigma, \tag{3.11}$$

where V_j is given by (3.5).

It is easy to see that the gauge capacitance matrix is tridiagonal, non-symmetric, and is given by

$$C^\gamma_{i,j}:=\begin{cases} \dfrac{\gamma}{s_1}\dfrac{\ell_1}{1-e^{-\gamma\ell_1}}, & i=j=1,\\ \dfrac{\gamma}{s_i}\dfrac{\ell_i}{1-e^{-\gamma\ell_i}}-\dfrac{\gamma}{s_{i-1}}\dfrac{\ell_i}{1-e^{\gamma\ell_i}}, & 1<i=j<N,\\ -\dfrac{\gamma}{s_i}\dfrac{\ell_i}{1-e^{-\gamma\ell_j}}, & 1\le i=j-1\le N-1,\\ \dfrac{\gamma}{s_j}\dfrac{\ell_i}{1-e^{\gamma\ell_j}}, & 2\le i=j+1\le N,\\ -\dfrac{\gamma}{s_{N-1}}\dfrac{\ell_N}{1-e^{\gamma\ell_N}}, & i=j=N, \end{cases} \tag{3.12}$$

while all the other entries are zero. More visually, we can display the capacitance matrix for $\ell_i = \ell$ and $s = s_i$ for all i as

$$C^\gamma := \frac{\gamma}{s} \begin{pmatrix} \frac{\ell}{1-e^{-\gamma\ell}} & -\frac{\ell}{1-e^{-\gamma\ell}} & & & & & & \\ \frac{\ell}{1-e^{\gamma\ell}} & \frac{\ell}{1-e^{-\gamma\ell}} - \frac{\ell}{1-e^{\gamma\ell}} & -\frac{\ell}{1-e^{-\gamma\ell}} & & & & & \\ & \frac{\ell}{1-e^{\gamma\ell}} & \ddots & \ddots & & & & \\ & & \ddots & \ddots & \ddots & & & \\ & & & \ddots & \ddots & -\frac{\ell}{1-e^{-\gamma\ell}} & & \\ & & & & \frac{\ell}{1-e^{\gamma\ell}} & \frac{\ell}{1-e^{-\gamma\ell}} - \frac{\ell}{1-e^{\gamma\ell}} & -\frac{\ell}{1-e^{-\gamma\ell}}^{-1} & \\ & & & & & \frac{\ell}{1-e^{\gamma\ell}} & -\frac{\ell}{1-e^{\gamma\ell}} & \end{pmatrix}. \tag{3.13}$$

The following result from [1], that is the analogue of Proposition 3.2, describes how the gauge capacitance matrix characterises the nontrivial solutions to (3.10).

Proposition 3.4. *The N subwavelength eigenfrequencies ω_i satisfy, as $\delta \to 0$,*

$$\omega_i = v_b\sqrt{\delta\lambda_i} + \mathcal{O}(\delta),$$

where $(\lambda_i)_{1\le i\le N}$ are the eigenvalues of the eigenvalue problem

$$V^2\, C^\gamma\, \boldsymbol{a}_i = \lambda_i L \boldsymbol{a}_i, \qquad 1 \le i \le N \tag{3.14}$$

with V and L being as in Proposition 3.2. Furthermore, let u_i be a subwavelength eigenmode corresponding to ω_i and let $\boldsymbol{a}_i$ be the corresponding eigenvector of C^γ. Then,

$$u_i(x) = \sum_j \boldsymbol{a}_i^{(j)} V_j(x) + \mathcal{O}(\delta),$$

where V_j is defined by (3.5) *and $\boldsymbol{a}_i^{(j)}$ denotes the j^{th} entry of the eigenvector $\boldsymbol{a}_i$.*

Part II. Applications

4. Topological interface modes

In this section, we consider wave localisation at the interface between two systems of *finitely many* subwavelength resonators. These resonators are arranged in pairs or dimers, such that the model we consider shares many of the features of the Su-Schrieffer-Heeger (SSH) model in quantum mechanics [44, 57]. We show the existence of exponentially localised interface eigenmodes in this finite structure. These interface modes have been subject to numerous studies in the setting of infinite structures. A particular focus has been put on studying the topological properties of infinite periodic structures and then introducing carefully designed interfaces so as to create the so-called *topologically protected* eigenmodes [12]. These modes have significant implications for applications since they are expected to be robust with respect to imperfections in the design. These concepts have been widely studied in a variety of settings, most notably in quantum mechanics for the Schrödinger operator [25, 26] and more recently, for related continuous models of classical wave systems in [19, 22, 39, 53, 58, 59]. In finite-sized systems, these eigenmodes have been observed both experimentally and numerically; see, for instance, [2, 12, 18, 69] and the references therein.

As mentioned before, here we consider the far less-explored but more realistic physical setting of interface modes in finite dimer structures. We present a one-to-one correspondence between the position of the eigenfrequency in the spectrum of the corresponding infinite periodic structure (*i.e.*, in the asymptotic spectral bulk, its boundary or the asymptotic spectral gap; see Definition 4.3) and the behaviour (localised versus delocalised) of the corresponding eigenmode. Our results hold for any finite and large enough chain of dimers with a geometric defect satisfying a mild condition. Furthermore, we show that the eigenfrequencies

lying in the gap converge exponentially as the size of the structure goes to infinity and provide an explicit and simple formula for the limit. The results of this section are from [3].

4.1. Dimer chains with a geometric defect

Systems of repeated dimers (that is, $s_i = s_{i-2}$ for $3 \leq i \leq N$) are of particular interest as the corresponding infinite structure can be studied with Floquet–Bloch band theory [2]; when the two repeating separation distances are distinct, this provides a nontrivial example of a band gap between the subwavelength spectral bands. Here, we consider systems of dimers with a defect in the geometric structure, so that at some point the repeating pattern of alternating separation distances is broken. This is inspired by the famous Su-Schrieffer-Heeger (SSH) model from quantum settings and is the canonical example of a topologically protected interface mode [57]. It is a system of $N = 4m + 1$ for $m \in \mathbb{N}$ resonators such that

$$\begin{aligned} s_i &= s_{i-2} \quad \text{for } 3 \leq i \leq 2m, \\ s_i &= s_{i+2} \quad \text{for } 2m+1 \leq i \leq 4m-2, \end{aligned}$$

where we typically assume $s_1 = s_{2m+2}$ and $s_2 = s_{2m+1}$ so that the system is symmetric with respect to the center of the $(2m+1)^{\text{th}}$ resonator with spacings s_1 and s_2. A sketch of this system with a geometric defect is shown in Figure 4.1.

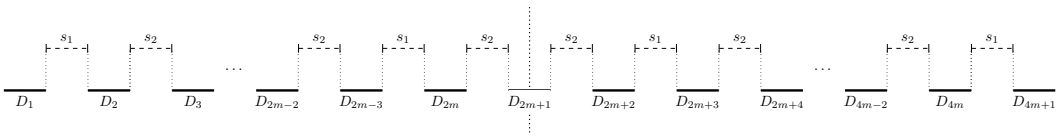


FIGURE 4.1. Dimer structure with a geometric defect.

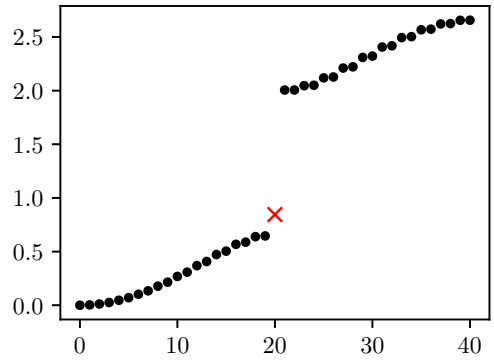
For such systems the geometric symmetries mean that the capacitance matrix from (3.7) has the following tridiagonal block structure:

$$C = \begin{pmatrix} \widetilde{\alpha} & \beta_1 & & & & & & & & & \\ \beta_1 & \alpha & \beta_2 & & & & & & & & \\ & \beta_2 & \alpha & \beta_1 & & & & & & & \\ & & \ddots & \ddots & \ddots & & & & & & \\ & & & \beta_2 & \alpha & \beta_1 & & & & & \\ & & & & \beta_1 & \alpha & \beta_2 & & & & \\ & & & & & \beta_2 & \eta & \beta_2 & & & \\ & & & & & & \beta_2 & \alpha & \beta_1 & & \\ & & & & & & & \beta_1 & \alpha & \beta_2 & \\ & & & & & & & & \ddots & \ddots & \ddots \\ & & & & & & & & & \beta_1 & \alpha & \beta_2 \\ & & & & & & & & & & \beta_2 & \alpha & \beta_1 \\ & & & & & & & & & & & \beta_1 & \widetilde{\alpha} \end{pmatrix}, \tag{4.1}$$

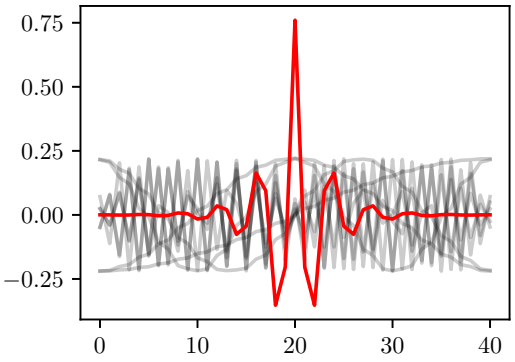
where

$$\beta_1 = -s_1^{-1}, \quad \beta_2 = -s_2^{-1}, \quad \alpha = s_1^{-1} + s_2^{-1}, \quad \eta = 2s_2^{-1}, \quad \widetilde{\alpha} = s_1^{-1}. \tag{4.2}$$

It will be useful to have notation for the top left $(2m+1) \times (2m+1)$-submatrix C_1 and the bottom right $(2m+1) \times (2m+1)$-submatrix C_2 (as highlighted by the shading in (4.1)). Figure 4.2b shows the spectrum and the eigenvectors of the capacitance matrix (4.1). It is immediately clear that there exists a spectral gap and there exists a localised eigenmode associated to an eigenvalue in the gap.



(A) Eigenvalues of (4.1). As red cross a specific eigenvalue lying isolated from the others.



(B) A selection of eigenvectors of C from (4.1). All eigenvectors are superimposed and with unit norm. The red solid eigenvector corresponds to the red cross eigenvalue in Figure 4.2a.

FIGURE 4.2. Eigenvalues and eigenvectors of the capacitance matrix (4.1) for $N = 41, s_1 = 1$ and $s_2 = 3$.

4.2. Perturbed tridiagonal 2-Toeplitz matrices

In this section, we will briefly recall results established in Section 2.4 about eigenvalues and eigenvectors of tridiagonal 2-Toeplitz matrices with perturbations on the corners. By slightly abusing the notation, we denote by $A_{2m+1}^{(a,b)}$ in (2.8) and $A_{2m}^{(a,b)}$ in (2.9) the corresponding Hermitian tridiagonal 2-Toeplitz matrices with $\alpha_1 = \alpha_2 = \alpha \in \mathbb{R}, \eta_j = \beta_j \in \mathbb{R}, j = 1, 2$.

The eigenvalues of $A_{2m+1}^{(a,b)}$ and $A_{2m}^{(a,b)}$ are given by the roots of the characteristic polynomials (2.11) and (2.12). On the other hand, by Theorem 2.12, the eigenvectors $\boldsymbol{x}$ of $A_{2m+1}^{(a,b)}$ and $A_{2m}^{(a,b)}$ are given as follows.

PROPOSITION 4.1. *Let λ be an eigenvalue of $A_{2m+1}^{(a,b)}$ in (2.8) with $\alpha_1 = \alpha_2 = \alpha \in \mathbb{R}, \eta_j = \beta_j \in \mathbb{R}, j = 1, 2$. Then, using $\mu := y(\lambda)$ where*

$$y(\lambda) := \frac{(\alpha - \lambda)^2 - (\beta_1^2 + \beta_2^2)}{2\beta_1\beta_2}, \tag{4.3}$$

the eigenvector corresponding to λ is given by

$$\boldsymbol{x} = \left(\widehat{q}_0^{(\xi_p,\xi_q)}(\mu), -\frac{1}{\beta_1}(\alpha - \lambda)\widehat{p}_0^{(\xi_p,\xi_q)}(\mu), \widehat{q}_1^{(\xi_p,\xi_q)}(\mu), -\frac{1}{\beta_1}(\alpha - \lambda)\widehat{p}_1^{(\xi_p,\xi_q)}(\mu), \right.$$
$$\left. \ldots, -\frac{1}{\beta_1}(\alpha - \lambda)\widehat{p}_{m-1}^{(\xi_p,\xi_q)}(\mu), \widehat{q}_m^{(\xi_p,\xi_q)}(\mu) \right). \tag{4.4}$$

If λ is an eigenvalue of $A_{2m}^{(a,b)}$, then the corresponding eigenvector is given by

$$\boldsymbol{x} = \left(\widehat{q}_0^{(\xi_p,\xi_q)}(\mu), -\frac{1}{\beta_1}(\alpha - \lambda)\widehat{p}_0^{(\xi_p,\xi_q)}(\mu), \widehat{q}_1^{(\xi_p,\xi_q)}(\mu), -\frac{1}{\beta_1}(\alpha - \lambda)\widehat{p}_1^{(\xi_p,\xi_q)}(\mu), \right.$$
$$\left. \ldots, -\frac{1}{\beta_1}(\alpha - \lambda)\widehat{p}_{m-1}^{(\xi_p,\xi_q)}(\mu) \right). \tag{4.5}$$

In both cases, $\xi_q = (\alpha - \lambda), \xi_p = (\alpha + a - \lambda)$ and $\widehat{p}_j^{(\xi_p,\xi_q)}, \widehat{q}_j^{(\xi_p,\xi_q)}$'s are given by (2.23) for $\beta = \beta_2/\beta_1$.

Observing that the two blocks in the capacitance matrix C defined by (4.1) are two Hermitian tridiagonal 2-Toeplitz matrices with perturbations on diagonal corners and based on the theorem above, we can characterise the eigenvectors of C as follows.

PROPOSITION 4.2. *Let $(\lambda, \boldsymbol{v})$ be an eigenpair of C defined by (4.1). Then $\boldsymbol{v}$ is given by*

$$\boldsymbol{v} = (\boldsymbol{x}^{(1)}, \boldsymbol{x}^{(2)}, \dots, \boldsymbol{x}^{(2m)}, \boldsymbol{x}^{(2m+1)}, (-1)^{\sigma}\boldsymbol{x}^{(2m)}, \dots, (-1)^{\sigma}\boldsymbol{x}^{(2)}, (-1)^{\sigma}\boldsymbol{x}^{(1)})^{\top}, \tag{4.6}$$

where $\boldsymbol{x} = (\boldsymbol{x}^{(1)}, \boldsymbol{x}^{(2)}, \dots, \boldsymbol{x}^{(2m)}, \boldsymbol{x}^{(2m+1)})^{\top} \in \mathbb{R}^{2m+1}$ is as in (4.4) with $\xi_q = (\alpha - \lambda), \xi_p = (\alpha + a - \lambda)$ and $\sigma = 0$ or 1 for all $\boldsymbol{x}$ except for $\boldsymbol{x} \in span\{\mathbf{1}\}$ where $\sigma = 0$.

4.3. Asymptotic spectral gap and localised interface modes

In this section, we show the existence of a spectral gap for a defectless structure of dimers. Furthermore, we establish a direct relationship between an eigenvalue being within the spectral gap and the localisation of its corresponding eigenvector.

We first define a spectral gap for the capacitance matrix of an unperturbed structure of dimers.

DEFINITION 4.3 (Spectral bulk and gaps). Consider a finite structure of resonators. We define the *asymptotic spectral bulk* Σ and *asymptotic spectral gap* Γ of the structure as the spectral bulk and spectral gap (also known as band gap) of the associated infinite periodic system, respectively.

The spectral gap and spectral bulk of infinite periodic dimer systems have been computed in [2, Lemma 5.3].

PROPOSITION 4.4. *Consider a system of repeated dimers (without defect) with $N = 2m$ resonators. Denote by C_N the associated capacitance matrix and let Σ be the asymptotic spectral bulk. Then,*

$$\Sigma = \overline{\lim_{N\to\infty} \sigma(C_N)} = \left[0, \frac{2}{s_2}\right] \cup \left[\frac{2}{s_1}, \frac{2}{s_1} + \frac{2}{s_2}\right],$$

where lim *denotes the Hausdorff limit. Consequently, the asymptotic spectral gap is*

$$\Gamma = \left(\frac{2}{s_2}, \frac{2}{s_1}\right) \subset \mathbb{R}\,.$$

In view of Proposition 3.2, we can refer to spectral bulk and spectral gap of the physical system and of the capacitance matrix interchangeably.

Last, we show that an eigenvalue in the gap is associated with an eigenvector that is exponentially localised in the sense that it decays exponentially away from the interface in both directions, within the limits of the finite structure.

DEFINITION 4.5 (Localised interface mode). Let $v(x)$ be an eigenmode. Then we say that v is a *localised interface mode* at the point x_0, if both $|v(x - x_0)|$ for $x_0 < x \in D$ and $|v(x_0 - x)|$ for $x_0 > x \in D$ decay exponentially as a function of $x \in D$. The same terminology applies to the corresponding eigenvector of the capacitance matrix.

PROPOSITION 4.6 (Eigenvectors of C). *Let $C \in \mathbb{R}^{4m+1\times 4m+1}$ be the capacitance matrix of a defected structure as illustrated in Figure 4.1 and let (λ, v) be an eigenpair of C. Then, there exists $|r| \geq 1$ independent of m and $A, B, \widetilde{A}, \widetilde{B} \in \mathbb{R}$ dependent on m such that, for $y(\lambda)$ defined by (4.3),*

if $y(\lambda)^2 > 1$**:**

$$v^{(|2m-2j|)} = Ar^j + Br^{-j},$$
$$v^{(|2m-2j-1|)} = \widetilde{A}r^j + \widetilde{B}r^{-j},$$

with $A = \frac{r^{1-m}(c_1 r - c_2)}{r^2-1} = \mathcal{O}(\frac{1}{r^m})$ and $B = \frac{r^m(c_2 r - c_1)}{r^2-1} = \mathcal{O}(r^{m-1})$ as $m \to \infty$ for $c_1, c_2 \in \mathbb{R}$ independent of m. The same asymptotics (with a slight different formula) hold for $\widetilde{A}$ and $\widetilde{B}$;

if $y(\lambda)^2 < 1$**:**

$$v^{(|2m-2j|)} = A\cos(j\theta) + B\sin(j\theta),$$
$$v^{(|2m-2j-1|)} = \widetilde{A}\cos(j\theta) + \widetilde{B}\sin(j\theta),$$

with $r = e^{\mathbf{i}\theta}$ *and* $A, B, \widetilde{A}, \widetilde{B}$ *bounded as* $m \to \infty$*;*
if $y(\lambda)^2 = 1$**:** $r = \pm 1$ *and*

$$v^{(|2m-2j|)} = Ar^j + Br^j \cdot j,$$
$$v^{(|2m-2j-1|)} = \widetilde{A}r^j + \widetilde{B}r^j \cdot j,$$

with $A = \frac{r^{1-m}(c_1 m r - c_1 r - c_2 m)}{mr^2 - m - r^2}$ *and* $B = \frac{r^m(c_2 r - c_1)}{mr^2 - m - r^2}$ *as* $m \to \infty$ *for* $c_1, c_2 \in \mathbb{R}$ *independent of* m*. The same asymptotics (with a slight different formula) hold for* $\widetilde{A}$ *and* $\widetilde{B}$*.*

4.4. Existence, uniqueness, and convergence of the eigenvalue in the gap

In this section, we will show the existence of a unique eigenvalue in the gap for the defected structure and consequently the existence of a unique localised interface eigenvector. Furthermore, we analyse the behaviour as the size of the system grows, specifically the limiting behaviour as $N \to \infty$. We will show that the eigenvalue of C lying in the asymptotic spectral gap converges exponentially fast to a value in the gap.

Existence. We first show the existence of an eigenvalue in the band gap. To illustrate how the existence of the interface eigenvalue is related to the Chebyshev polynomial, we outline the main steps of the proof. For further details on the derivation, we refer the reader to [3, Section 5].

By performing Laplace expansion on the top block of rows $1 \le i \le 2m+1$ of $C - xI$, we obtain the characteristic polynomial of $C \in \mathbb{R}^{(4m+1)\times(4m+1)}$, that is,

$$\begin{aligned} p(x) = \big(&\left[(x-\alpha-\beta_2-(\beta_1-\beta_2))\,P_m^*(x) + \left(\beta_2(\beta_1-\beta_2)(x-\alpha) - \beta_2\beta_1^2 - (\beta_1-\beta_2)\beta_2^2\right)P_{m-1}^*(x)\right] \\ &- \beta_2^2\left[(x-\alpha-\beta_2)\,P_{m-1}^*(x) + \left(-\beta_2\beta_1^2\right)P_{m-2}^*(x)\right]\big)\chi_{A_{2m}^{(a,0)}(\alpha,\beta_1,\beta_2)}(x), \end{aligned} \tag{4.7}$$

where we have used (2.11) and (2.12).

For the sake of brevity, we rewrite

$$p(x) = \chi_{A_{2m}^{(a,0)}(\alpha,\beta_1,\beta_2)}(x)\left(\left[A(x)P_m^*(x) + B(x)P_{m-1}^*(x)\right] - \beta_2^2\left[E(x)P_{m-1}^*(x) + F(x)P_{m-2}^*(x)\right]\right),$$

where $A(x), B(x), E(x)$, and $F(x)$ are defined as

$$A(x) = x-\alpha-\beta_1, \quad B(x) = \beta_2(\beta_1-\beta_2)(x-\alpha) - \beta_2\beta_1^2 - (\beta_1-\beta_2)\beta_2^2,$$
$$E(x) = x-\alpha-\beta_2, \quad F(x) = -\beta_2\beta_1^2.$$

For simplicity, we abbreviate $A(x), B(x), E(x)$, and $F(x)$ as A, B, D, and F respectively in the subsequent discussions. Thus, $\lambda \in \Gamma$ is an eigenvalue if and only if

$$\begin{aligned} &\left[AP_m^*(\lambda) + BP_{m-1}^*(\lambda)\right] = \beta_2^2\left[EP_{m-1}^*(\lambda) + FP_{m-2}^*(\lambda)\right] \\ \Leftrightarrow\ &P_m^*(\lambda)\left[A + B\frac{P_{m-1}^*(\lambda)}{P_m^*(\lambda)}\right] = \beta_2^2 P_{m-1}^*(\lambda)\left[E + F\frac{P_{m-2}^*(\lambda)}{P_{m-1}^*(\lambda)}\right]. \end{aligned} \tag{4.8}$$

In the above step, we were able to divide by $\chi_{A_{2m}^{(a,0)}}(\lambda)$ because it is nonzero in Γ as will be shown by Proposition 4.8. In addition, $P_k^*(\lambda) = (\beta_1\beta_2)^k U_k(y(\lambda))$ with $y(\lambda) := \frac{(\lambda-\alpha)^2-\beta_1^2-\beta_2^2}{2\beta_1\beta_2}$ and $\lambda \in \Gamma$ corresponds to the case when $y(\lambda) < -1$. Since the Chebyshev polynomials $U_k(\cdot)$'s only have roots in $(-1,1)$, $P_{m-1}^*(\lambda)$ and $P_m^*(\lambda)$ are nonzero in Γ and we are able to divide by them in (4.8).

Moreover, since

$$U_m(y) = \frac{\left(y+\sqrt{y^2-1}\right)^{m+1} - \left(y-\sqrt{y^2-1}\right)^{m+1}}{2\sqrt{y^2-1}},$$

the limit $L(\lambda) \coloneqq \lim_{m\to\infty} \frac{P^*_{m-1}(\lambda)}{P^*_m(\lambda)}$ exists for all $\lambda \in \mathbb{R}$. Then,

$$[A+BL] = \beta_2^2 L\,[E+FL] \Leftrightarrow L^2(\beta_2^2 F) + L(\beta_2^2 E - B) - A = 0,$$

from which we get the condition

$$L(\lambda) = \frac{B - E\beta_2^2 \pm \sqrt{4AF\beta_2^2 + B^2 - 2BE\beta_2^2 + E^2\beta_2^4}}{2F\beta_2^2}. \tag{4.9}$$

On the other hand, by the recurrence formula of U_m, for $\lambda \in \Gamma$ with $y(\lambda) < -1$ and using again the shorthand y for $y(\lambda)$, it follows that

$$\begin{aligned} L(\lambda) = \lim_{m\to\infty} \frac{P^*_{m-1}(\lambda)}{P^*_m(\lambda)} &= \frac{y - \sqrt{y^2-1}}{\beta_1\beta_2} \\ &= \frac{(\lambda-\alpha)^2 - \beta_1^2 - \beta_2^2 - 2\beta_1\beta_2\sqrt{\frac{\left(\beta_1^2+\beta_2^2-(\lambda-\alpha)^2\right)^2}{4\beta_1^2\beta_2^2} - 1}}{2\beta_1^2\beta_2^2}. \end{aligned} \tag{4.10}$$

Now, an algebraic manipulation shows that conditions (4.9) and (4.10) have exactly one common solution $\lambda_0 \in \Gamma$ given by

$$\lambda_0 = \alpha + \frac{1}{2}\left(-\sqrt{9\beta_1^2 - 14\beta_1\beta_2 + 9\beta_2^2} - \beta_1 - \beta_2\right). \tag{4.11}$$

We can then state the results of the existence of the interface eigenvector (modes) of C.

Proposition 4.7. *Consider a perturbed structure of dimers as illustrated in Figure 4.1. For N large enough, there exists at least one localised interface eigenvector of C with eigenvalue $\lambda_{\mathsf{i}}^{(N)}$ in the band gap Γ.*

Proof. Denote by

$$\begin{aligned} f_m(\lambda) &\coloneqq \left[A + B\frac{P^*_{m-1}(\lambda)}{P^*_m(\lambda)}\right] - \beta_2^2 \frac{P^*_{m-1}(\lambda)}{P^*_m(\lambda)}\left[E + F\frac{P^*_{m-2}(\lambda)}{P^*_{m-1}(\lambda)}\right], \\ f_\infty &\coloneqq [A + BL(\lambda)] - \beta_2^2 L(\lambda)\,[E + FL(\lambda)], \end{aligned}$$

and note that $f_\infty(\lambda) = \lim_{m\to\infty} f_m(\lambda)$. By (4.11), there exists a λ_0 in the band gap such that $f_\infty(\lambda_0) = 0$. Furthermore, by the above formula of $f_\infty(\lambda)$, we have $f_\infty(\lambda_0-\zeta)f_\infty(\lambda_0+\zeta) < 0$ for some $\zeta > 0$ satisfying $[\lambda_0-\zeta, \lambda_0+\zeta] \subset \Gamma$. By the sign-preserving property, we have $f_m(\lambda_0-\zeta)f_m(\lambda_0+\zeta) < 0$ for large enough m, which proves the existence of roots of $f_m(\lambda)$ in the band gap Γ. By Proposition 4.6, the corresponding eigenvector is then a localised interface eigenvector. ∎

Uniqueness. We now show the uniqueness of the eigenvalue in the band gap. The proof utilises the Cauchy interlacing theorem [36] and the monotonicity of Chebyshev polynomials of the second kind in Proposition 2.1. We refer the reader to [3, Section 5] for further details.

Proposition 4.8. *There exists at most one eigenvalue of C as defined in* (4.1) *lying in the asymptotic spectral gap $\Gamma = (2/s_2, 2/s_1)$. In particular, for m large enough, there exists exactly one eigenvalue in Γ.*

Remark 4.9. We remark that if one can show the existence of an eigenfrequency in the band gap Γ for the capacitance matrix C with general size m, then by Proposition 4.8, it is unique.

Convergence. Last, we show the exponential convergence of the resonant frequency in the gap and conclude the section by the following theorem.

Theorem 4.10. *Consider a perturbed structure of dimers as illustrated in Figure 4.1. For N large enough, there exists a unique interface mode with eigenfrequency $\omega_{\mathrm{i}}^{(N)}$ in the band gap. The associated eigenfrequency $\omega_{\mathrm{i}}^{(N)}$ converges to*

$$\omega_{\mathrm{i}} = v_b \sqrt{\delta \frac{1}{2} \left(-\sqrt{\frac{9}{s_1^2} - \frac{14}{s_1 s_2} + \frac{9}{s_2^2}} + \frac{3}{s_1} + \frac{3}{s_2} \right)} \tag{4.12}$$

exponentially as $N \to \infty$. In particular, for N large enough,

$$|\omega_{\mathrm{i}} - \omega_{\mathrm{i}}^{(N)}| < A e^{-BN}, \tag{4.13}$$

for some $A, B > 0$ independent of N.

Proof. The limit λ_i can be computed from (4.11) and ω_i is $v_b\sqrt{\delta\lambda_i}$ by Corollary 3.4. The only part left to prove is the convergence rate, which is derived from the pseudospectrum theory. We refer the reader to [3, Section 5] for further details. ∎

We remark that, combined with Proposition 4.6, Theorem 4.10 also gives the decaying rate of the interface mode for a structure with sufficiently many resonators.

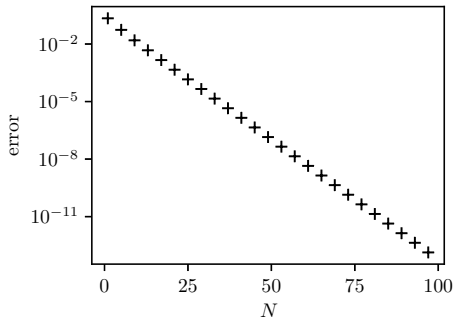


Figure 4.3. Convergence of the eigenvalue in the gap (y-axis in *log* scale). We display the left-hand side of (4.13) for a structure with $s_1 = 1$ and $s_2 = 2$.

4.5. Stability analysis

Interface modes of SSH-like structures are well-known to be stable, *i.e.*, perturbations of the system affect them only slightly. In this section, we show that perturbations in the geometry have limited effect on both the resonant frequencies and the associated modes. Then we quantify this effect.

To this end, we consider a system of $N = 4m + 1$ resonators as shown in Figure 4.1 but where the spacings s_i are now perturbed:

$$s_i = \begin{cases} s_1 + \widetilde{\varepsilon}_i, & 1 \le i \le 2m, \ i \text{ odd}, \\ s_2 + \widetilde{\varepsilon}_i, & 1 \le i \le 2m, \ i \text{ even}, \\ s_1 + \widetilde{\varepsilon}_i, & 2m+1 \le i \le 4m, \ i \text{ even}, \\ s_2 + \widetilde{\varepsilon}_i, & 2m+1 \le i \le 4m, \ i \text{ odd}. \end{cases} \tag{4.14}$$

Furthermore, we denote

$$\varepsilon_i = \begin{cases} -\dfrac{\widetilde{\varepsilon}_i}{s_1(s_1+\widetilde{\varepsilon}_i)}, & 1 \le i \le 2m,\ i \text{ odd}, \\ -\dfrac{\widetilde{\varepsilon}_i}{s_2(s_2+\widetilde{\varepsilon}_i)}, & 1 \le i \le 2m,\ i \text{ even}, \\ -\dfrac{\widetilde{\varepsilon}_i}{s_1(s_1+\widetilde{\varepsilon}_i)}, & 2m+1 \le i \le 4m,\ i \text{ even}, \\ -\dfrac{\widetilde{\varepsilon}_i}{s_2(s_2+\widetilde{\varepsilon}_i)}, & 2m+1 \le i \le 4m,\ i \text{ odd}. \end{cases} \tag{4.15}$$

The following proposition handles stability of the eigenvalues and is a direct application of the well-known Weyl theorem.

PROPOSITION 4.11. *Let $\widehat{C}$ be the capacitance matrix associated to the structure described in* (4.14) *and let*

$$\varepsilon \coloneqq \max_{1\le i\le N-2} |\varepsilon_i| + |\varepsilon_{i+1}|. \tag{4.16}$$

Then, the eigenvalues $\widehat{\lambda}_k$ (sorted increasingly) satisfy

$$|\widehat{\lambda}_k - \lambda_k| \le 2\varepsilon, \quad 1 \le k \le N, \tag{4.17}$$

where λ_k are the eigenvalues of C.

Applying Proposition 4.11 to our system of dimers where the perturbations $|\widetilde{\varepsilon}_i| \le \eta$ are in the interval $(-\eta, \eta)$ for some $\eta > 0$, we obtain that the eigenvalue perturbation is bounded by

$$\frac{2\eta}{s_1(s_1-\eta)} + \frac{2\eta}{s_2(s_2-\eta)} = 2\eta\left(\frac{1}{s_1^2} + \frac{1}{s_2^2}\right) + \mathcal{O}(\eta^2) \quad \text{as } \eta \to 0.$$

Now, we analyse the stability of the eigenvectors. As a direct consequence of Davis–Kahan theorem for Hermitian matrices [23], we have the following result on the stability of the interface eigenmodes.

Theorem 4.12. *Let $\varepsilon < \frac{1}{2}\left(\frac{1}{s_1} - \frac{1}{s_2}\right)$ in (4.16). Let $\boldsymbol{v}$ and $\widehat{\boldsymbol{v}}$ be the eigenvectors corresponding to the eigenvalues λ_i and $\widehat{\lambda}_i$ in the gap of C and $\widehat{C}$, respectively. Then,*

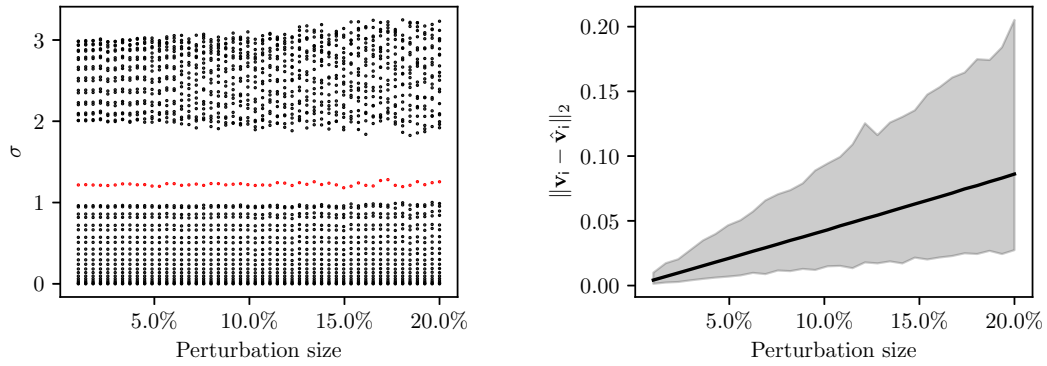
$$\|\boldsymbol{v} - \widehat{\boldsymbol{v}}\|_2 \le \frac{2\sqrt{2}\varepsilon}{\delta} \tag{4.18}$$

$$\le \frac{2\sqrt{2}\varepsilon}{\delta_0 - 2\varepsilon}, \tag{4.19}$$

where $\delta \coloneqq \min\{|\lambda_i - \widehat{\lambda}_{i+1}|, |\lambda_i - \widehat{\lambda}_{i-1}|\}$ and $\delta_0 = \min\{|\lambda_i - \lambda_{i+1}|, |\lambda_i - \lambda_{i-1}|\}$. The a priori *estimate* (4.19) *holds for $\delta_0 > 2\varepsilon$.*

Remark that, for $s_1 = 1$ and $s_2 = 2$ and m large, we have $\delta_0 \approx 0.219$ so that the *a priori* estimate (4.19) holds for $\varepsilon < 0.1$. This *a priori* estimate is, however, suboptimal as Figure 4.4b shows.

In Figure 4.4, we show numerically the high stability of the interface modes. We let $\mathcal{U}_{[-\eta,\eta]}$ be a uniform distribution with support in $[-\eta, \eta]$. We consider perturbations of the type $\widetilde{\varepsilon}_i \sim \mathcal{U}_{[-\eta,\eta]}$, where we call η the perturbation size and display it as percentage relative to the resonator's size. Figure 4.4a shows that the interface eigenfrequency (lying in the gap) is only minimally perturbed even by perturbation in the size of 20%. We remark that numerically the bound of (4.17) can even be sharpened to $|\widehat{\lambda_k} - \lambda_k| \le \frac{3}{2}\varepsilon$. Figure 4.4b shows $\|\boldsymbol{v} - \widehat{\boldsymbol{v}}\|_2$ for various perturbation sizes and normalised $\boldsymbol{v}$ and $\widehat{\boldsymbol{v}}$. The black lines shows the average over 10^4 runs while the gray area encloses the range from the minimum to the maximum value of $\|\boldsymbol{v} - \widehat{\boldsymbol{v}}\|_2$.



(A) Spectrum of the capacitance matrix with perturbations given by $\widetilde{\varepsilon}_i \sim \mathcal{U}_{[-\eta,\eta]}$. For every perturbation size the spectrum of one realisation is shown. The eigenvalue in red corresponds to the localised interface mode.

(B) Stability of the interface mode. The solid black line shows the average dislocation over 10^4 runs, while the gray area encloses the range from the minimum to the maximum dislocation observed over these realisations.

FIGURE 4.4. The interface eigenvalue and the corresponding interface mode are very stable also in presence of large perturbations. Simulations in a system of $N = 41$ resonators with $s_1 = 1$ and $s_2 = 2$. Perturbations are uniformly distributed in $(-\eta, \eta)$ where we call η the perturbation size, expressed relatively to the resonators' sizes.

5. Non-Hermitian skin effect

Understanding the skin effect in non-Hermitian physical systems has been one of the hottest research topics in recent years [16, 38, 40, 50, 62, 65, 68]. The skin effect is the phenomenon whereby the bulk eigenmodes of a non-Hermitian system are all localised at one edge of an open chain of resonators. This phenomenon is unique to non-Hermitian systems with non-reciprocal coupling. It has been realised experimentally in topological photonics, phononics, and other condensed matter systems [29, 31, 41, 63]. By introducing an imaginary gauge potential, all the bulk eigenmodes condensate in the same direction [34, 55, 65]. This has deep implications for the fundamental physics of the system. For example, the non-Hermitian skin effect means that the conventional bulk-edge correspondence principle is violated. This section is dedicated to demonstrating that a non-Hermitian system with an imaginary gauge potential as introduced in Section 3.2 exhibits an eigenmode condensation that is typical of the skin effect. To this end, we will make extensive use of the theory of Toeplitz matrices and operators.

5.1. The skin effect in monomer systems of subwavlength resonators

We will first consider a system of equally spaced identical resonators (monomers), that is, a chain of N resonators with $s_i = s$ and $\ell_i = \ell$ for all $1 \leq i \leq N$. For this case, the particular structure of the capacitance matrix allows us to apply existing results concerning the spectra of tridiagonal Toeplitz matrices, which we have briefly recalled in Section 2.2. We will be able to derive a variety of explicit results that are not possible for the more complex situations analysed in the subsequent sections. Nevertheless, Proposition 3.4 applies for more general cases and the numerical results which we present below.

Applying the explicit formula for the eigenpairs of perturbed tridiagonal Toeplitz matrices from Lemma 2.7 to the gauge capacitance matrix C^γ given by (3.11), we obtain the following theorem from [1].

Theorem 5.1. *The eigenvalues of C^γ are given by*

$$\lambda_1 = 0,$$
$$\lambda_k = \frac{\gamma}{s}\coth(\gamma\ell/2) + \frac{2|\gamma|}{s}\frac{e^{\frac{\gamma\ell}{2}}}{|e^{\gamma\ell}-1|}\cos\left(\frac{\pi}{N}(k-1)\right), \quad 2 \le k \le N. \tag{5.1}$$

Furthermore, the associated eigenvector $\boldsymbol{a}_k$ satisfies the following inequality, for $2 \le k \le N$,

$$|\boldsymbol{a}_k^{(i)}| \le \kappa_k e^{-\gamma\ell\frac{i-1}{2}} \quad \textit{for all } 1 \le i \le N, \tag{5.2}$$

for some $\kappa_k \le (1+e^{\frac{\gamma\ell}{2}})^2$.

Here, $\boldsymbol{a}_k^{(i)}$ denotes the i^{th} component of the k^{th} eigenvector. It is easy to show that the first eigenvector $\boldsymbol{a}_1$ is a constant vector (*i.e.*, $\boldsymbol{a}_1^{(i)}$ is the same for all i). From Theorem 5.1, we can see that the eigenmodes display exponential decay both with respect to the site index i and the factor γ.

Of particular interest is the application of Propositions 2.2 and 2.5 to the gauge capacitance matrix C^γ. These results show that the localisation of the eigenvectors of both the finite and semi-infinite capacitance matrices depends on the Fredholm index of the symbol of the associated Toeplitz operator at the corresponding eigenvalue or, equivalently, of its winding number.

Indeed, the Toeplitz symbol of the Toeplitz operator associated to the capacitance matrix C^γ encloses the ellipse $E \subseteq \mathbb{C}$

$$z - b \in E \Leftrightarrow \frac{\Re(z)^2}{a+c} + \frac{\Im(z)^2}{a-c} \le 1,$$

where a, b and c are the below diagonal, diagonal and above diagonal elements of the Toeplitz operator. In particular, the boundary of the ellipses is drawn by $\theta \mapsto ae^{\mathbf{i}\theta} + b + ce^{-\mathbf{i}\theta}$ so that the winding in the interior of the ellipse is negative for $\gamma > 0$ and positive for $\gamma < 0$. It is thus easy to show that

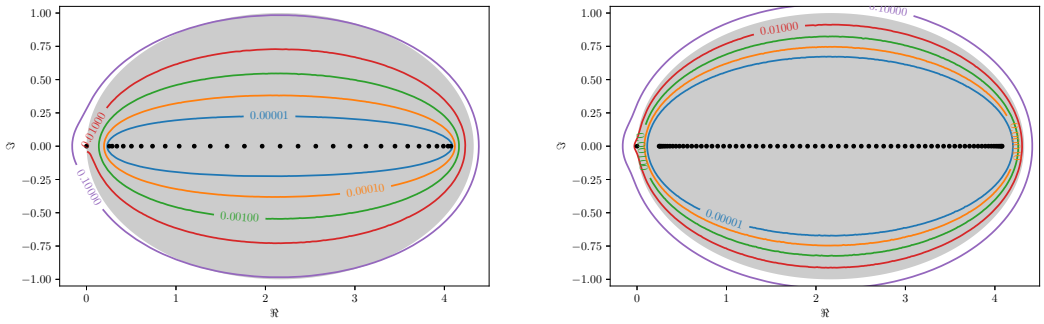
$$\lambda \in \sigma(C^\gamma) \setminus \{0\} \Rightarrow \lambda \in \text{int}(E) \quad \text{and} \quad 0 \in \partial E. \tag{5.3}$$

Specifically, every eigenvector having the corresponding eigenvalue laying in the region of the complex plane where the Fredholm index (or equivalently, the winding number of the symbol) is negative, has to be exponentially localised. This shows the intrinsic topological nature of the skin effect.

In Figure 5.1, we display the convergence of the pseudospectrum and the topologically protected region of negative winding number. We remark that the trivial eigenvalue 0 is outside of the region as the winding number is not defined there. As a consequence, the corresponding eigenvector is not localised.

The explicit formula for eigenvalues from Lemma 2.7 also gives some insight on the distribution of the *density of states*. The property of the cosine to have minimal slope when it is close to its maxima and minima, causes eigenvalues to cluster at the edges of the range of the spectrum. This is demonstrated by the nonuniform distribution of the black dots in Figure 5.1.

We conclude this section with a qualitative analysis of the spectral decomposition of C^γ. In Figure 5.3a, we show the eigenvector localisation as a function of the site index for finite arrays of various sizes. The localisation of a vector v is measured using the quantity $\|v\|_\infty/\|v\|_2$. After rescaling the site index, we expect there to be some invariance to the array size N, based on the formulas of Lemma 2.7. Figure 5.3b shows, on the other hand, the singular values of the eigenvector matrix, again with the indices normalised. The number of nonzero singular values is a proxy for the dimension of the range of the matrix. This has an exponential dependence on N. As a result, Figure 5.3 shows that as N increases, despite the number of eigenvalues growing like N, the rank of the matrix of eigenvectors is fixed.



(A) $N = 30$. (B) $N = 70$.

FIGURE 5.1. ε-pseudospectra of C^γ for $\varepsilon = 10^{-k}$ for $k = 1, \ldots, 5$. Shaded in grey is the region where the symbol f_T has negative winding, for T the Toeplitz operator corresponding to the semi-infinite structure. The pseudospectra are computed using [30].

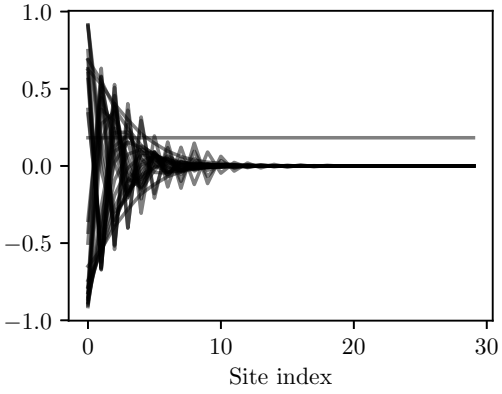


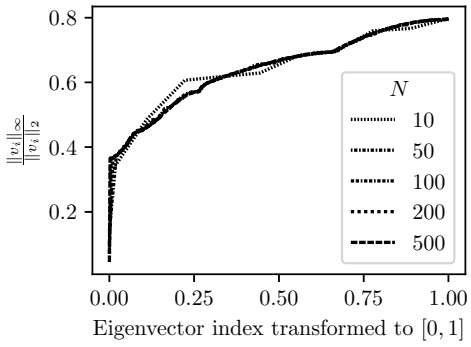
FIGURE 5.2. Eigenvectors of the capacitance matrix superimposed to display an exponential decay.

5.2. Non-Hermitian skin effect in dimer systems of subwavelength resonators

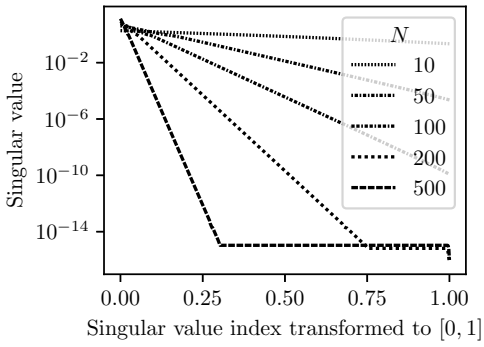
In Section 2.4, we have discussed the general form of eigenvalues and eigenvectors of tridiagonal 2-Toeplitz matrices with perturbations in the corners. In this subsection, we will use those results to show that the skin effect — whose existence has been shown in the previous subsection — is a feature present also in dimer systems. To do this, we will use quite different tools from those used for the case of identical and equally spaced resonators.

We consider a system as in Figure 3.1 composed of dimers — that is $s_i = s_{i+2}$ for all $1 \leq i \leq N-3$ and $\ell_i = \ell$ for all $1 \leq i \leq N$ — governed by (3.9). The gauge capacitance matrix from (3.12) takes the form

$$C^\gamma = \begin{pmatrix} \widetilde{\alpha}_1 & \beta_1 & & & & & \\ \eta_1 & \alpha_2 & \beta_2 & & & & \\ & \eta_2 & \alpha_1 & \beta_1 & & & \\ & & \eta_1 & \alpha_2 & \ddots & & \\ & & & \ddots & \ddots & \ddots & \\ & & & & \eta_2 & \alpha_1 & \beta_1 \\ & & & & & \eta_1 & \widetilde{\alpha}_2 \end{pmatrix}, \tag{5.4}$$



(A) The eigenvector localisation $\frac{|v_i|_\infty}{|v_i|_2}$ does not depend on N after rescaling.



(B) The singular values of the eigenvector matrix decay exponentially in N. This shows that the rank of the eigenvector matrix is independent of the size.

FIGURE 5.3. As $N \to \infty$, arbitrarily many eigenmodes become close to parallel. Here, this is shown in the case $s = \ell = 1$ and $\gamma = 0.5$.

where

$$\alpha_1 = \frac{\gamma}{s_1}\frac{\ell}{1-e^{-\gamma\ell}} - \frac{\gamma}{s_2}\frac{\ell}{1-e^{\gamma\ell}}, \qquad \alpha_2 = \frac{\gamma}{s_2}\frac{\ell}{1-e^{-\gamma\ell}} - \frac{\gamma}{s_1}\frac{\ell}{1-e^{\gamma\ell}},$$
$$\widetilde{\alpha}_1 = \frac{\gamma}{s_1}\frac{\ell}{1-e^{-\gamma\ell}}, \qquad \widetilde{\alpha}_2 = -\widetilde{\alpha}_1,$$
$$\beta_1 = -\frac{\gamma}{s_1}\frac{\ell}{1-e^{-\gamma\ell}}, \qquad \beta_2 = -\frac{\gamma}{s_2}\frac{\ell}{1-e^{-\gamma\ell}},$$
$$\eta_1 = \frac{\gamma}{s_1}\frac{\ell}{1-e^{\gamma\ell}}, \qquad \eta_2 = \frac{\gamma}{s_2}\frac{\ell}{1-e^{\gamma\ell}}.$$

One may remark that all rows of C^γ sum to 0 and thus $\mathbf{1} \in \ker(C^\gamma)$. We will see that this is the only eigenvector of C^γ that is not localised.

The first result consists in showing that the eigenvectors of the capacitance matrix exhibit an exponential decay and that the eigenvectors therefore condense. Its proof is nearly a direct application of the eigenvector formula (2.27) in Theorem 2.12. In particular, employing (2.27) we only need to control the "Chebyshev-like" polynomials $\widehat{p}_j^{(\xi_p,\xi_q)}(\lambda), \widehat{q}_j^{(\xi_p,\xi_q)}(\lambda)$'s. This then utilises the boundedness of Chebyshev polynomials in $[-1,1]$ shown in (2.4) and the eigenvalue distribution derived in Theorem 2.8. We thus see that the interface modes and the skin effect actually correspond to the opposite behaviors of the Chebyshev polynomials in and outside the interval $[-1,1]$; see Figure 2.1. We refer the reader to [6] for a detailed proof.

LEMMA 5.2. *Except for at most* 11 *eigenvalues* $\{\lambda_r\}$ *of* $A_{2m+1}^{(a,b)}$*, the corresponding eigenvectors* $\boldsymbol{x}$ *in Theorem 2.12 satisfy*

$$\left|\boldsymbol{x}^{(j)}\right| \leq Mj\left(\sqrt{\frac{\eta_1\eta_2}{\beta_1\beta_2}}\right)^{\lfloor\frac{j-1}{2}\rfloor} \tag{5.5}$$

for some constant $M > 0$ *independent of the* λ_r*'s, where* $\boldsymbol{x}^{(j)}$ *is the* j^{th} *component of* $\boldsymbol{x}$*. The estimate* (5.5) *holds also for the eigenvectors* $\boldsymbol{x}$ *of* $A_{2m}^{(a,b)}$ *associated with the eigenvalue* λ_r *in Theorem 2.12, except for at most* 12 *r's.*

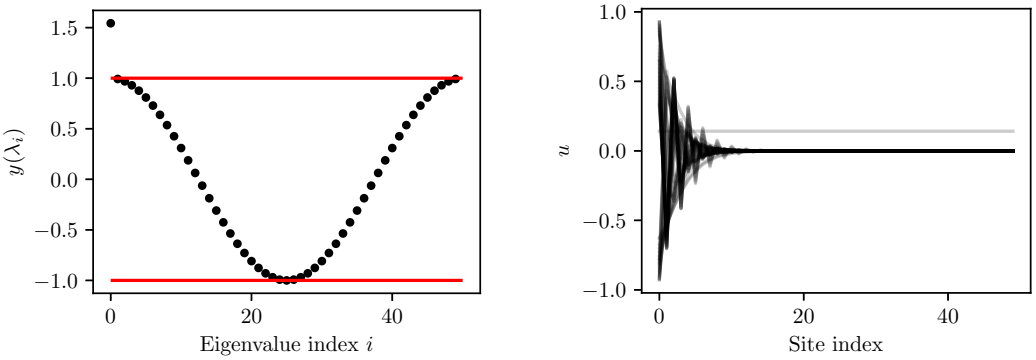
As shown in [6], the natural consequence of this theorem is the condensation of the eigenvectors of the gauge capacitance matrix.

Theorem 5.3. *All but a few (independent of N) eigenvectors of the gauge capacitance matrix C^γ satisfy the following estimate:*

$$\left|\boldsymbol{x}^{(j)}\right| \leq Mje^{-\ell\gamma\lfloor\frac{j-1}{2}\rfloor}, \tag{5.6}$$

where $\boldsymbol{x}^{(j)}$ is the j^{th} component of the eigenvector $\boldsymbol{x}$.

Lemma 5.2 and Theorem 5.3 are stated to hold up to a finite number of eigenpairs. This is due to the fact that the proof relies on multiple applications of Cauchy's interlacing Theorem. Nevertheless, numerically, we can verify that there is exactly one eigenvector which is not localised. More precisely, we show in Figure 5.4a that only the eigenvalue $\lambda_1 = 0$ satisfies $|y(\lambda_i)| \geq 1$ for y as in (2.14). In Figure 5.4b, we plot the eigenmodes of a system of 25 dimers.



(A) The black dots show the value $y(\lambda_i)$ for the eigenvalues λ_i of C^γ. The red line show the boundaries stability zone $y = \pm 1$. Only for $\lambda = 0$, $y(\lambda)$ lays outside of this zone.

(B) Eigenmodes superimposed on one another to portray the skin effect: all modes except one are exponentially localised on the left edge of the system.

FIGURE 5.4. Eigenmode localisation for a system of 25 dimers ($N = 50$), $\ell_i = 1$, $s_1 = 1$, $s_2 = 2$ and $\gamma = 1$.

It is interesting to remark that the eigenvalue 0 is both the only outlier of Figure 5.4a and the only point laying on the trace of the eigenvalues of the symbol of the 2-Toeplitz operator; see Figure 5.8 for an illustration and Theorem 5.11 for a theoretical demonstration.

5.3. Stability of the skin effect

In this section, we present a stability estimate of the skin effect. We illustrate the stability of the skin effect for monomer systems of subwavelength resonators. For the case of dimer systems, one can derive similar results based on the constructions in Sections 2.4 and 5.2.

According to the theory in Section 5.1, the capacitance matrix in this case is given by

$$C^\gamma = T_N^{(\eta,\beta)},$$

for $T_N^{(\eta,\beta)}$ defined as in (2.7) and η, α, β are such that

$$\eta\beta > 0, \quad \text{and} \quad \eta + \alpha + \beta = 0.$$

In order to study the stability of the non-Hermitian skin effect with respect to random imperfections in the system design, we either add random errors to the positions of the resonators (keeping the length of the resonators unchanged) or to the γ-term and then repeatedly compute the subwavelength eigenfrequencies and their associated eigenmodes. The perturbations in the positions and in the values of the γ-parameter are drawn at random from uniform distributions with zero-mean values. Since these random perturbations affect

only the tridiagonal entries of the gauge capacitance matrix $\widehat{C}^{\gamma}$ of the randomly perturbed system, we can write in both cases that

$$\widehat{C}^{\gamma} = \widehat{T}_N^{(a,b)} := \begin{pmatrix} \alpha + a + \varepsilon_{\alpha,1} & \beta + \varepsilon_{\beta,1} & 0 & \dots & 0 & 0 \\ \eta + \varepsilon_{\eta,2} & \alpha + \varepsilon_{\alpha,2} & \beta + \varepsilon_{\beta,2} & \dots & 0 & 0 \\ 0 & \eta + \varepsilon_{\eta,3} & \alpha + \varepsilon_{\alpha,3} & \dots & 0 & 0 \\ \dots & \dots & \dots & \dots & \dots & \dots \\ \dots & \dots & \dots & \dots & \alpha + \varepsilon_{\alpha,N-1} & \beta + \varepsilon_{\beta,N-1} \\ 0 & 0 & 0 & \dots & \eta + \varepsilon_{\eta,N} & \alpha + b + \varepsilon_{\alpha,N} \end{pmatrix} \tag{5.7}$$

with $a = \eta, b = \beta, \eta = -\frac{\ell\gamma}{s}\frac{1}{1-e^{-\gamma\ell}}, \alpha = \coth(\gamma\ell/2), \beta = \frac{\ell\gamma}{s}\frac{1}{1-e^{\gamma\ell}}$.

We first derive stability results for the eigenvalues of $T_N^{(a,b)}$. This relies on a crucial observation that the tridiagonal matrix $T_N^{(a,b)}$ always has the same eigenvalues as a Hermitian matrix. Thus we first recall the following well-known Weyl theorem for the stability of eigenvalues of Hermitian matrices; see [56, Theorem 1.1.7], [32, Theorem 8.1.6] and [52, Theorem 10.3.1].

PROPOSITION 5.4. *Let A and E be $N \times N$ Hermitian matrices. For $k \in \{1, \dots, N\}$, denote by $\lambda_k(A+E), \lambda_k(A)$ the k^{th} eigenvalue of $A+E$ and A, respectively. Assume these to be arranged in a decreasing sequence. Then,*

$$|\lambda_k(A+E) - \lambda_k(A)| \leqslant \|E\|_2,$$

where $\|E\|_2$ is the operator norm of E.

Now we introduce the following result for the stability of the eigenvalues of $T_N^{(a,b)}$; see [4] for a detailed justification. From this we can state that the eigenvalues of matrices of the type $T_N^{(a,b)}$ with $a, b \in \mathbb{R}$ are stable under *physical* perturbations. We remark here that physical means perturbing either the geometry or the imaginary gauge potential. It is well-known that $T_N^{(a,b)}$ is not stable under arbitrary perturbations, but these do not occur as a result of physical modifications to the system.

PROPOSITION 5.5. *The eigenvalues of $T_N^{(a,b)}$ and $\widehat{T}_N^{(a,b)}$ are all real numbers. Let $\{\lambda_k\}, \{\widehat{\lambda}_k\}$ be respectively the eigenvalues of $T_N^{(a,b)}$ and $\widehat{T}_N^{(a,b)}$, arranged in decreasing sequences. Assuming that*

$$\max_{j=1,\dots,N} \left(|\varepsilon_{\eta,j}|, |\varepsilon_{\alpha,j}|, |\varepsilon_{\beta,j}|\right) =: \varepsilon \tag{5.8}$$

with $\varepsilon \leqslant \min(|\eta|, |\beta|)$, then we have

$$\left|\widehat{\lambda}_k - \lambda_k\right| \leqslant C_1(\eta, \beta, \varepsilon)\varepsilon,$$

where

$$C_1(\eta, \beta, \varepsilon) = \frac{|\beta| + |\eta| + \varepsilon}{\sqrt{\beta\eta}} + 1. \tag{5.9}$$

Applying Proposition 5.5 to the eigenvalues of $T_N^{(\eta,\beta)}$ (stated in Lemma 2.7) yields the following stability estimate first derived in [4].

Theorem 5.6. *For the eigenvalue $\widehat{\lambda}_k$ of the perturbed capacitance matrix $\widehat{C^{\gamma}}$ with*

$$\max_{j=1,\dots,N} \left(|\varepsilon_{\eta,j}|, |\varepsilon_{\alpha,j}|, |\varepsilon_{\beta,j}|\right) =: \varepsilon \tag{5.10}$$

and $\varepsilon \leqslant \min(|\eta|, |\beta|)$, we have $\widehat{\lambda}_1 = \varepsilon_1$ and

$$\widehat{\lambda}_k = \lambda_k + \varepsilon_k = \alpha + 2\sqrt{\eta\beta}\cos\left(\frac{(k-1)\pi}{N}\right) + \varepsilon_k, \quad k = 2, \cdots, N, \tag{5.11}$$

with $|\varepsilon_k| \leqslant C_1(\eta, \beta, \varepsilon)\varepsilon, 1 \leqslant k \leqslant N$ and $C_1(\eta, \beta, \varepsilon)$ being defined by (5.9). In particular, all the $\widehat{\lambda}_k$'s are real numbers.

Remark 5.7. One can apply Proposition 5.5 and Theorem 5.8 to derive similar stability results for $T_N^{(0,0)}$. This corresponds to many examples of the non-Hermitian skin effect in condensed matter theory and quantum mechanics. The stability results presented here can therefore be immediately applied to these examples. For the eigenvalues of tridiagonal Toeplitz matrices with various perturbations on the corners, we refer the reader to [66, 67].

Next, we estimate the stability of the eigenvectors of $C^\gamma = T_N^{(\eta,\beta)}$. For λ_k an eigenvalue of C^γ, we let

$$p_j(\lambda_k) = \left(\eta \sin\left(\frac{(j+1)(k-1)\pi}{N}\right) - \eta\sqrt{\frac{\eta}{\beta}}\sin\left(\frac{j(k-1)\pi}{N}\right)\right), \quad j = 0, \cdots, N-1. \tag{5.12}$$

Note that

$$|p_j(\lambda_k)| \leqslant |\eta|\left(1 + \sqrt{\frac{\eta}{\beta}}\right), \quad j = 0, \cdots, N-1. \tag{5.13}$$

The following results hold.

Theorem 5.8. *For $\widehat{T}_N^{(\eta,\beta)}$ defined by (5.7) and satisfying (5.10) with $\varepsilon \leqslant \min(|\eta|, |\beta|)$ and its eigenvalues $\widehat{\lambda}_k = \lambda_k + \varepsilon_k, k = 2, \cdots, N$ defined by (5.11), the corresponding eigenvectors are given by*

$$\begin{aligned}\widehat{\boldsymbol{x}}_k = \big(&p_0(\lambda_k) + \delta_0(\lambda_k), s\left(p_1(\lambda_k) + \delta_1(\lambda_k)\right), s^2\left(p_2(\lambda_k) + \delta_2(\lambda_k)\right), \cdots, \\ &s^{N-1}\left(p_{N-1}(\lambda_k) + \delta_{N-1}(\lambda_k)\right)\big)^\top, \quad k = 2, \cdots, N,\end{aligned} \tag{5.14}$$

where $s = \sqrt{\frac{\eta}{\beta}}$ and $p_j(\lambda_k)$ is defined in (5.12). Moreover, we have

$$\left|(-s)^j p_j(\lambda_k)\right| \leqslant \left(\frac{\eta}{\beta}\right)^{\frac{j}{2}} |\eta|\left(1 + \sqrt{\frac{\eta}{\beta}}\right), \quad j = 0, 1, \cdots, N-1, \tag{5.15}$$

and

$$\left|s^j \delta_j(\lambda_k)\right| \leqslant \zeta_{k,j}\varepsilon, \quad j = 0, 1, \cdots, N-1, \tag{5.16}$$

where

$$\zeta_{k,j} = \left(\sqrt{\frac{\eta}{\beta}}\left(\frac{|\beta|\left(|\eta| + \varepsilon\right)}{(|\beta| - \varepsilon)|\eta|}\right)\right)^j \left(a_+ r_{k,+}^j(\eta,\beta,\varepsilon) + a_- r_{k,-}^j(\eta,\beta,\varepsilon) - \zeta\right)$$

with

$$\begin{aligned}&r_{k,\pm}(\eta,\beta,\varepsilon) \\ &= \left(\left|\cos\left(\frac{(k-1)\pi}{N}\right)\right| + \frac{C_2(\eta,\beta,\varepsilon)\varepsilon}{\sqrt{\eta\beta}}\right) \pm \sqrt{\left(\left|\cos\left(\frac{(k-1)\pi}{N}\right)\right| + \frac{C_2(\eta,\beta,\varepsilon)\varepsilon}{\sqrt{\eta\beta}}\right)^2 + 1},\end{aligned} \tag{5.17}$$

$C_2(\eta,\beta,\varepsilon) = \frac{|\beta|+|\eta|+\varepsilon}{2\sqrt{\beta\eta}} + 1$, and a_+, a_-, ζ being bounded constants. In particular, for those indices k such that

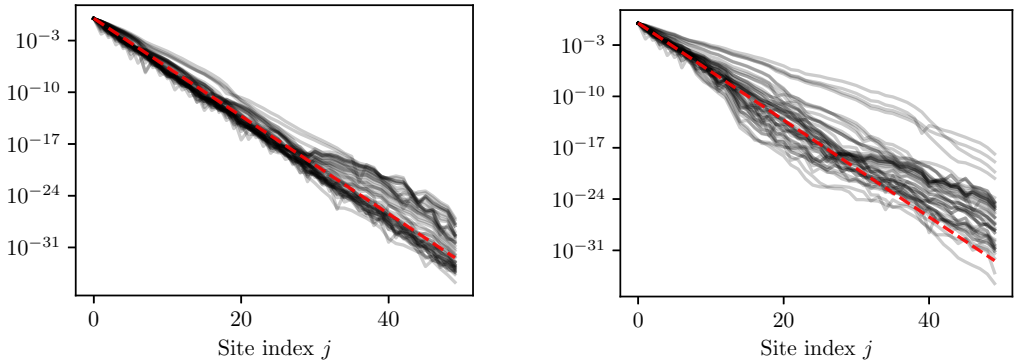
$$\left|\sqrt{\frac{\eta}{\beta}}\left(\frac{|\beta|\left(|\eta| + \varepsilon\right)}{(|\beta| - \varepsilon)|\eta|}\right) r_{k,+}\right| < 1, \tag{5.18}$$

the corresponding eigenvector still has an exponential decay.

As a result, there exists a constant c such that if $\sqrt{\eta/\beta} < \sqrt{2} - 1$ and $\varepsilon < \frac{c}{N^2}$, then we still have an exponential decay for all the corresponding eigenvectors $\widehat{\boldsymbol{x}}_k, 2 \leqslant k \leqslant N$, of $\widehat{T}_N^{(a,b)}$. Furthermore, if we require $\sqrt{\eta/\beta}$ to be even smaller, then this exponential decay will remain for even larger values of ε.

Before applying Theorem 5.8 to show the stability of the skin effect, we illustrate numerically the results stated there. In particular, we consider typical values in physical applications. We let $\eta = 0.15$, $\beta = 3.15$ (which corresponds to $\ell = s = 1$ and $\gamma = 3$) and ε satisfying (5.18). The results are presented in Figure 5.5, where we show the eigenvectors of a 50×50 matrix on a logarithmic axis. If the perturbations are sufficiently small that the condition (5.18) is satisfied, then the eigenvectors still all have the $(\sqrt{\beta/\eta})$ decay rate. However, when

the perturbations are large enough that condition (5.18) does not hold for some indices, the corresponding eigenmodes have a much lower decay rate.



(A) Exponential decay of the eigenvectors for ε satisfying (5.18). The eigenvectors superimposed on one another on a semi-log plot. The red dashed line represents $(\sqrt{\beta/\eta})^j$. We observe the same decay rate as the unperturbed case.

(B) Decay of the eigenvectors for ε *not* satisfying (5.18). The eigenvectors superimposed on one another on a semi-log plot. The red dashed line represents $(\sqrt{\beta/\eta})^j$. We observe several eigenvectors with lower decay rate than the one in Figure 5.5a.

FIGURE 5.5. Numerical illustration of the stability of the eigenvector decay rate predicted by Theorem 5.8. The Toeplitz matrix has coefficients $\eta = 0.15$, $\beta = 3.15$ and is of size 50×50.

Now, since a perturbation of order ε to the spacings $\{s_i\}$ between the subwavelength resonators or the coefficient γ results in an $\mathcal{O}(\varepsilon)$ perturbation in the nonzero entries of the gauge capacitance matrix C^γ, Theorem 5.8 can be immediately applied to $\widehat{C}^\gamma$ to obtain the stability of the eigenvectors of C^γ and the skin effect in the structure. We present below a corollary for a simplified stability estimate on the spectrum of C^γ.

COROLLARY 5.9. *Let $\widehat{C}^\gamma$ be defined by (5.7). Assume that (5.10) holds with $\varepsilon \leqslant \min(|\eta|, |\beta|)$. Then the normalised eigenvector $\widehat{\boldsymbol{x}}_k$ corresponding to the eigenvalue $\widehat{\lambda}_k = \lambda_k + \varepsilon_k, k = 2, \cdots, N$, defined by (5.11) is given by*

$$\widehat{\boldsymbol{x}}_k = \boldsymbol{x}_k + \boldsymbol{\Delta}_k, \quad k = 2, \cdots, N,$$

where $\boldsymbol{x}_k$ is the eigenvector of C^γ and $\boldsymbol{\Delta}_k$ satisfies

$$||\boldsymbol{\Delta}_k||_\infty \leq C_1 \varepsilon,$$

for some constant C_1 independent of ε, when

$$\left| \sqrt{\frac{\eta}{\beta}} \left(\frac{|\beta| \left(|\eta| + \varepsilon \right)}{(|\beta| - \varepsilon)|\eta|} \right) r_{k,+}(\eta, \beta, \varepsilon) \right| < 1,$$

with $r_{k,+}(\eta, \beta, \varepsilon)$ being given by (5.17). In particular, $\widehat{\boldsymbol{x}}_k$ still has an exponential decay.

It is important to notice that the asymptotic approximations of the resonant eigenfrequencies and eigenmodes through the spectrum of the gauge capacitance matrix hold also for the perturbed structure. The stability of the spectrum of the gauge capacitance matrix C^γ implies the stability of the skin effect in the subwavelength regime. In particular, we have the following corollary on the stability of the eigenfrequencies and eigenmodes of the system (3.9).

COROLLARY 5.10. *Let*

$$\max_{j=1,\cdots,N} (|\varepsilon_{\alpha,j}|, |\varepsilon_{\beta,j}|, |\varepsilon_{\eta,j}|) \leqslant \frac{\ell\gamma}{s} \coth(\frac{\gamma\ell}{2})\varepsilon := \widehat{\varepsilon}, \tag{5.19}$$

and

$$\boldsymbol{x}_k^{(j)} = \left(\frac{\eta}{\beta}\right)^{\frac{j-1}{2}} \left(\eta \sin\left(\frac{j(k-1)\pi}{N}\right) - \eta\sqrt{\frac{\eta}{\beta}} \sin\left(\frac{(j-1)(k-1)\pi}{N}\right)\right), \ j = 1, \cdots, N. \tag{5.20}$$

For a perturbed structure of resulting in (5.7) *such that*

$$s_i = s(1+\varepsilon_i), \quad i = 1, \cdots, N, \tag{5.21}$$

with $|\varepsilon_i| \leqslant \varepsilon$ *for* ε *sufficiently small, the* N *subwavelength eigenfrequencies* $\widehat{\omega}_i$ *of (3.9) satisfy, as* $\delta \to 0$*,*

$$\widehat{\omega}_i = \omega_i + \mathcal{O}(\delta + \sqrt{\delta\varepsilon}),$$

where $(\omega_i)_{1\leqslant i\leqslant N}$ *are the eigenfrequencies for the unperturbed structure. Furthermore, let* $\widehat{u}_i$ *be a subwavelength eigenmode corresponding to* $\widehat{\omega}_i$ *and let* $\boldsymbol{a}_i$ *be the corresponding eigenvector of* $\ell^{-1}\, C^\gamma$*. Then, for* $\ell \mathbf{a}_i, i = 2, \cdots, n$*, given by (5.20) and those index* i *satisfying*

$$\left|\sqrt{\frac{\eta}{\beta}} \left(\frac{|\beta|\,(|\eta| + \widehat{\varepsilon})}{(|\beta| - \widehat{\varepsilon})|\eta|}\right) r_{i,+}(\eta, \beta, \widehat{\varepsilon})\right| < 1$$

with $r_{i,+}(\eta, \beta, \widehat{\varepsilon})$*,* $\widehat{\varepsilon}$ *being given by (5.17),(5.19), respectively, we have*

$$\widehat{u}_i(x) = \sum_j \boldsymbol{a}_i^{(j)} V_j(x) + \mathcal{O}(\delta + \varepsilon), \quad i = 2, \cdots, N,$$

where the V_j*'s are defined by* (3.11)*.*

Random perturbations of the geometry. In this subsection, we will provide numerical evidence of the stability of the non-Hermitian skin effect and show how it competes with Anderson-type localisation of the eigenmodes in the bulk when the disorder is large. We can consider perturbations in both the geometry and the local values of the damping parameter (*i.e.*, the imaginary gauge potential). We will present here the case of a perturbed geometry and refer the reader to [4] for the other case. For the sake of brevity, we fix the size ℓ of the resonators and perturb independently the spacing s between the resonators. The numerical experiments presented here are for the discrete approximation (5.7) and not for the damped wave equation (3.9).

We consider the following perturbation:

$$s_i = 1 + \varepsilon_i, \qquad \varepsilon_i \sim \mathcal{U}_{[-\varepsilon,\varepsilon]}. \tag{5.22}$$

Here, we recall that $\mathcal{U}_{[-\varepsilon,\varepsilon]}$ is a uniform distribution with support in $[-\varepsilon, \varepsilon]$. In Figure 5.6a, we study how the eigenmodes of a system of 30 subwavelength resonators behave as the disorder increases. These results are averaged based on 500 independent realisations. We show the relative proportion of eigenvalues that fall within the region of negative winding of the associated Toeplitz operator, as well as the proportion of eigenmodes accumulating at the left edge (which for this and the following figures has been defined as the number of eigenvectors that attain their maximal values, in absolute terms, in one of the first four resonators). We consider values of the disorder strength that are small enough to ensure that the resonators do not overlap. Both these quantities are constant for small disorder strengths then decrease once the disorder strength passes a certain threshold (as predicted by Theorem 5.8). The intersection of these two sets is also shown.

One notices very similar trends in the three lines in Figure 5.6a, with small differences due to the imperfect formulation of the accumulation measure and the perturbations. On the other hand, Figure 5.6b shows the localisation of the eigenvectors of $\widehat{C}^\gamma$ from (5.7) for different disorder strengths. The localisation of the eigenvectors is measured using the quantity $\|v_i\|_\infty / \|v_i\|_2$ and the different lines correspond to different disorder strengths ε. We notice that the lines are indistinguishable, indicating that the localisation of the eigenvectors is independent of any random perturbation of the positions of the resonators.

Figure 5.6d shows similar stability properties as those in Figure 5.6a, but here the relative number of eigenvalues falling within the region with negative winding is plotted for different

values of ε and γ. On the left side of the figure, we see the topologically protected region: for these values of γ any small perturbation size ε will not cause any eigenvalue to exit the region and thus the corresponding eigenvector remains accumulated at the left edge of the structure.

In Figure 5.6c, the localisation of the eigenvectors is measured using the inverse participation ratio (IPR) defined as $\|v_i\|_4/\|v_i\|_2$. IPR is commonly used to distinguish Anderson localised and extended eigenmodes [42, 49]. One notices that the results in Figure 5.6c are similar to those in Figure 5.6b.

The results in Figure 5.6 show how the proportion of eigenvectors localised to the left edge of the system decreases as the disorder increases. Studying in the eigenvectors themselves, as shown in Figure 5.7 for three different values of the disorder strength, we see that increasing disorder means an increasing number of eigenvectors that are localised in the bulk rather than on the left edge. This behaviour is typical of Anderson-type localisation in disordered systems and demonstrates the internal competition between the skin effect and Anderson localisation.

5.4. Topological origin of the skin effect

In this section, employing the Toeplitz theory in Section 2.5, we elucidate the topological origin of the skin effect in the polymer systems of subwavelength resonators which includes the monomer and dimer systems as special cases. For the semi-infinite polymer systems of subwavelength resonators, we obtain a perturbed tridiagonal k-Toeplitz operator

$$T^a(f) = \begin{pmatrix} \alpha_1 + a & \beta_1 & & & & & \\ \eta_1 & \alpha_2 & \beta_2 & & & & \\ & \ddots & \ddots & \ddots & & & \\ & & \eta_{k-1} & \alpha_k & \beta_k & & \\ & & & \eta_k & \alpha_1 & \beta_1 & \\ & & & & \ddots & \ddots & \ddots \end{pmatrix}$$

with f being the symbol defined in (2.33).

It has been observed in [6] that the exponential decay of the eigenvectors of k-Toeplitz matrices for $k \geq 2$ is due to the winding of the eigenvalues of the symbol being nontrivial. Now, by the spectral theory for the tridiagonal k-Toeplitz operators introduced in Section 2.5, we have the following results for the topological origin of the skin effect in subwavelength resonator systems, validating the observation made in [6].

Theorem 5.11. *Suppose $\Pi_{j=1}^k \eta_j \neq 0$ and $\Pi_{j=1}^k \beta_j \neq 0$. Let $f(z) \in \mathbb{C}^{k\times k}$ be the symbol (2.33) and let $\lambda \in \mathbb{C} \setminus \sigma_{\rm ess}(T^a(f))$. If $\sum_{j=1}^k \mathrm{wind}(\lambda_j, \lambda) < 0$, then there exists an eigenvector $\boldsymbol{x}$ of $T^a(f)$ associated to λ and some $\rho < 1$ such that*

$$\frac{|\boldsymbol{x}_j|}{\max_i |\boldsymbol{x}_i|} \leq C_1 \lceil j/k \rceil \rho^{\lceil j/k \rceil - 1}, \tag{5.23}$$

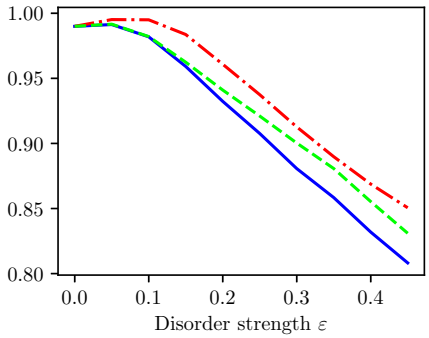
where $C_1 > 0$ is a constant depending only on $\lambda, \alpha_j, \beta_j, \eta_j, j = 1, \cdots, k$. If $\sum_{j=1}^k \mathrm{wind}(\lambda_j, \lambda) > 0$, then the above results hold for the left eigenvectors.

Theorem 5.11 elucidates the topological origin of the skin effect in the polymer system of subwavelength resonators. In particular, the skin effect holds for all λ in the region

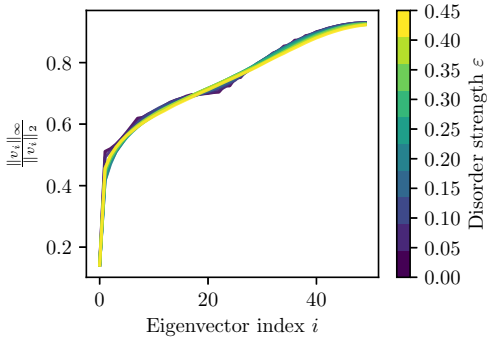
$$G := \left\{ \lambda \in \mathbb{C} \setminus \sigma_{\rm det}(f) : \sum_{j=1}^k \mathrm{wind}(\lambda_j, \lambda) \neq 0 \right\}. \tag{5.24}$$

This is a generalisation for the topological origin of the skin effect in the Toeplitz operator case given in Section 5.1.

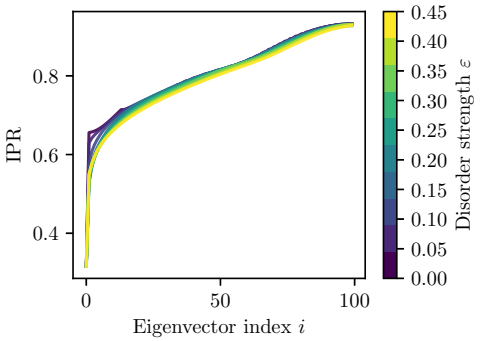
The last part of this section is devoted to illustrating numerically the skin effect and its topological origin in chains of 2, 3, and 4 periodically repeated resonators. We start by



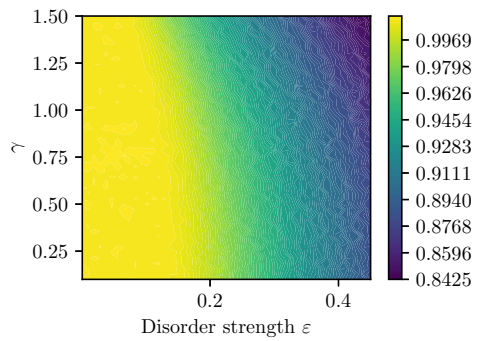
(A) Eigenmode accumulation at one edge and topological winding. The green dashed line shows the average proportion of eigenvectors which are localised at the left edge. The red dash-dot line shows the average proportion of eigenvalues that lay in the topologically protected region. The blue solid line shows the proportion of eigenpairs that have *both* eigenvalues in the topologically protected region and eigenvectors accumulated on the left edge.



(B) Eigenmode localisation. Each line shows the average eigenmode localisation for a different value of the disorder strength ε. For small ε, the localisation is due to the skin effect while, for large ε, it is consequence of the Anderson localisation. As the lines are indistinguishable we conclude that the eigenmode localisation is independent of disorder strength; as ε increases, modes might be localised in the bulk but will not become delocalised.



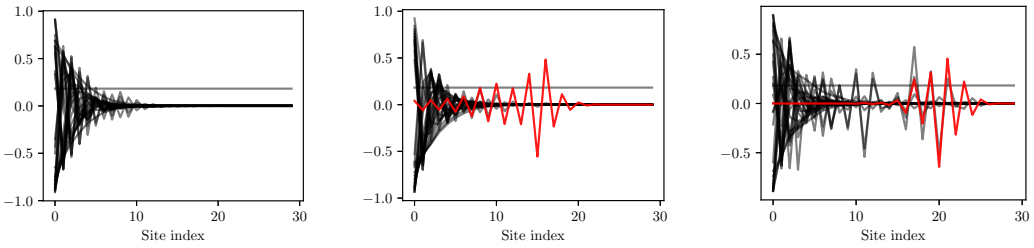
(C) Similar plot as in Figure 5.6b but using IPR as localisation measure. No significant difference is noticed.



(D) Phase change and topological protection. The color scale shows the average proportion of eigenvalues that lay in the topologically protected region for different values of γ. The left yellow zone is the stability region.

FIGURE 5.6. Competition between the non-Hermitian skin effect and Anderson localisation when perturbing the geometry. The non-Hermitian skin effect shows stability with respect to random perturbations. Outside of the stability region, there is competition with Anderson localisation. Averages are computed over 500 runs for a system of 50 resonators with $\ell = s = 1$.

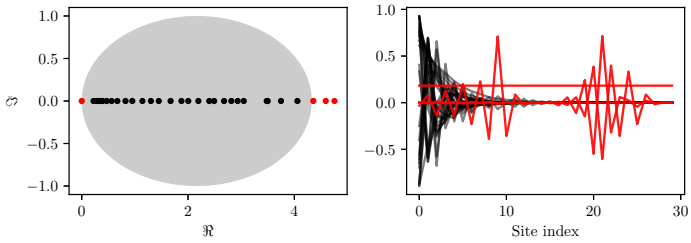
illustrating in Figure 5.8 the results of a system of 2 periodically repeated resonators as in [6]. In Figure 5.8a, we show the spectrum and pseudospectrum of the gauge capacitance matrix of a system of 25 dimers together with the winding of the two eigenvalues of the symbol of the corresponding 2-Toeplitz operator. Figure 5.8b shows that all the eigenvectors (black eigenvectors) associated with eigenvalues inside the region G in (5.24) are localised



(A) Single realisation with disorder strength $\varepsilon = 0.1$. All eigenmodes are accumulated on the left edge.

(B) Single realisation with disorder strength $\varepsilon = 0.2$. One eigenmode localised in the bulk is highlighted in red.

(C) Single realisation with disorder strength $\varepsilon = 0.4$. One eigenmode localised in the bulk is highlighted in red.



(D) Relation between the eigenvalues in the topologically protected region and the condensation of eigenvectors in a single realisation with $\varepsilon = 0.4$. Eigenvalues laying outside the protected region and the corresponding eigenvectors are shown in red.

FIGURE 5.7. Stability of the non-Hermitian skin effect under perturbations of the geometry. Eigenmode condensation on the left edge of the structure with some eigenmodes localised in the bulk. Single realisations with $N = 30$, $s = \ell = 1$, and $\varepsilon = 0.1, 0.2, 0.4, 0.4$ for Figure 5.7a, 5.7b, 5.7c and 5.7d, respectively. This should be compared with Figure 5.2, where there is no disorder.

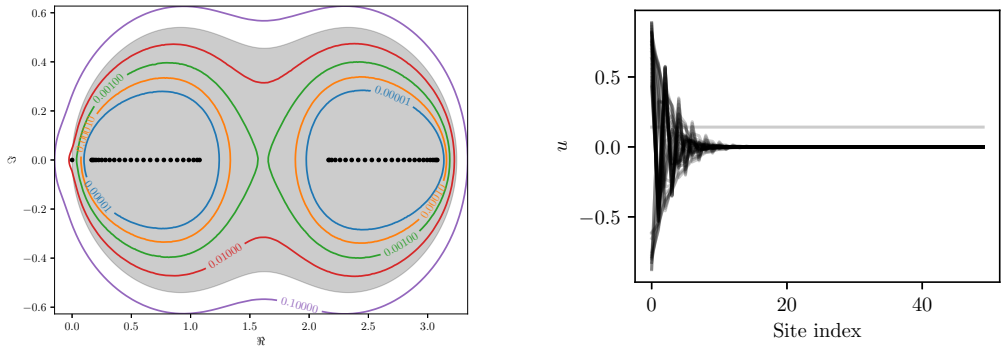
and the only nondecreasing eigenvector (gray eigenvector) corresponds to the eigenvalue 0 in the boundary of the region G. On the other hand, in [6] it is observed that the nontrivial winding of the eigenvalues $\lambda_j(z)$ predicts the exponential decay of the eigenmodes. This is due to $\mathrm{wind}(\lambda_j, \lambda) \leq 0, j = 1, 2$ in the example, which yields

$$G = \left\{ \lambda \in \mathbb{C} \setminus \sigma_{\mathrm{det}}(f) : \bigcup_{j=1}^{2} \mathrm{wind}(\lambda_j, \lambda) \neq 0 \right\}.$$

Figure 5.9 illustrates the results for 3 and 4 periodically repeated resonators. We numerically verify that indeed all the eigenvectors, except the one associated with eigenvalue 0 on the boundary of G, are localised at the left edge of the structure. We remark that due to the higher freedom in the parameter choice, for $n \geq 3$ periodically repeated resonators, various topologies are achievable for the area G and the one presented in Figure 5.9 is only one of the possibilities.

5.5. Non-Hermitian interface modes between opposing signs of the gauge potential

We now briefly consider interface modes between two structures where the sign of γ is switched from negative (on the left part) to positive (on the right part). Most commonly,



(A) The region of nontrivial winding of the eigenvalues and the pseudospectrum.

(B) Eigenmodes superimposed on one another to portray the skin effect.

FIGURE 5.8. The region of λ so that $\sum_{j=1}^{k} \operatorname{wind}(\lambda_j(\mathbb{T}), \lambda) \neq 0$ and the localisation of the eigenvectors. Computation performed for $s_1 = 1, s_2 = 2$, and $N = 50$.

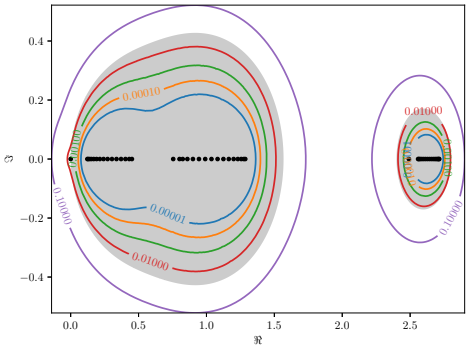
localised interface modes are formed by creating a defect in the system's geometric periodicity (see, for example, [12]). In non-Hermitian systems based on complex material parameters, similar localised interface modes have been shown to exist in the presence of a defect in the periodicity of the material parameters [2, 14]. Given the existence of the skin effect, demonstrated in the previous section, it is reasonable to expect that we might be able to produce a similar localisation effect using systems of resonators with imaginary gauge potentials. With this in mind, we consider the following system of $N = 2n + 1$ resonators:

$$\begin{cases} u''(x) + \gamma u'(x) + \dfrac{\omega^2}{v_b^2} u = 0, & x \in \displaystyle\bigcup_{i=1}^{n} (x_i^{\mathsf{L}}, x_i^{\mathsf{R}}), \\ u''(x) - \gamma u'(x) + \dfrac{\omega^2}{v_b^2} u = 0, & x \in \displaystyle\bigcup_{n+1}^{N} (x_i^{\mathsf{L}}, x_i^{\mathsf{R}}), \\ u''(x) + \dfrac{\omega^2}{v^2} u = 0, & x \in \mathbb{R} \setminus \displaystyle\bigcup_{i=1}^{N} (x_i^{\mathsf{L}}, x_i^{\mathsf{R}}), \\ u|_{\mathsf{R}}(x_i^{\mathsf{L,R}}) - u|_{\mathsf{L}}(x_i^{\mathsf{L;R}}) = 0, & \text{for all } 1 \leq i \leq N, \\ \dfrac{\mathrm{d}u}{\mathrm{d}x}\Big|_{\mathsf{R}} (x_i^{\mathsf{L}}) = \delta \dfrac{\mathrm{d}u}{\mathrm{d}x}\Big|_{\mathsf{L}} (x_i^{\mathsf{L}}), & \text{for all } 1 \leq i \leq N, \\ \dfrac{\mathrm{d}u}{\mathrm{d}x}\Big|_{\mathsf{R}} (x_i^{\mathsf{R}}) = \delta \dfrac{\mathrm{d}u}{\mathrm{d}x}\Big|_{\mathsf{R}} (x_i^{\mathsf{L}}), & \text{for all } 1 \leq i \leq N, \\ \dfrac{\mathrm{d}u}{\mathrm{d}\,|x|} u - \mathbf{i}ku = 0, & x \in (-\infty, x_1^{\mathsf{L}}) \cup (x_N^{\mathsf{R}}, \infty). \end{cases} \tag{5.25}$$

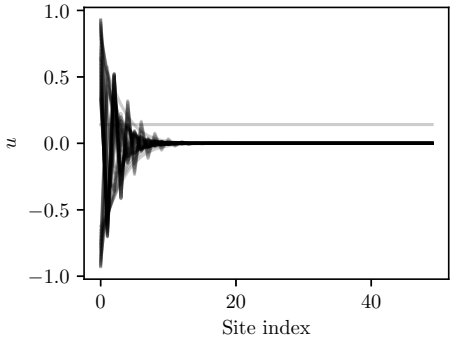
It is not difficult to see that also with this system we can recover a capacitance matrix for which a similar result as the one in Proposition 3.4 holds. In particular, generalising (3.11), we get

$$C_{i,j}^{\gamma,-\gamma} = \begin{cases} C_{i,j}^{\gamma}, & i \leq n, \\ C_{i,j}^{-\gamma}, & i \geq n+1. \end{cases}$$

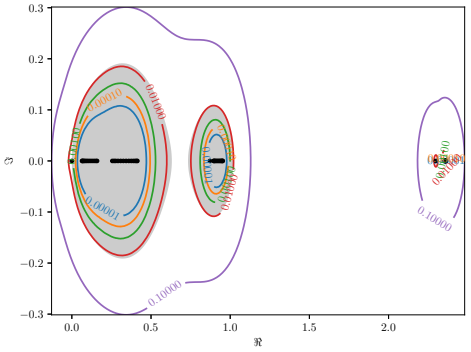
The decay properties of the eigenvectors (5.2) and the symmetry property with respect to γ show that this symmetric system (5.25) has all but two modes localised at the interface.



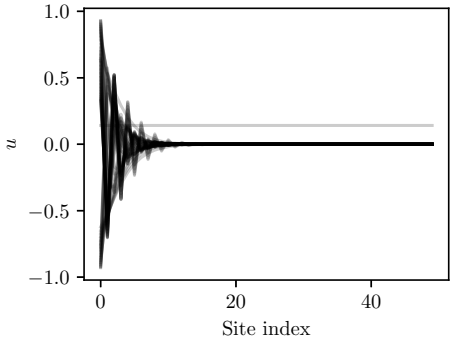
(A) Computation performed for $s_1 = 1, s_2 = 2, s_3 = 3$, and $N = 48$.



(B) Simulation performed with $s_1 = 1, s_2 = 2, s_3 = 3$, and $N = 48$.



(C) Computation performed for $s_1 = 2, s_2 = 3, s_3 = 4$, and $N = 52$.



(D) Simulation performed with $s_1 = 2, s_2 = 3, s_3 = 4$, and $N = 52$.

FIGURE 5.9. Figures A and C show the spectrum of the operator. The green regions consist of all the eigenvalues λ that satisfy $\sum_{j=1}^{3} \text{wind}(\lambda_j, \lambda) \neq 0$. The black dots along the real line denote the spectrum of the gauge capacitance matrix C^γ and the solid blue and orange lines around the spectrum are the ε-pseudospectra for $\varepsilon = 10^k$ and $k = -5, -2$. Figures B and D show the eigenvectors of C^γ.

These interface modes are shown in Figure 5.10, superimposed on one another to portray the general trend.

The case presented here is the choice of γ's that generates localised mode at the middle of the structure as do defected Hermitian interface structures in Section 4. In the next section, we consider the other case, which generates localisation at the edges of the system.

6. Tunable localisation in parity-time symmetric systems

The aim of this section is to consider a mirrored system with two imaginary gauge potentials (opposite to each other as presented briefly in Section 5.5) and study the phase change of the spectrum from purely real to complex when gain and loss are introduced in a balanced way into the system as a function of the gain to loss ratio. This ensures that parity–time ($\mathcal{PT}$-) symmetry is preserved as this ratio is increased. Crucially, the parity–time symmetry of the system is reflected in the gauge capacitance matrix C^γ, ensuring that it is *pseudo–Hermitian*, that is there exists some invertible self-adjoint matrix M so that the adjoint $(C^\gamma)^*$ of C^γ is given by $(C^\gamma)^* = MC^\gamma M^{-1}$. We observe that the eigenmodes of the parity–time symmetric system decouple when going through an exceptional point. Tuning the

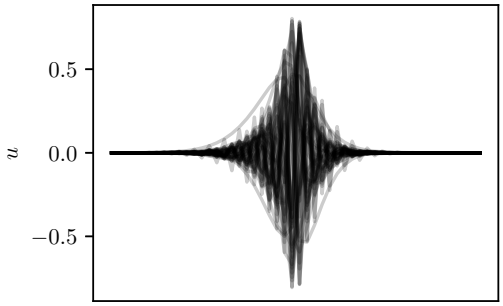


Figure 5.10. Plot of all the eigenmodes localised at the interface associated to a system described by (5.25). The x-axis encodes the site index of the resonators. The simulation is performed with a structure of $N = 50$ resonators, $\ell = s = 1$ and $\gamma = 1$. The two trivial eigenmodes are not shown.

gain-to-loss ratio, we change the system from a phase with unbroken parity-time symmetry to a phase with broken parity-time symmetry where the condensed eigenmodes at one edge are decoupled from the ones at the opposite edge of the structure. To understand this behaviour we extend the standard Toeplitz theory to encompass symmetrical parameter changes across an interface. We show that the intrinsic nature of this switch from unbroken to broken $\mathcal{PT}$-symmetry is due to a change in the topological nature of the mode. Furthermore, we are able to show that as the number of resonators is increased, the amount of tuning required for exceptional points and the corresponding decoupling to occur goes to zero. This leads to an increasingly dense concentration of exceptional points. The results in this section are from [8].

We will only consider systems of equally spaced identical resonators, that is,

$$\ell_i = \ell \in \mathbb{R}_{>0} \text{ for all } 1 \leq i \leq N \quad \text{and} \quad s_i = s \in \mathbb{R}_{>0} \text{ for all } 1 \leq i \leq N-1,$$

and apply an imaginary gauge potential as illustrated in Figure 6.1. On one side, the

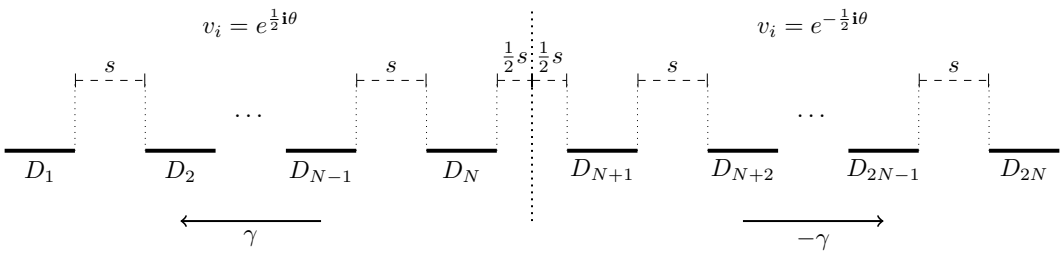


Figure 6.1. A chain of $2N$ one-dimensional identical and equally spaced resonators. Material parameters and sign of the imaginary gauge potentials depend on the resonator's position.

gauge capacitance matrix is given by

$$C^\gamma = \left(\begin{array}{cccccc|cccccc} \alpha+\beta & \eta & & & & & & & & & & \\ \beta & \alpha & \ddots & & & & & & & & & \\ & \ddots & \ddots & & & & & & & & & \\ & & & \alpha & \eta & & & & & & & \\ & & & \beta & \alpha & & \eta & & & & & \\ \hline & & & & & \eta & \alpha & \beta & & & & \\ & & & & & & \eta & \alpha & \ddots & & & \\ & & & & & & & \ddots & \ddots & & & \\ & & & & & & & & & \alpha & \beta & \\ & & & & & & & & & \eta & \alpha+\beta \end{array}\right) \in \mathbb{R}^{2N\times 2N} \tag{6.1}$$

with

$$\alpha = \frac{\gamma}{1-e^{-\gamma}} - \frac{\gamma}{1-e^{\gamma}} = \gamma\coth(\gamma/2), \quad \eta = \frac{-\gamma}{1-e^{-\gamma}}, \quad \beta = \frac{\gamma}{1-e^{\gamma}}, \tag{6.2}$$

because of the sign change of the imaginary gauge potential. On the other side, we have to model the complex (and varying) material parameters. Thus, we consider the *generalised gauge capacitance matrix*

$$C^{\theta,\gamma} = V^\theta C^\gamma \quad \text{with} \quad V^\theta = \left(\begin{array}{c|c} e^{\mathbf{i}\theta} I_N & \mathbf{0} \\ \hline \mathbf{0} & e^{-\mathbf{i}\theta} I_N \end{array}\right) \in \mathbb{C}^{2N\times 2N}. \tag{6.3}$$

The same result as the one stated in Proposition 3.4 holds for the system described by Figure 6.1 when considering the generalised gauge capacitance matrix from (6.3) (generalising the proof presented in [1] is easily achieved by the same procedure as the one used in [2]). Throughout this section, $C^{\theta,\gamma}$ and C^γ are $2N \times 2N$ matrices.

This section will extensively study *non-diagonalisability* of $C^{\theta,\gamma}$.

Definition 6.1. A setup for which $C^{\theta,\gamma}$ is *not* diagonalisable is called an *exceptional point*.

Specifically, we will study setups where the geometry and the imaginary gauge potentials remain fixed and the material parameters (here modelled by θ) lay in a specific range.

6.1. Properties of the generalised gauge capacitance matrix

Let $P \in \mathbb{R}^{2N\times 2N}$ be the anti-diagonal involution, *i.e.*, $P_{ij} = \delta_{i,2N-i+1}$ and $D^\gamma = \operatorname{diag}(1, e^\gamma, \dots, (e^\gamma)^{N-1}, (e^\gamma)^{N-1}, \dots, e^\gamma, 1) \in \mathbb{R}^{2N\times 2N}$. We refer, for instance, to [8] for the precise definitions of pseudo–Hermitian and quasi-Hermitian matrices. Here and elsewhere in this section, M^* denotes the adjoint of M: $(M^*)_{i,j} = \overline{M_{j,i}}$.

Proposition 6.2. *The generalised gauge capacitance matrix has the following symmetry:*

$$PC^{\theta,\gamma}P = \overline{C^{\theta,\gamma}}. \tag{6.4}$$

For the unmodified gauge capacitance matrix C^γ, we have

$$PC^\gamma P = C^\gamma. \tag{6.5}$$

Proposition 6.3. *Let $M^{\theta,\gamma} = PV^\theta D^\gamma$. Then, $M^{\theta,\gamma}$ is invertible and Hermitian and we have*

$$M^{\theta,\gamma}C^{\theta,\gamma} = (C^{\theta,\gamma})^* M^{\theta,\gamma}. \tag{6.6}$$

Since $C^{\theta,\gamma}$ as in (6.3) is pseudo–Hermitian, its spectrum must be invariant under complex conjugation [8], that is,

$$\sigma(C^{\theta,\gamma}) = \overline{\sigma(C^{\theta,\gamma})}.$$

For the case $\theta = 0$, the matrix $C^{0,\gamma} = C^\gamma$ satisfies an even stronger notion of Hermiticity.

Proposition 6.4. *Let $C^\gamma = C^{\theta=0,\gamma}$ as in equation (6.1). Then, C^γ is quasi-Hermitian with* metric operator *D, that is,*

$$D^{-1}C^\gamma = (C^\gamma)^* D^{-1}. \tag{6.7}$$

As a quasi-Hermitian matrix, C^γ is diagonalisable with real spectrum.

Finally, we characterise the kernel of $C^{\theta,\gamma}$.

Lemma 6.5. *For any $\gamma > 0$ and $\theta \in [0, 2\pi)$, we have $(1, \dots, 1)^\top \in \ker C^{\theta,\gamma} \subset \mathbb{R}^{2N}$.*

As a consequence of Proposition 6.6, the eigenspaces of $C^{\theta,\gamma}$ are always one-dimensional. Consequently, the kernel of $C^{\theta,\gamma}$ is also one-dimensional and is exactly the span of $\mathbf{1} = (1, \dots, 1)^\top$.

The fact that $C^{\theta,\gamma}$ is tridiagonal allows us to determine the eigenvectors recursively. The symmetry of $C^{\theta,\gamma}$ across the interface in the middle will yield very similar forms for the first and second half of its eigenvectors. The eigenvalues will then be characterised by a compatibility condition across this interface.

Proposition 6.6. *Let the affine transformation $\mu^\theta : \mathbb{C} \to \mathbb{C}$ be defined by*

$$\mu^\theta(\lambda) \coloneqq \frac{e^{-\mathbf{i}\theta}\lambda - \alpha}{2\sqrt{\beta\eta}} = e^{-\mathbf{i}\theta}\lambda\frac{1}{\gamma}\sinh\frac{\gamma}{2} - \cosh\frac{\gamma}{2}. \tag{6.8}$$

For $\lambda \in \mathbb{C}$ an eigenvalue of $C^{\theta,\gamma}$, the corresponding eigenvector is given by $\boldsymbol{v} = (\boldsymbol{x}, \boldsymbol{y})^\top$, where

$$\begin{aligned} \boldsymbol{x} &= \left(P_0(\mu^\theta(\lambda)), \left(e^{-\frac{\gamma}{2}}\right) P_1(\mu^\theta(\lambda)), \cdots, \left(e^{-\frac{\gamma}{2}}\right)^{N-1} P_{N-1}(\mu^\theta(\lambda))\right)^\top, \\ \boldsymbol{y} &= C_1 \left(\left(e^{-\frac{\gamma}{2}}\right)^{N-1} P_{N-1}(\mu^{-\theta}(\lambda)), \cdots, \left(e^{-\frac{\gamma}{2}}\right) P_1(\mu^{-\theta}(\lambda)), P_0(\mu^{-\theta}(\lambda))\right)^\top. \end{aligned} \tag{6.9}$$

Here, $P_n(x) = U_n(x) + e^{-\frac{\gamma}{2}}U_{n-1}(x)$ is the sum of two Chebyshev polynomials of the second kind, with $P_0 = 1$. Specifically, $U_{n+1}(x) \coloneqq 2xU_n(x) - U_{n-1}(x)$ for $n \geq 1$ with $U_0(x) = 1$ and $U_1(x) = 2x$. Furthermore, we have

$$C_1 = e^{-\frac{\gamma}{2}}\frac{P_N(\mu^\theta(\lambda))}{P_{N-1}(\mu^{-\theta}(\lambda))} = e^{\frac{\gamma}{2}}\frac{P_{N-1}(\mu^\theta(\lambda))}{P_N(\mu^{-\theta}(\lambda))}, \tag{6.10}$$

which yields the following characterisation of the spectrum of $C^{\theta,\gamma}$:

$$\frac{P_N(\mu^\theta(\lambda))P_N(\mu^{-\theta}(\lambda))}{P_{N-1}(\mu^\theta(\lambda))P_{N-1}(\mu^{-\theta}(\lambda))} = e^\gamma. \tag{6.11}$$

Namely, $\lambda \in \mathbb{C}$ is an eigenvalue of $C^{\theta,\gamma}$ if and only if it satisfies (6.11)*. Moreover, its corresponding eigenspace is always one-dimensional.*

These final two facts immediately yield the following characterisation for the exceptional points of $C^{\theta,\gamma}$.

Corollary 6.7. *An exceptional point occurs when* (6.11) *has less than $2N$ distinct solutions.*

We aim to use this corollary to show that for a given $\theta > 0$, any nonreal eigenvalue $\lambda \in \mathbb{C} \setminus \mathbb{R}$ of $C^{\theta,\gamma}$ must have passed through an exceptional point. However, we must first formalise the notion of an eigenvalue "having passed through" an exceptional point. To that end, we would like to associate each eigenvalue λ_i of $C^{\theta,\gamma}$ with some corresponding continuous path $\lambda_i(\theta)$ such that $\lambda_i(\theta)$ is an eigenvalue of $C^{\theta,\gamma}$ for all values of θ and all $i = 1, \dots, 2N$. However, precisely because exceptional points occur, we cannot choose these paths in a canonical fashion, as at these exceptional points, two eigenvalue paths $\lambda_i(\theta)$ and $\lambda_j(\theta)$, $i \neq j$, meet and cannot be distinguished. What we can do is the following: Let $0 < \theta' < \frac{\pi}{2}$ be fixed. For any simple eigenvalue λ of $C^{\theta',\gamma}$, we can then define the maximal unique continuous *eigenvalue path* $\lambda : \theta \in [\theta_0, \theta'] \to \mathbb{C}$ such that $\lambda(\theta)$ is always an eigenvalue of $C^{\theta,\gamma}$ for any $\theta \in [\theta_0, \theta']$ and $\lambda(\theta') = \lambda$. θ_0 is chosen to be either the largest $\theta < \theta'$ such that $\lambda(\theta)$ is an exceptional point, or zero - whichever is greater.

For some $0 < \theta' < \frac{\pi}{2}$ and $\lambda \in \mathbb{C}$ eigenvalue of $C^{\theta',\gamma}$, we can then say that λ *has passed through an exceptional point* if and only if θ_0 is greater than zero. Note also that because C^γ is diagonalisable, $\lambda(0)$ is never an exceptional point.

We can now state the following result.

COROLLARY 6.8. *Let $0 < \theta' < \frac{\pi}{2}$ and let $\lambda \in \mathbb{C}$ be an eigenvalue of $C^{\theta,\gamma}$. If λ is in $\mathbb{C} \setminus \mathbb{R}$, it must have passed through an exceptional point.*

This corollary is very useful because it allows us to prove the existence of exceptional points merely from the fact that some eigenvalues are nonreal.

The final result of this section characterises the relation between the factors C_λ and $C_{\overline{\lambda}}$ for complex conjugate pairs $\lambda, \overline{\lambda}$ of $C^{\theta,\gamma}$.

COROLLARY 6.9. *Let $\lambda, \overline{\lambda}, \in \mathbb{C}$ be a pair of eigenvalues of $C^{\theta,\gamma}$ and let $C_\lambda, C_{\overline{\lambda}}$ be the corresponding factors as defined in (6.10). Then, we have*

$$\overline{C_\lambda} C_{\overline{\lambda}} = 1. \tag{6.12}$$

In particular, we have $|C_\lambda| = 1$ for $\lambda \in \mathbb{R}$.

6.2. Eigenvalue of the generalised gauge capacitance matrix

In this section, we study the eigenvalues of the generalised gauge capacitance matrix $C^{\theta,\gamma}$ for the system described in the previous section. We prove that for small θ all the eigenvalues of $C^{\theta,\gamma}$ are real, which corresponds to the coupled regime. We also prove existence and density of exceptional points. Finally, we approximate the locations of eigenvalues. Understanding the movement of eigenvalues will prove to be a crucial prerequisite to understand the decoupling behaviour of the eigenvectors in the next section.

Coupled regime. This subsection is dedicated to the case where all eigenvalues of $C^{\theta,\gamma}$ are real. We will show that for small θ the eigenvalues behave similarly to the ones of the gauge capacitance matrix $C^{\theta=0,\gamma}$. Consequently, as we will show in Section 6.3, also the eigenvectors of $C^{\theta,\gamma}$ will have a form similar to that of $C^{\theta=0,\gamma}$.

PROPOSITION 6.10. *For any $N \in \mathbb{N}$ and $\gamma > 0$, there exists an $\varepsilon > 0$ such that for $0 \leq \theta < \varepsilon$ all the eigenvalues of $C^{\theta,\gamma}$ are real. For a real eigenvalue λ of $C^{\theta,\gamma}$, the eigenvector $= (\boldsymbol{x}, \boldsymbol{y})^\top$ decomposed as in Proposition 6.6, has the following symmetry:*

$$\boldsymbol{y} = e^{\mathbf{i}\phi} P \overline{\boldsymbol{x}} \tag{6.13}$$

for some $\phi \in [0, 2\pi)$. In particular, we have $|\boldsymbol{x}^{(j)}| = |\boldsymbol{y}^{(2N+1-j)}|$ for $j = 1, \dots N$.

Existence of exceptional points. In this subsection, our aim is to show that regardless of N and γ, all eigenvalues must pass through an exceptional point as θ is increased from 0 to $\frac{\pi}{2}$.

Theorem 6.11. *Let $\gamma > 0$ and $N \in \mathbb{N}$. Then, all but two eigenvalues $\lambda \in \mathbb{C}$ of $C^{\theta,\gamma}$ for $\theta = \frac{\pi}{2}$ must have passed through an exceptional point. The remaining two eigenvalues experience an exceptional point at $\theta = \frac{\pi}{2}$.*

In line with Corollary 6.8, in order to show that an eigenvalue λ of $C^{\theta,\gamma}$ for $\theta = \frac{\pi}{2}$ has passed through an exceptional point, it is sufficient to show that λ lies in $\mathbb{C} \setminus \mathbb{R}$. Indeed, for $\theta = \frac{\pi}{2}$ we will show that the spectrum of $C^{\theta,\gamma}$ lies entirely on the imaginary axis. All nonzero eigenvalues must thus have gone through an exceptional point. Two eigenvalues will turn out to be zero, yielding another exceptional point exactly at $\theta = \frac{\pi}{2}$.

We will need a good understanding of the zeros of Chebyshev polynomials.

PROPOSITION 6.12. *$\mathcal{S}(\lambda)$ has exactly $(2N-2)$ distinct real zeros and a double zero $\lambda = 0$.*

The main idea of the proof is to exploit the heavily interlaced nature of the Chebyshev polynomials, which will prove to be a robust source of zeros of their composites. This will allow us to guarantee and bound N real zeros for P_N and $(N-1)$ real zeros for $P_N + P_{N-1}$. The evenness of $\mathcal{S}(\lambda)$ will then allow us to use these results to guarantee zeros of $\mathcal{S}$ as well.

We can then combine the arguments of this subsection to prove Theorem 6.11.

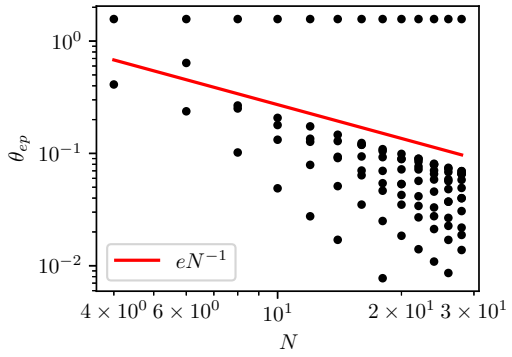


FIGURE 6.2. Distribution of the exceptional points for varying N. For any N, the system exhibits a trivial exceptional point at $\theta = \frac{\pi}{2}$. All other exceptional points concentrate in the interval $[0, e/N]$ and become increasingly dense as N grows.

Proof of Theorem 6.11. For $\theta = 0$, all the eigenvalues are real and for $\theta = \frac{\pi}{2}$ all but two eigenvalues are purely imaginary by Proposition 6.12. The two not purely imaginary eigenvalues are both zero, causing an exceptional point by Corollary 6.7. By Corollary 6.8, all the purely imaginary, nonzero eigenvalues must have passed through an exceptional point by $\theta = \frac{\pi}{2}$. Furthermore, these eigenvalues are distinct, which ensures that they passed through that exceptional point *before* $\theta = \frac{\pi}{2}$. ∎

Asymptotic density of exceptional points. We are now interested in showing that exceptional points do not only occur (as shown in the previous subsection) but also cluster creating a parameter region with high density of such points. Many of the results developed in this subsection will also be used in Section 6.2 and Section 6.3 as they enable the asymptotic characterisation of the eigenvalue locations and eigenvector growth.

Theorem 6.13. *Let $0 < \theta < \frac{\pi}{2}$ and $\gamma > 0$ be fixed. Then, there exists an $N_0 \in \mathbb{N}$ such that for every $N \geq N_0$, the corresponding $C^{\theta,\gamma}$ has exactly two real eigenvalues.*

By Corollary 6.8, this ensures that all other $2N-2$ eigenvalues in $\mathbb{C} \setminus \mathbb{R}$ must have already passed through an exceptional point before θ.

The building blocks for this result start with a helpful reformulation of the characterisation (6.11) for real eigenvalues.

PROPOSITION 6.14. *$\lambda \in \mathbb{R}$ is a real eigenvalue of $C^{\theta,\gamma}$ if and only if*

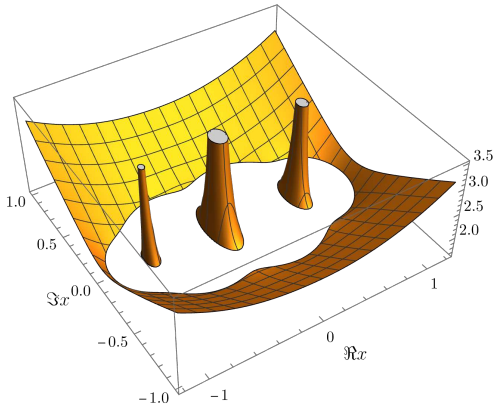
$$\left| \frac{P_N(\mu^\theta(\lambda))}{P_{N-1}(\mu^\theta(\lambda))} \right| = e^{\frac{\gamma}{2}}. \tag{6.14}$$

The transformation $\mu^\theta(\lambda) = e^{-\mathrm{i}\theta} \lambda \frac{1}{\gamma} \sinh \frac{\gamma}{2} - \cosh \frac{\gamma}{2}$ maps the real line $\mathbb{R}$ onto a line $\mu^\theta(\mathbb{R})$ in $\mathbb{C}$ rotated by $-\theta$ around the point $-\cosh \frac{\gamma}{2}$. This provides a very geometric view of the zeros of equation (6.14). In fact, the real spectrum of $C^{\theta,\gamma}$ corresponds to intersections of the line $\mu^\theta(\mathbb{R})$ and a level set of $\mu \mapsto |\frac{P_N(\mu)}{P_{N-1}(\mu)}|$:

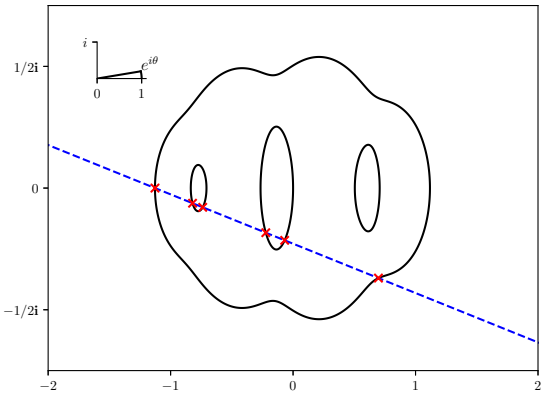
$$\sigma(C^{\theta,\gamma}) \cap \mathbb{R} = \mu^\theta(\mathbb{R}) \cap \left\{ \mu \in \mathbb{C} : |\frac{P_N(\mu)}{P_{N-1}(\mu)}| = e^{\frac{\gamma}{2}} \right\}.$$

Thus, in order to understand the real eigenvalues of $C^{\theta,\gamma}$, it is crucial to understand the level sets of $|\frac{P_N(\mu)}{P_{N-1}(\mu)}|$. We begin by recalling a well-known equivalent definition of the Chebyshev polynomials:

$$U_n(\mu) = \frac{a(\mu)^{n+1} - a(\mu)^{-(n+1)}}{2\sqrt{\mu+1}\sqrt{\mu-1}},$$



(A) Graph of $\mathbb{C} \ni \mu \mapsto |\frac{P_N(\mu)}{P_{N-1}(\mu)}|$ cut off by the plane $\mathbb{C} \times \{e^{\frac{\gamma}{2}}\}$.



(B) Intersection of $\mu^\theta(\mathbb{R})$ (in blue dashed) with the level set $\{\mu \in \mathbb{C} : |\frac{P_N(\mu)}{P_{N-1}(\mu)}| = e^{\frac{\gamma}{2}}\}$ (in black). The latter can be seen in Figure 6.3a. Intersection points are shown in red. The preimage of these are the real eigenvalues of $C^{\theta,\gamma}$.

FIGURE 6.3. Geometrical interpretation of the eigenvalues of $C^{\theta,\gamma}$ as given by Proposition 6.14. In this view, we can also clearly see the exceptional points, where two real eigenvalues meet and become complex. Namely, this happens exactly when $\mu^\theta(\mathbb{R})$ goes from passing through one of the inner regions in (B) to moving past them and two red crosses meet.

where $a(\mu) = \mu + \sqrt{\mu+1}\sqrt{\mu-1}$.

Eigenvalue locations. In this subsection, we aim to understand the position of the eigenvalues in the complex plane. This will prove crucial in understanding the behaviour of the eigenvectors in Section 6.3. As we will observe, for a fixed θ and increasing N, they move arbitrarily close to the two line segments $(\mu^\theta)^{-1}([-1,1]) \cup (\mu^{-\theta})^{-1}([-1,1])$.

The following result holds.

PROPOSITION 6.15. *Let $0 < \theta < \pi/2$ and let $\gamma > 0$ be fixed. For any $\varepsilon > 0$ small enough, there exists an $N_0 \in \mathbb{N}$ such that for any $N \geq N_0$, all but exactly two eigenvalues of $C^{\theta,\gamma}$ lie in an ε-neighbourhood of $K \coloneqq (\mu^\theta)^{-1}([-1,1]) \cup (\mu^{-\theta})^{-1}([-1,1])$. Indeed, because of the conjugation symmetry of eigenvalues, we have*

$$\left|\sigma(C^{\theta,\gamma}) \cap B_\varepsilon((\mu^{\sigma\cdot\theta})^{-1}([-1,1]))\right| = N - 1, \tag{6.15}$$

for $\sigma = \pm 1$.

6.3. Eigenvectors of the generalised gauge capacitance matrix

As shown in Section 5, systems with an imaginary gauge potential are known for the presence of skin effect, *i.e.*, the condensation of the eigenvectors at one edge of the system. This condensation is exponential [6]. The system studied here has a much more peculiar property. The symmetric change of sign in the gauge potential implies that the condensation happens on both edges of the system for small values of θ or N. Nevertheless, the non-Hermiticity introduced by θ can change this symmetry. The exponential nature of the modes has been shown to be caused by the Fredholm index of the Toeplitz operator associated to the system. The system studied here presented in Figure 6.1 does not yield a Toeplitz matrix, nevertheless we will show that the same theory can be modified to be used in this situation as well.

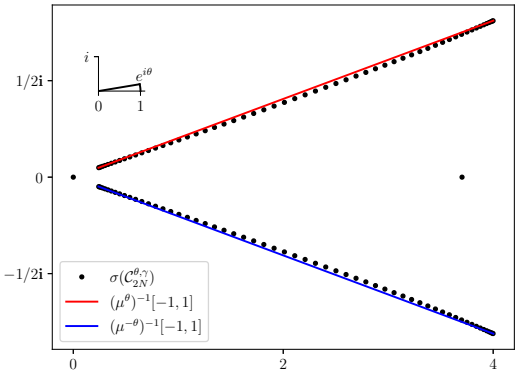


FIGURE 6.4. Eigenvalue locations close to the two line segments $(\mu^{\theta})^{-1}([-1,1]) \cup (\mu^{-\theta})^{-1}([-1,1])$ for $\theta = 0.2$, $\gamma = 1$ and $N = 60$.

Exponential decay and growth. As our matrix $C^{\theta,\gamma}$ is split into two parts by an interface we define the *upper and lower symbols* of $C^{\theta,\gamma}$ as

$$\begin{aligned} f_{\pm}^{\theta} : \mathbb{T}^1 &\to \mathbb{C} \\ e^{\mathbf{i}\phi} &\mapsto e^{\pm\mathbf{i}\theta}(\beta e^{\pm\mathbf{i}\phi} + \alpha + \eta e^{\mp\mathbf{i}\phi}). \end{aligned} \tag{6.16}$$

We further define the *upper and lower regions of topological convergence* as

$$E_{\pm}^{\theta} = \{z \in \mathbb{C} : \pm \operatorname{wind}(f_{\pm}^{\theta}, z) < 0\}, \tag{6.17}$$

where $\operatorname{wind}(f_{\pm}^{\theta}, z)$ denotes the winding number of $f_{\pm}^{\theta}$ around z.

These concepts are closely linked to our formalism based on Chebyshev polynomials. The following result holds.

LEMMA 6.16. *We have*

$$E_{\pm}^{\theta} = \left\{ (\mu^{\pm\theta})^{-1}(a^{-1}(re^{\mathbf{i}\phi})) \text{ for } r \in [1, e^{\gamma/2}), \phi \in [0, 2\pi) \right\}.$$

By Lemma 6.16 it makes thus sense to lighten the notation and use $E^{\theta} = E_{+}^{\theta}$ and $E^{-\theta} = E_{-}^{\theta}$.

Lemma 6.16 also justifies calling $E^{\pm\theta}$ "regions of topological convergence". Namely, for an eigenpair $(\lambda, \boldsymbol{v})$ of $C^{\theta,\gamma}$, Proposition 6.6 gives the following form for the eigenvector:

$$\boldsymbol{v} = (\boldsymbol{x}^{(1)}, \dots, \boldsymbol{x}^{(N)}, \boldsymbol{y}^{(1)}, \dots, \boldsymbol{y}^{(N)})^{\top}$$

with $\boldsymbol{x}^{(j)} = (e^{-\frac{\gamma}{2}})^{j-1} P_{j-1}(\mu^{\theta}(\lambda))$ and $\boldsymbol{y}^{(j)} = (e^{-\frac{\gamma}{2}})^{N-j} P_{N-j}(\mu^{-\theta}(\lambda))$.

The rates of growth for the left and right parts of this eigenvector are then given by

$$\frac{\boldsymbol{x}^{(j+1)}}{\boldsymbol{x}^{(j)}} = e^{-\frac{\gamma}{2}} \frac{P_j(\mu^{\theta}(\lambda))}{P_{j-1}(\mu^{\theta}(\lambda))}, \qquad \frac{\boldsymbol{y}^{(j+1)}}{\boldsymbol{y}^{(j)}} = e^{\frac{\gamma}{2}} \frac{P_{j-1}(\mu^{-\theta}(\lambda))}{P_j(\mu^{-\theta}(\lambda))}.$$

Focusing on the left part, we notice that its asymptotic growth behaviour is determined by whether $|\frac{P_j(\mu^{\theta}(\lambda))}{P_{j-1}(\mu^{\theta}(\lambda))}|$ is smaller or larger than $e^{\frac{\gamma}{2}}$. Furthermore, we have $\frac{P_j(\mu^{\theta}(\lambda))}{P_{j-1}(\mu^{\theta}(\lambda))} \to a(\mu^{\theta}(\lambda))$. $\boldsymbol{x}$ thus decays or grows asymptotically exactly if $|a(\mu^{\theta}(\lambda))|$ is smaller or larger than $e^{\frac{\gamma}{2}}$, respectively. But, by Lemma 6.16, we can see that λ lies in E^{θ} if and only if $|a(\mu^{\theta}(\lambda))| < e^{\frac{\gamma}{2}}$, justifying our naming.

For $\boldsymbol{y}$ the rate of growth is exactly the inverse of the rate of growth of $\boldsymbol{x}$ with $\mu^{\theta}(\lambda)$ replaced by $\mu^{-\theta}(\lambda)$. The above reasoning thus also holds for $\boldsymbol{y}$ with "growth" and "decay" as well as the sign of θ is flipped.

By Proposition 6.15, we know the approximate locations of the eigenvalues of $C^{\theta,\gamma}$. We will now make use of that and the topological convergence to formally prove the above intuition.

Theorem 6.17. *Let $0 < \theta < \pi/2$, $\gamma > 0$ and let N be large enough*[1]*. Fix, furthermore, a $0 < \sigma \ll 1$. Consider an eigenpair $(\lambda, \boldsymbol{v})$ of $C^{\theta,\gamma}$ fulfilling Proposition 6.6. Then, one of the following three cases realises:*

(i) If $\lambda \in B_\sigma(\partial E^\theta \cup \partial E^{-\theta}) =: \Theta$, then either $\lambda = 0$ and $\boldsymbol{v} = \mathbf{1}$ or no conclusion is made;

(ii) If $\lambda \in E^\theta \cap E^{-\theta} \setminus \Theta$, then there exist some $B_1, B_2, C_1, C_2 > 0$ independent of N so that

$$|\boldsymbol{v}^{(j)}| < C_1 e^{-B_1 \frac{j\gamma}{2}} \quad \text{and} \quad |\boldsymbol{v}^{(2N+1-j)}| < C_2 e^{-B_2 \frac{j\gamma}{2}},$$

for $1 \leq j \leq N$. In particular, if also $\lambda \in \mathbb{R}$, then $C_1 = C_2$ and $B_1 = B_2$.

(iii) If $\lambda \in E^\theta \triangle E^{-\theta} \setminus \Theta$, then there exit some $B, C > 0$ independent of N so that

$$|\boldsymbol{v}^{(j)}| < C e^{-B \frac{j\gamma}{2}} \quad \text{if } \lambda \in E^\theta,$$
$$|\boldsymbol{v}^{(2N+1-j)}| < C e^{-B \frac{j\gamma}{2}} \quad \text{if } \lambda \in E^{-\theta},$$

for $1 \leq j \leq 2N$.

In particular, for $\frac{\pi}{4} \leq \theta \leq \frac{\pi}{2}$, case (2) never realises for N large enough.

The implications of Theorem 6.17 are important as it shows that the eigenvectors of $C^{\theta,\gamma}$ are not only exponentially decaying or growing but also that the non-Hermiticity introduced by θ manifests itself at a macroscopic level as a decoupling of the eigenvectors. While for $\theta = 0$ the eigenvectors always present a symmetric exponential decay, the non-Hermiticity introduced by $\theta > 0$ brings the eigenvalue to eventually migrate to the complex plane and out of one of the two regions E^θ or $E^{-\theta}$. As a consequence of this, the symmetry is broken. It is also interesting to notice that this process happens pairwise. Since $C^{\theta,\gamma}$ is pseudo–Hermitian, the eigenvalues come in complex conjugated pairs and, as θ is varying, they meet pairwise at an exceptional point. After the exceptional points, one of the eigenvectors will be decaying while the other will be increasing. The decoupling of the eigenvectors is illustrated in Figure 6.5.

From the proof of Theorem 6.17, we can read out the decay or growth rate of the eigenvectors.

	Upper branch		Lower branch	
	$\lambda \in E^{-\theta}$	$\lambda \notin E^{-\theta}$	$\lambda \in E^{\theta}$	$\lambda \notin E^{\theta}$
$\boldsymbol{x}$	$e^{-\gamma/2}$	$e^{-\gamma/2}$	< 1	> 1
$\boldsymbol{y}$	> 1	< 1	$e^{\gamma/2}$	$e^{\gamma/2}$

TABLE 6.1. Approximated decay and growth rate of the left and right part of an eigenvector of the capacitance matrix depending on the location of the corresponding eigenvalue. Values greater than 1 correspond to growth and lower than 1 correspond to decay. Here, upper and lower branches refer respectively to $\lambda \in B_\varepsilon((\mu^{\pm\theta})^{-1}([-1,1]))$ as in Proposition 6.15.

[1]Specifically so that ε from Proposition 6.15 is smaller than $\sqrt{\alpha+\beta} - \sqrt{\beta+\eta}$ and thus $B_\varepsilon((\mu^{\pm\theta})^{-1}([-1,1])) \subset E^{\pm\theta}$.

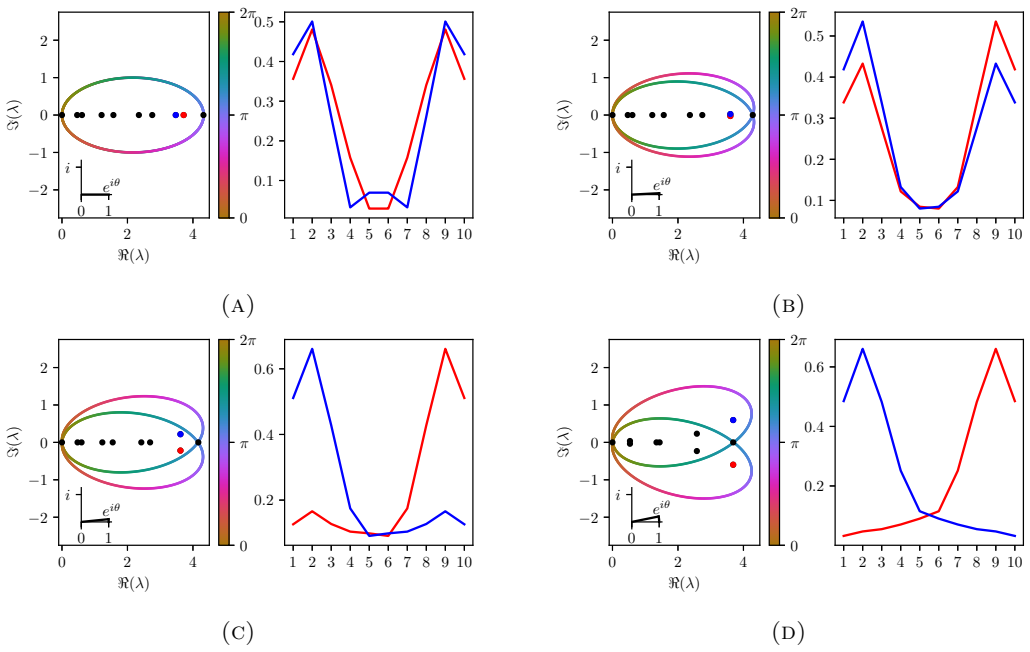


Figure 6.5. Decoupling of the eigenvectors of the gauge capacitance matrix. The macroscopic behaviour of the eigenvectors (exponential decay/growth) is predicted by the location of the eigenvalues in the complex plane with respect to the region of topological convergence defined in (6.17) displayed here as trace of (6.16). Looking at the two highlighted eigenvalues (red and blue), Figure (A-C) correspond to item (ii) in Theorem 6.17 while (D) corresponds to item (i).

Topological origin. This section is devoted to illustrating the topological origin of the specific condensation properties of $C^{\theta,\gamma}$'s eigenvectors that have been shown in Theorem 6.17. Especially, in Theorem 6.17 we demonstrate the condensation properties by the specific behaviours of $a(\mu)$, while here we concentrate on the Fredholm index theory of the symbol of the Toeplitz operator, which directly leads to considering $E^{\pm\theta}$ in (6.17) defined by symbols $f^{\theta}_{\pm}$. Instead of considering the eigenvector of a Toeplitz operator, we analyse the pseudoeigenvector of the corresponding matrix $C^{\theta,\gamma}$ to keep the boundary of the system. We first present the topological origin of the case (2) in Theorem 6.17.

Theorem 6.18. *Suppose that $\lambda \in E^{\theta} \cap E^{-\theta}$. For some $0 < \rho < 1$ and sufficiently large N, there exists a pseudoeigenvector $\boldsymbol{v}$ of $C^{\theta,\gamma}$ satisfying*

$$\frac{\|(C^{\theta,\gamma} - \lambda)\boldsymbol{v}\|}{\|\boldsymbol{v}\|} \leq \max(C_1, NC_2)\rho^{N-1}$$

such that

$$\begin{cases} \dfrac{|\boldsymbol{v}_j|}{\max_i |\boldsymbol{v}_i|} \leq C_3 N \rho^{j-1}, \quad j = 1, \cdots, N, \\ \dfrac{|\boldsymbol{v}_j|}{\max_i |\boldsymbol{v}_i|} \leq C_3 N \rho^{2N-j}, \quad j = N+1, \cdots, 2N, \end{cases}$$

where C_1, C_2, C_3 are constants independent of N.

Now, we present the topological origin of case (iii) in Theorem 6.17.

Theorem 6.19. *Suppose that $\lambda \in E^\theta \triangle E^{-\theta}$. For some $0 < \rho < 1$ and sufficiently large N, there exists a pseudoeigenvector $\boldsymbol{v}$ of $C^{\theta,\gamma}$ satisfying*

$$\frac{\|(C^{\theta,\gamma} - \lambda)\boldsymbol{v}\|}{\|\boldsymbol{v}\|} \leq \max(C_1, NC_2)\rho^{N-1}$$

such that

$$\begin{cases} \dfrac{|\boldsymbol{v}_j|}{\max_i |\boldsymbol{v}_i|} \leq C_3 N \rho^{j-1}, \quad j = 1, \cdots, 2N, \ \text{if } \lambda \in E^\theta, \\ \dfrac{|\boldsymbol{v}_j|}{\max_i |\boldsymbol{v}_i|} \leq C_3 N \rho^{2N-j}, \quad j = 1, \cdots, 2N, \ \text{if } \lambda \in E^{-\theta}, \end{cases}$$

where C_1, C_2, C_3 are constants independent of N.

7. Generalised Brillouin zone for non-reciprocal problems

Various physical systems are modelled through Toeplitz matrices and operators and variations thereof. In the previous sections, we have seen systems of subwavelength resonators in (classical) one-dimensional wave physics [1, 3] but also other system as the tight-binding model with nearest neighbour approximation in condensed matter theory [24, 47, 48, 51, 60] falls into this category. The tools developed in this section apply to all of these models.

System are typically constituted by resonators or particles all of which we will call sites in this section.

7.1. Physical systems and their mathematical models

We assume that the interactions between the sites repeat periodically with period k, so that if the interactions are all the same $k = 1$ holds. We denote by L the spatial period of recurrence.

In all of the aforementioned examples, the following modelling applies:

Finite systems: are constituted by a finite number of sites. These are modelled by tridiagonal k-Toeplitz matrices;

Semi-infinite systems: are constituted by an infinite number of sites but only in one direction from a fixed origin. These are modelled by tridiagonal k-Toeplitz operators;

Infinite systems: are constituted by an infinite number of sites where no point is a privileged choice of origin. These are modelled by tridiagonal k-Laurent operators.

In the literature, these three cases are also known as open boundary conditions, semi-infinite boundary conditions, and periodic boundary conditions [51]. The subsequent theory recently introduced in [7] applies to all physical systems that can be modelled through these mathematical objects.

7.2. Floquet–Bloch theory in the Hermitian case

Floquet–Bloch theory is the appropriate tool for analysing periodic systems in the Hermitian case, in particular because Floquet's theorem relates the spectra of the infinite operator to the spectra of the corresponding quasiperiodic operators. Here, the Hermiticity of the system is reflected in the Hermiticiy of the matrices and operators, *i.e.*, $M = M^* \coloneqq \overline{M}^\top$.

One may quickly notice that when studying a tridiagonal system associated to a tridiagonal k-Laurent operator $L(f)$ (defined in Section 2.5) and denoting by α the quasiperiodicity, the operator associated to the Floquet-transformed system is simply given by the symbol $f(e^{-\mathbf{i}\alpha\,\mathsf{L}})$. Using [5, Theorem 2.8], we can find that

$$\sigma(L(f)) = \bigcup_{\alpha \in Y^*} \sigma(f(e^{-\mathbf{i}\alpha\,\mathsf{L}})), \tag{7.1}$$

where $Y^* \coloneqq [-\pi/\mathsf{L}, \pi/\mathsf{L})$ is the first *Brillouin zone*. This exactly mirrors the Floquet–Bloch decomposition of the spectrum for a periodic self-adjoint elliptic operator.

Combining the Bauer–Fike theorem together with [17, Corollary 6.16] shows that for these Hermitian systems, the spectrum of the finite system converges to the spectrum of the infinite one, meaning that

$$\sigma(T_{mk}(f)) \xrightarrow{m\to\infty} \sigma(L(f)) \tag{7.2}$$

in the Hausdorff sense. Recall that $T_{mk}(f)$ denotes a k-Toeplitz matrix of order mk and $T(f)$ a k-Toeplitz operator as defined in Section 2.5. On the other side, the Hermiticity of the symbol immediately implies that

$$\sigma(T(f)) = \sigma(L(f)).$$

7.3. The non-reciprocal case

We now shift our focus to the case of non-reciprocal systems, that is the case where the matrices and operators we are working with are no longer Hermitian. Non-reciprocal systems are peculiar for having eigenmodes which are condensed on one edge of the system as shown in Section 5 (see also [1, 64]) and therefore present a privileged choice of origin, making a semi-infinite system the natural corresponding physical structure.

We consider the following prototypical example:

$$f(z) = \begin{pmatrix} 0 & -2 + -\frac{z}{10} \\ -\frac{9}{10} + \frac{1}{z} & 0 \end{pmatrix}, \tag{7.3}$$

and look at the spectra plotted in Figure 7.1.

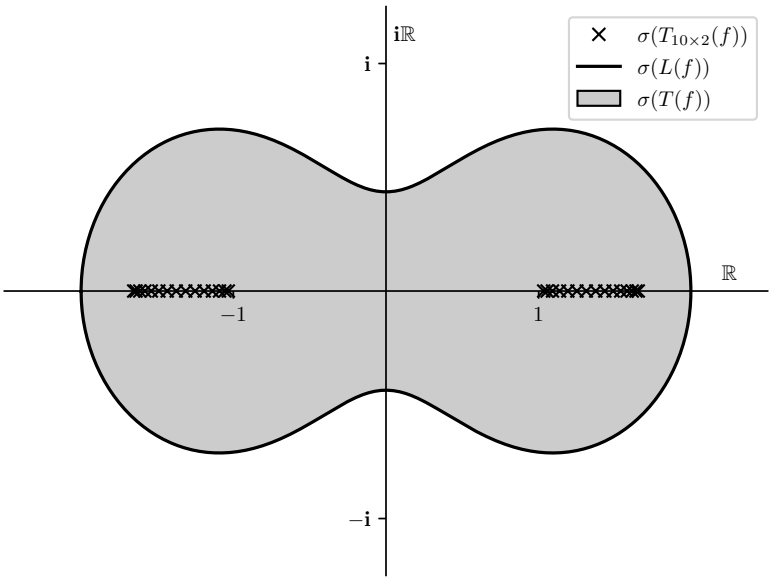


Figure 7.1. Spectra of the different mathematical objects related to the symbol f from (7.3).

We observe the following:

(i) The symbol $f(z)$ is no longer collapsed (see Lemma 2.17) and now has nonempty interior. This will prove to be the crucial difference between the non-reciprocal and the reciprocal cases, as in the non-reciprocal setting the spectra $\sigma(L(f))$ and $\sigma(T(f))$ do not agree anymore.

(ii) $\sigma(L(f)) = \bigcup_{\alpha\in Y^*} \sigma(f(e^{-\mathbf{i}\alpha\,\mathsf{L}}))$ still holds also in the non-reciprocal case. Nevertheless, non-reciprocal systems have a privileged choice of origin as they present an exponential decay in their eigenmodes. One would wish that the Floquet–Bloch decomposition could model this decay and would cover $\sigma(T(f))$ and not only $\sigma(L(f))$.

(iii) The convergence $\sigma(T_{mk}(f)) \xrightarrow{m\to\infty} \sigma(L(f))$ does not hold anymore and neither does $\sigma(T_{mk}(f)) \xrightarrow{m\to\infty} \sigma(T(f))$. The spectrum of $T_{mk}(f)$ is purely real while the ones of $L(f)$ and of $T(f)$ have nontrivial imaginary parts.

In the following sections, we will address the issues (ii) and (iii) above and resolve both of them.

7.4. k-Toeplitz operators and the generalised Brillouin zone

As it can be seen for the non-Hermitian skin effect in Section 5, the classical Floquet–Bloch transform with real quasiperiodicities $\alpha \in Y^*$ fails to capture non-reciprocal decay and only covers the k-Laurent operator $L(a) \subsetneq T(a)$ (identity (7.1) still holds). In order to rectify this, we extend the allowable quasiperiodicities into the complex plane. This is a natural extension. Indeed, considering the quasiperiodicity condition

$$u(x + \mathsf{L}) = e^{\mathbf{i}\,\mathsf{L}\,\alpha} u(x),$$

one immediately notices that decaying functions (as are the eigenmodes of non-reciprocal systems) cannot be described through this relation for $\alpha \in \mathbb{R}$. This would, however, be the case if we allow $\alpha \in \mathbb{C}$.

Definition 7.1. For a tridiagonal k-Toeplitz operator with symbol

$$f : z \mapsto \begin{pmatrix} a_1 & b_1 & 0 & \cdots & 0 & c_k z \\ c_1 & a_2 & b_2 & & & 0 \\ 0 & c_2 & \ddots & \ddots & & \vdots \\ \vdots & & \ddots & \ddots & b_{k-2} & 0 \\ 0 & & & c_{k-2} & a_{k-1} & b_{k-1} \\ b_k z^{-1} & 0 & \cdots & 0 & c_{k-1} & a_k \end{pmatrix} \tag{7.4}$$

with nonzero off-diagonal entries we define the *non-reciprocity rate* as

$$\Delta = \ln \prod_{j=1}^{k} \left| \frac{b_j}{c_j} \right|. \tag{7.5}$$

Furthermore, we define the *generalised Brillouin zone* to be

$$\mathcal{B} = \left\{ \alpha + \mathbf{i}\beta \mid \alpha \in [-\pi/\mathsf{L}, \pi/\mathsf{L}), \beta \in [0, \Delta/\mathsf{L}] \right\}, \tag{7.6}$$

where L denotes the physical length of the unit cell.

We aim at showing that this expansion of the Brillouin zone allows us to reinstate the Floquet–Bloch theorem in a physical sense, which we encompass in the following theorem.

Theorem 7.2. *Consider a tridiagonal k-Toeplitz operator with symbol f as in* (7.4) *and with nonzero off-diagonal entries and let $\mathcal{B}$ be the generalised Brillouin zone from* (7.6)*. Then,*

$$\sigma(T(f)) = \bigcup_{\alpha+\mathbf{i}\beta\in\mathcal{B}} \sigma(f(e^{-\mathbf{i}\,\mathsf{L}(\alpha+\mathbf{i}\beta)})), \tag{7.7}$$

up to at most $(k-1)$ points which may be in $\sigma(T(f))$ but not in $\bigcup_{\alpha+\mathbf{i}\beta\in\mathcal{B}} \sigma(f(e^{-\mathbf{i}\,\mathsf{L}(\alpha+\mathbf{i}\beta)}))$. Furthermore, for every $\lambda \in \sigma(T(f))$, the Brillouin zone $\mathcal{B}$ contains exactly two corresponding quasiperiodicities

$$\alpha + \mathbf{i}\beta \in [-\pi/\mathsf{L}, \pi/\mathsf{L}) + \mathbf{i}[0, \Delta/(2\,\mathsf{L})],$$
$$\alpha' + \mathbf{i}\beta' = (-\zeta/\mathsf{L} - \alpha) + \mathbf{i}(\Delta/\mathsf{L} - \beta) \in [-\pi/\mathsf{L}, \pi/\mathsf{L}) + \mathbf{i}[\Delta/(2\,\mathsf{L}), \Delta/\mathsf{L}]$$

such that $\lambda \in \sigma(a(e^{-\mathbf{i}\,\mathsf{L}(\alpha+\mathbf{i}\beta)}) = \sigma(a(e^{-\mathbf{i}\,\mathsf{L}(\alpha'+\mathbf{i}\beta')}))$. Here, ζ denotes the shift $\zeta := \operatorname{Arg}(\prod_{i=1}^{k} \frac{b_i}{c_i})$.

Remark 7.3.

- From now on, we will take $\mathsf{L} = 1$ without any loss of generality. To reintroduce L, we simply rescale $\mathcal{B}$ by $1/\mathsf{L}$ and all occurrences of $\alpha + \mathbf{i}\beta$ in the formulas by L.

- We will also use $\alpha + \mathbf{i}\beta$ and $z = e^{-\mathbf{i}(\alpha+\mathbf{i}\beta)}$ interchangeably and refer to them as *associated*.
- For a given quasiperiodicity $\alpha + \mathbf{i}\beta \in \mathcal{B}$ with $\beta \in [0, \Delta/(2\,\mathsf{L})]$, we call $\alpha' + \mathbf{i}\beta'$ with $\alpha' = \zeta/\,\mathsf{L} - \alpha$ and $\beta' = \Delta/\,\mathsf{L} - \beta$ the *conjugate quasiperiodicities*.
- In the above definition, we have assumed that $\Delta > 0$. However, this is not necessarily the case. If $\Delta < 0$, then the eigenmodes[2] of $T(a)$ will turn out to be exponentially growing and we observe a *negative* decay parameter β. We can then let $\beta \in [\Delta/\,\mathsf{L}, 0]$ and all of the arguments below work analogously.
- As $\alpha \mapsto e^{-\mathbf{i}(\alpha+\mathbf{i}\beta)}$ is periodic in α with period 2π we consider equality with respect to α modulo 2π and choose the convention $\alpha \in [-\pi, \pi)$.
- For reciprocal systems (*i.e.*, for $\Delta = 0$), the generalised Brillouin zone reduces to the standard Brillouin zone, effectively making $\mathcal{B}$ an extension of Y^*.

To prove Theorem 7.2, we will need Theorem 2.15 for the spectra of tridiagonal k-Toeplitz operators and the following lemma.

Lemma 7.4. *Let $T(f)$ be a tridiagonal k-Toeplitz operator with symbol $f(z)$ as in* (7.4)*. Then, we have*

$$\det(f(z) - \lambda) = \psi(z) + g(\lambda) \qquad \lambda, z \in \mathbb{C},$$

where

$$\psi(z) = (-1)^{k+1} \left((\prod_{i=1}^{k} c_i) z + (\prod_{i=1}^{k} b_i) z^{-1} \right), \tag{7.8}$$

and $g(\lambda)$ is a polynomial[3] *of degree k.*

As a consequence of the above two results, we can see that if we define E to be the ellipse (with interior) traced out by $\psi(\mathbb{T}^1)$, then we have

$$\sigma_{\mathrm{det}}(f) = (-g)^{-1}(\partial E) \quad \text{and} \quad \sigma_{\mathrm{wind}}(f) = (-g)^{-1}(\operatorname{int} E), \tag{7.9}$$

where $\sigma_{\mathrm{det}}(f), \sigma_{\mathrm{wind}}(f)$ are given by (2.35) and (2.38), respectively.

The following results hold.

Lemma 7.5. *The map*

$$\psi : \mathcal{B} \to E$$
$$\alpha + \mathbf{i}\beta \mapsto \psi(e^{-\mathbf{i}(\alpha+\mathbf{i}\beta)})$$

is well-defined, surjective and for every $\xi \in E$, there exist unique

$$\alpha \in [-\pi, \pi], \beta \in [0, \Delta/2]$$

such that

$$\psi^{-1}(\xi) = \{\alpha + \mathbf{i}\beta, \alpha' + \mathbf{i}\beta'\}.$$

Furthermore, if we denote by E_β the (with interior) ellipse traced out by $\psi([-\pi, \pi] + \mathbf{i}\beta)$, then we have $E_\beta = E_{\Delta-\beta}$ and $\operatorname{int} E_{\beta_1} \supset E_{\beta_2}$ for $0 \le \beta_1 < \beta_2 \le \Delta/2$.

The proof of Lemma 7.5 can be found in [7]. An immediate consequence of this lemma is that for a given quasiperiodicity $\alpha + \mathbf{i}\beta$ we have $\sigma(f(\alpha + \mathbf{i}\beta)) = \sigma(f(\alpha' + \mathbf{i}\beta'))$. We show graphically the statement of Lemma 7.5 in Section 7.4. We can prove Theorem 7.2 by using Lemma 7.5. We omit the details which can be found in [7].

At the beginning of this section, we have motivated the introduction of an imaginary part with the heuristic of taking into account the possible decay of the eigenvectors. This heuristic is made formal with the following proposition.

[2]While these eigenmodes $\boldsymbol{u}$ are eigenmodes in the symbolic sense $(T(a) - \lambda I)\boldsymbol{u} = 0$, they no longer lie in ℓ^2 due to their exponential growth.

[3]See [5, Appendix A] for further details.

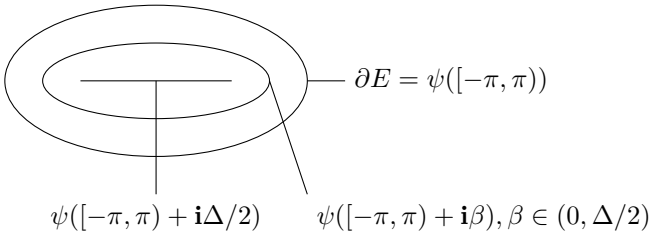


FIGURE 7.2. Parametrisation of the ellipse E by ψ for $\alpha \in Y^* \simeq \mathbb{T}^1$ and $\beta \in [0, \Delta/2]$. As β increases from 0 to $\Delta/2$ the corresponding ellipse drawn out by $\psi(\mathbb{T}^1 + \mathbf{i}\beta)$ shrinks uniformly.

Theorem 7.6. *Let $\lambda \in \sigma_{\mathrm{det}}(f) \cup \sigma_{\mathrm{wind}}(f)$, with the uniquely determined corresponding quasiperiodicities $\alpha + \mathbf{i}\beta, \alpha' + \mathbf{i}\beta'$. Let $\boldsymbol{u}_1, \boldsymbol{u}_2$ be eigenvectors of $f(\alpha + \mathbf{i}\beta)$, $f(\alpha' + \mathbf{i}\beta')$ associated with that eigenvalue λ. Then, we can obtain a symbolic eigenvector $T(f)\boldsymbol{u} = \lambda\boldsymbol{u}$ of the Toeplitz operator as a linear combination of the $(\alpha + \mathbf{i}\beta)$-quasiperiodic extension $\widetilde{\boldsymbol{u}}_1$ and the $(\alpha' + \mathbf{i}\beta')$-quasiperiodic extension $\widetilde{\boldsymbol{u}}_2$ of $\boldsymbol{u}_1, \boldsymbol{u}_2$, respectively. Furthermore, all eigenvectors $\boldsymbol{u}$ of $T(f)$ are of this form. Here, the $(\alpha + \mathbf{i}\beta)$-quasiperiodic extension of a vector $\boldsymbol{v}$ is defined as*

$$\widetilde{\boldsymbol{v}} \coloneqq (\boldsymbol{v}^\top, z^{-1}\boldsymbol{v}^\top, z^{-2}\boldsymbol{v}^\top, \dots)^\top$$

for $z = e^{-\mathbf{i}(\alpha + \mathbf{i}\beta)}$. Consequently, for every $j \in \mathbb{N}$,

$$\frac{|\boldsymbol{u}^{(j+k)}|}{|\boldsymbol{u}^{(j)}|} = e^{-\beta}. \tag{7.10}$$

REMARK 7.7. Theorem 7.6 hence justifies why Δ is called the *non-reciprocity rate*, as it directly translates into the decay rate of the eigenvector, a peculiarity of non-reciprocal systems. However, in the generic case an eigenvector $\boldsymbol{u}$ of $T(a)$ will be a linear combination of $\widetilde{\boldsymbol{u}}_1$ and $\widetilde{\boldsymbol{u}}_2$ with decay rates β and $\Delta - \beta$ and thus has decay rate $\max\{\beta, \Delta - \beta\}$ which is maximised if $\beta = \Delta/2$. Hence, the actual *maximal rate of decay* is $\Delta/2$.

We can also see that the construction in Theorem 7.6 is independent of the actual entries of $T(a)$ in its first row. Hence, it continues to work even if the top left edge of $T(a)$ is perturbed.

7.5. Three spectral limits

Having restored the Floquet–Bloch decomposition for the Toeplitz operator limit $T(f)$, we now aim to understand how and if finite Toeplitz matrices $T_{mk}(f)$ converge to this limit as $m \to \infty$. Crucially, while in the Hermitian setting the symbol $f(z)$ is collapsed, in general its eigenvalues trace out a path with nonempty interior. Any point in this interior is exponentially close to a pseudoeigenvalue of $T_{mk}(f)$ in the limit $m \to \infty$. This in turn causes the finite system and its limiting spectrum to be highly sensitive to boundary conditions. Figure 7.3 shows the finite spectra under different boundary conditions as well as the pseudospectrum. The collapsed symbol causes their respective limits to coincide in the Hermitian setting but we can see that they diverge in the non-reciprocal setting.

The appropriate generalisation of the Brillouin zone depends on the limit of interest and does not necessarily match the generalised Brillouin zone for the Toeplitz operator limit $T(f)$ as defined in (7.6). For open and periodic boundary conditions, we will now characterise the limiting spectrum and give the appropriate generalised Brillouin zone. Finally, we will investigate the limiting pseudospectrum and see how this connects the two boundary conditions.

Open limit. First, we aim to characterise the limiting spectrum $\sigma(T_{mk}(f))$ as $m \to \infty$, which corresponds to a growing finite system. The main idea is that for non-reciprocal tridiagonal systems, we can perform a change of basis to obtain a similar symmetric system. The symbol

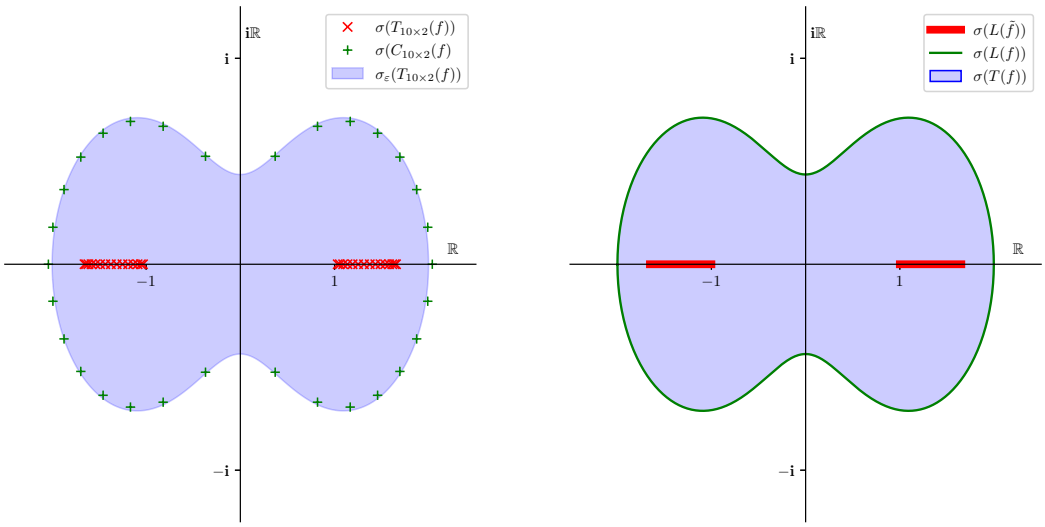


FIGURE 7.3. Illustration of the three spectral limits. We see that the eigenvalues of the circulant matrix $C_{2\times10}(f)$ (green) arrange around the symbol curve and hence converge to the Laurent operator limit $L(f)$. The eigenvalues of the Toeplitz matrix $T_{2\times10}(f)$ (red) arrange around the collapsed symbol $\widetilde{f}$ (as defined in the proof of Theorem 7.8) and hence converge to the collapsed Toeplitz (or Laurent) operator $T(\widetilde{f})$. The ε-pseudospectrum of $T_{mk}(f)$ corresponds exactly to the interior of the symbol curve and thus converges to the actual Toeplitz limit $T(f)$.

of this system is collapsed and we can recover the traditional spectral convergence and decomposition. Then we may transform back into the original basis in order to achieve a Floquet–Bloch relation, but with a Brillouin zone shifted into the complex plane to account for the exponential decay of the eigenvectors.

Theorem 7.8. *Let $T(f)$ be a tridiagonal Toeplitz operator with symbol $f(z)$ and $b_i, c_i \neq 0$ for all $1 \leq i \leq k$. We then have*

$$\lim_{m\to\infty} \sigma(T_{mk}(f)) = \bigcup_{\alpha\in Y^*} \sigma(f(e^{-\mathbf{i}\,\mathsf{L}(\alpha+\mathbf{i}\Delta/(2\,\mathsf{L}))})).$$

This result is illustrated in Figure 7.3 where the spectrum of the Toeplitz matrix on the left-hand side (corresponding to the open boundary condition) converges to the spectrum of the Toeplitz operator with collapsed symbol $T(\widetilde{f})$ on the right-hand side. As we just proved the appropriate *generalised Brillouin zone* to decompose the spectrum of this operator is the classical Brillouin zone, shifted into the complex plane:

$$\mathcal{B}_{\mathrm{OBC}} = \left\{\alpha + \mathbf{i}\Delta/(2\,\mathsf{L}) \mid \alpha \in Y^*\right\}.$$

Consequently, for tridiagonal Toeplitz systems with open boundary conditions, shifting the Brillouin zone by $\Delta/(2\,\mathsf{L})$ restores spectral convergence as well as the Floquet–Bloch decomposition. This corresponds to the fact that in the tridiagonal case, all the eigenmodes have the same rate of decay. Namely, this decay is the maximal decay that is given explicitly by $\Delta/(2\,\mathsf{L})$.

Periodic boundary conditions and the Laurent operator limit. We can impose periodic boundary conditions on $T_{mk}(f)$ and get the tridiagonal k-circulant matrix

$$(C_{mk}(f))_{ij} \coloneqq \begin{cases} c_k & \text{for } i = 0, j = mk, \\ b_k & \text{for } i = mk, j = 0, \\ (T_{mk}(f))_{ij} & \text{otherwise.} \end{cases} \tag{7.11}$$

The following result holds.

Theorem 7.9. *Let $C_{mk}(f)$ be a tridiagonal k-circulant matrix as above. Then, we have the following spectral decomposition:*

$$\sigma(C_{mk}(f)) = \bigcup_{j=0}^{m-1} \sigma(f(e^{2\pi \mathbf{i} j/m})).$$

Furthermore, if we let $m \to \infty$,

$$\sigma(C_{mk}(f)) = \bigcup_{j=0}^{m-1} f(e^{2\pi \mathbf{i} j/m}) \to \bigcup_{\alpha \in Y^*} f(e^{-\mathbf{i} \mathsf{L} \alpha}) = \sigma(L(f)). \tag{7.12}$$

We have thus shown the analogue of Theorem 7.8 for periodic boundary conditions. As we can see in Figure 7.3, imposing periodic boundary conditions on the finite system causes the spectrum of $C_{mk}(f)$ to diverge drastically from the spectrum of $T_{mk}(f)$. This corresponds to the fact that while the eigenmodes of $T_{mk}(f)$ have a decay of $\Delta/2L$, imposing periodic boundary conditions forces the eigenmodes to be decay-free, causing a large perturbation. The non-Hermitian non-reciprocity thus causes the system to be highly sensitive to boundary conditions. Figure 7.3 further illustrates how the spectrum of the circulant matrices $C_{mk}(f)$ arranges around the symbol curve and thus converges to the Laurent operator limit as $m \to \infty$. The above theorem therefore shows that the appropriate Brillouin zone for this setting is the classical Brillouin zone with no decay:

$$\mathcal{B}_{\mathrm{PBC}} = Y^*.$$

Pseudospectrum and the Toeplitz operator limit. Finally, we investigate the pseudospectrum of the finite system $T_{mk}(a)$. Crucially, while the spectrum of Toeplitz matrices is highly sensitive to boundary conditions, the pseudospectrum is not and using [17, Corollary 6.16], we find that it converges to the Toeplitz operator limit.

Theorem 7.10. *Consider a continuous symbol $f \in L^\infty(\mathbb{T}^1, \mathbb{C}^{k\times k})$ so that $T(f)$ is tridiagonal. Then, for every $\varepsilon > 0$,*

$$\lim_{m\to\infty} \sigma_\varepsilon(T_{mk}(f)) = \sigma_\varepsilon(T(f)). \tag{7.13}$$

In particular, the previous theorem implies that

$$\lim_{\varepsilon\to 0} \lim_{m\to\infty} \sigma_\varepsilon(T_{mk}(f)) = \lim_{\varepsilon\to 0} \sigma_\varepsilon(T(f)) = \sigma(T(f)).$$

Hence, by Theorem 7.2, the appropriate generalised Brillouin zone to recover the pseudospectral limit is the same as for the Toeplitz operator:

$$\mathcal{B} = \left\{ \alpha + \mathbf{i}\beta \mid \alpha \in [-\pi/\mathsf{L}, \pi/\mathsf{L}), \beta \in [0, \Delta/\mathsf{L}] \right\}.$$

Notably, this Brillouin zone is of higher dimension than the previous two Brillouin zones (*i.e.*, a two dimensional region in $\mathbb{C}$ different from the previous $\mathbb{T}^1 \cong Y^*$) as it contains a range of possible decay rates. Furthermore, it contains the shifted Brillouin zone of the open boundary condition and the classical Brillouin zone of the periodic boundary condition as special cases ($\beta = \Delta/(2\mathsf{L})$ and $\beta = 0$). This is in line with the fact that the Toeplitz operator spectrum contains both the Laurent operator spectrum, as well as the collapsed Toeplitz spectrum, as seen in Figure 7.3. The open and periodic boundary condition settings thus correspond to the maximal decay and zero decay extremes of a range of possible pseudospectral decays, captured by the Toeplitz operator spectrum.

Appendix A. Capacitance matrix

The capacitance matrix introduced in Section 3 plays a crucial role throughout the presented work. In this appendix, we present the details of its derivation referring to [28] in the Hermitian case and to [1] for the non-Hermitian proofs.

We consider the non-reciprocal case first and think of the reciprocal one as the special case where $\gamma = 0$.

The use of the Dirichlet-to-Neumann map has proven itself to be an effective tool to find solutions to (3.10) that lend themselves to asymptotic analysis in the high-contrast regime. Hereafter, we will adapt the methods of [28] to (3.10).

The first step is to solve the outer problem

$$\begin{cases} w''(x) + \dfrac{\omega^2}{v^2} w(x) = 0, & x \in \mathbb{R} \setminus \bigcup_{i=1}^{N} (x_i^{\mathsf{L}}, x_i^{\mathsf{R}}), \\ w(x_i^{\mathsf{L,R}}) = f_i^{\mathsf{L,R}}, & \text{for all } 1 \le i \le N, \\ \dfrac{\mathrm{d}w}{\mathrm{d}\,|x|}(x) - \mathbf{i}kw(x) = 0, & x \in (-\infty, x_1^{\mathsf{L}}) \cup (x_N^{\mathsf{R}}, \infty), \end{cases} \tag{A.1}$$

for some boundary data $f_i^{\mathsf{L,R}} \in \mathbb{C}^{2N}$. Its solution is simply given by

$$w(x) = \begin{cases} f_1^{\mathsf{L}} e^{-\mathbf{i}k(x - x_1^{\mathsf{L}})}, & x \le x_1^{\mathsf{L}}, \\ a_i e^{\mathbf{i}kx} + b_i e^{-\mathbf{i}kx}, & (x_i^{\mathsf{R}}, x_{i+1}^{\mathsf{L}}), \\ f_N^{\mathsf{R}} e^{-\mathbf{i}k(x - x_N^{\mathsf{R}})}, & x_N^{\mathsf{R}} \le x, \end{cases} \tag{A.2}$$

where a_i and b_i are given by

$$\begin{pmatrix} a_i \\ b_i \end{pmatrix} = -\frac{1}{2\mathbf{i}\sin(ks_i)} \begin{pmatrix} e^{-\mathbf{i}kx_{i+1}^{\mathsf{L}}} & -e^{-\mathbf{i}kx_i^{\mathsf{R}}} \\ -e^{\mathbf{i}kx_{i+1}^{\mathsf{L}}} & e^{\mathbf{i}kx_i^{\mathsf{R}}} \end{pmatrix} \begin{pmatrix} f_i^{\mathsf{R}} \\ f_{i+1}^{\mathsf{L}} \end{pmatrix},$$

as shown in [28, Lemma 2.1]. The second and harder step is to combine the expression for the outer solution (A.2) with the boundary conditions in order to find the full solution. We will handle this information through the Dirichlet-to-Neumann map.

Definition A.1 (Dirichlet-to-Neumann map). For any $k \in \mathbb{C}$ which is not of the form $n\pi/s_i$ for some $n \in \mathbb{Z}\setminus\{0\}$ and $1 \le i \le N-1$, the *Dirichlet-to-Neumann map* with wave number k is the linear operator $\mathcal{T}^k : \mathbb{C}^{2N} \to \mathbb{C}^{2N}$ defined by

$$\mathcal{T}^k[(f_i^{\mathsf{L,R}})_{1\le i\le N}] = \left(\pm \frac{\mathrm{d}w}{\mathrm{d}x}(x_i^{\mathsf{L,R}}) \right)_{1\le i\le N},$$

where w is the unique solution to (A.1).

We refer to [28, Section 2] for a more extensive discussion of this operator, but recall that $\mathcal{T}^k$ has a block-diagonal matrix representation

$$T^k \begin{pmatrix} f_1^{\mathsf{L}} \\ f_1^{\mathsf{R}} \\ \vdots \\ f_N^{\mathsf{L}} \\ f_N^{\mathsf{R}} \end{pmatrix} = \begin{pmatrix} \mathbf{i}k & & & & \\ & A^k(s_1) & & & \\ & & A^k(s_2) & & \\ & & & \ddots & \\ & & & & A^k(s_{(N-1)}) \\ & & & & & \mathbf{i}k \end{pmatrix} \begin{pmatrix} f_1^{\mathsf{L}} \\ f_1^{\mathsf{R}} \\ \vdots \\ f_N^{\mathsf{L}} \\ f_N^{\mathsf{R}} \end{pmatrix}, \tag{A.3}$$

where, for any real $\ell \in \mathbb{R}$, $A^k(\ell)$ denotes the 2×2 symmetric matrix given by

$$A^k(\ell) := \begin{pmatrix} -\dfrac{k\cos(k\ell)}{\sin(k\ell)} & \dfrac{k}{\sin(k\ell)} \\ \dfrac{k}{\sin(k\ell)} & -\dfrac{k\cos(k\ell)}{\sin(k\ell)} \end{pmatrix}. \tag{A.4}$$

Consequently, T^k is holomorphic in k in a neighbourhood of the origin and admits a power series representation $T^k = \sum_{n\geq 0} k^n T_n$, where

$$T_0 = \begin{pmatrix} 0 & & & & & \\ & A^0(s_1) & & & & \\ & & A^0(s_2) & & & \\ & & & \ddots & & \\ & & & & A^0(s_{(N-1)}) & \\ & & & & & 0 \end{pmatrix}, \tag{A.5}$$

and $A^0(s) := \lim_{k\to 0} A^k(s)$.

The above properties of the Dirichlet-to-Neumann map will be crucial to find subwavelength eigenfrequencies. We will use $\mathcal{T}^k$ and T^k interchangeably.

Characterisation of the subwavelength eigenfrequencies. The Dirichlet-to-Neumann map allows us to reformulate (3.10) as follows:

$$\begin{cases} u''(x) + \gamma u'(x) + \dfrac{\omega^2}{v_b^2} u = 0, & x \in \displaystyle\bigcup_{i=1}^{N} (x_i^{\mathsf{L}}, x_i^{\mathsf{R}}), \\ \left.\dfrac{\mathrm{d}u}{\mathrm{d}x}\right|_{\mathsf{R}} (x_i^{\mathsf{L}}) = -\delta\, \mathcal{T}^{\frac{\omega}{v}} [u]_i^{\mathsf{L}}, & \forall\ 1 \leq i \leq N, \\ \left.\dfrac{\mathrm{d}u}{\mathrm{d}x}\right|_{\mathsf{L}} (x_i^{\mathsf{R}}) = \delta\, \mathcal{T}^{\frac{\omega}{v}} [u]_i^{\mathsf{R}}, & \forall\ 1 \leq i \leq N. \end{cases} \tag{A.6}$$

We can then further rewrite (A.6) in weak form by multiplying it by a test function $w \in H^1(D)$ and integrating on the intervals. Explicitly, we obtain that u is a solution to (A.6) if and only if

$$a(u, w) = 0 \tag{A.7}$$

for any $w \in H^1(D)$, where

$$\begin{aligned} a(u,w) = &\sum_{i=1}^{N} \int_{x_i^{\mathsf{L}}}^{x_i^{\mathsf{R}}} u'\overline{w}' - \gamma u'\overline{w} - \frac{\omega^2}{v_b^2} u\overline{w}\,\mathrm{d}x \\ &- \delta \sum_{i=1}^{N} \overline{w}(x_i^{\mathsf{R}})\, \mathcal{T}^{\frac{\omega}{v}} [u]_i^{\mathsf{R}} + \overline{w}(x_i^{\mathsf{L}})\, \mathcal{T}^{\frac{\omega}{v}} [u]_i^{\mathsf{L}}. \end{aligned} \tag{A.8}$$

We also introduce a slightly modified bilinear form

$$\begin{aligned} a_{\omega,\delta}(u,w) = &\sum_{i=1}^{N} \left(\int_{x_i^{\mathsf{L}}}^{x_i^{\mathsf{R}}} u'\overline{w}' - \gamma u'\overline{w}\,\mathrm{d}x + \int_{x_i^{\mathsf{L}}}^{x_i^{\mathsf{R}}} u\,\mathrm{d}x \int_{x_i^{\mathsf{L}}}^{x_i^{\mathsf{R}}} \overline{w}\,\mathrm{d}x \right) \\ &- \sum_{i=1}^{N} \left(\int_{x_i^{\mathsf{L}}}^{x_i^{\mathsf{R}}} \frac{\omega^2}{v_b^2} u\overline{w}\,\mathrm{d}x + \delta \left(\overline{w}(x_i^{\mathsf{R}})\, \mathcal{T}^{\frac{\omega}{v}} [u]_i^{\mathsf{R}} + \overline{w}(x_i^{\mathsf{L}})\, \mathcal{T}^{\frac{\omega}{v}} [u]_i^{\mathsf{L}} \right) \right). \end{aligned} \tag{A.9}$$

This new form parametrised by ω is an analytic perturbation of the $a_{0,\delta}$ form, which is continuous and its associated variational problem is well-posed on $H^1(D)$ and so $a_{\omega,\delta}$ inherits

this property. Specifically, for every summand of $\Re(a_{0,\delta})$ the following holds for any $\varepsilon > 0$

$$\begin{aligned}
&\sum_{i=1}^{N}\left[\int_{x_i^{\mathsf{L}}}^{x_i^{\mathsf{R}}} u'\overline{u}'\,\mathrm{d}x - \gamma\int_{x_i^{\mathsf{L}}}^{x_i^{\mathsf{R}}} u'\overline{u} + \int_{x_i^{\mathsf{L}}}^{x_i^{\mathsf{R}}} u\,\mathrm{d}x\int_{x_i^{\mathsf{L}}}^{x_i^{\mathsf{R}}}\overline{u}\,\mathrm{d}x\right]\\
\geq&\sum_{i=1}^{N}\left[\|u'\|^2_{L^2(x_i^{\mathsf{L}},x_i^{\mathsf{R}})} - \frac{\varepsilon\gamma}{2}\|u'\|^2_{L^2(x_i^{\mathsf{L}},x_i^{\mathsf{R}})} - \frac{\gamma}{2\varepsilon}\|u\|^2_{L^2(x_i^{\mathsf{L}},x_i^{\mathsf{R}})} + \left|\int_{x_i^{\mathsf{L}}}^{x_i^{\mathsf{R}}} u\,\mathrm{d}x\right|^2\right]\\
=&\sum_{i=1}^{N}\left[(1-\frac{\gamma\varepsilon}{2})\|u'\|^2_{L^2(x_i^{\mathsf{L}},x_i^{\mathsf{R}})} - \frac{\gamma}{2\varepsilon}\|u\|^2_{L^2(x_i^{\mathsf{L}},x_i^{\mathsf{R}})} + \left|\int_{x_i^{\mathsf{L}}}^{x_i^{\mathsf{R}}} u\,\mathrm{d}x\right|^2\right].
\end{aligned}$$

From the compactness of the injection of H^1 into L^2 and for ε small enough, it follows that $\Re(a_{0,\delta})$ satisfies a Gårding inequality. On the other hand, it follows from the explicit form (A.3) of the Dirichlet-to-Neumann operator that

$$\Im(a_{0,\delta}(u,u)) = 0,$$

which implies that u is constant on each $[x_i^{\mathsf{L}}, x_i^{\mathsf{R}}]$. But, $\Re(a_{0,\delta}(u,u)) = 0$ for u constant on each $[x_i^{\mathsf{L}}, x_i^{\mathsf{R}}]$ implies that the constants are all zero. Thus one obtains the well-posedness of the associated variational problem.

We exploit this, by defining the $h_j(\omega,\delta)$ functions as the Lax–Milgram solutions to the variational problem

$$a_{\omega,\delta}(h_j(\omega,\delta), w) = \int_{x_j^{\mathsf{L}}}^{x_j^{\mathsf{R}}}\overline{w}\,\mathrm{d}x \tag{A.10}$$

for every $w \in H^1(D)$ and $1 \leq j \leq N$. In the following lemma, we show that the functions h_j allow us to reduce (A.7) to a finite dimensional $N \times N$ linear system by acting as basis functions.

Lemma A.2. *Let $\omega \in \mathbb{C}$ and $\delta \in \mathbb{R}$ belong to a neighbourhood of zero such that $a_{\omega,\delta}$ is coercive. The variational problem* (A.7) *admits a nontrivial solution $u \equiv u(\omega,\delta)$ if and only if the $N \times N$ nonlinear eigenvalue problem*

$$(I - \mathbf{C}(\omega,\delta))\boldsymbol{x} = 0$$

has a solution ω and $\boldsymbol{x} := (x_i(\omega,\delta))_{1\leq i\leq N}$, where $\mathbf{C}(\omega,\delta)$ is the matrix given by

$$\mathbf{C}(\omega,\delta) \equiv (\mathbf{C}(\omega,\delta)_{ij})_{1\leq i,j\leq N} := \left(\int_{x_i^{\mathsf{L}}}^{x_i^{\mathsf{R}}} h_j(\omega,\delta)\,\mathrm{d}x\right)_{1\leq i,j\leq N}. \tag{A.11}$$

Proof. This can be shown using the arguments presented in [28, Lemma 3.4]. ∎

Subwavelength eigenfrequencies are thus the values $\omega(\delta)$ satisfying (3.4) for which $I - \mathbf{C}(\omega,\delta)$ is not invertible.

Acknowledgements

This work was partially supported by Swiss National Science Foundation grant number 200021-200307.

Code Availability

The data that support the findings of this work are openly available at `https://doi.org/10.5281/zenodo.10438679`, `https://zenodo.org/doi/10.5281/zenodo.10361315`,`https://doi.org/10.5281/zenodo.8210678`, and `https://doi.org/10.5281/zenodo.8081076`.

Conflict of interest

The authors have no competing interests to declare that are relevant to the content of this article.

References

[1] Ammari Habib, Barandun Silvio, Cao Jinghao, Davies Bryn and Hiltunen Erik Orvehed, "Mathematical Foundations of the Non-Hermitian Skin Effect", in: *Arch. Ration. Mech. Anal.* 248.3 (2024), Paper No. 33, 34.

[2] Ammari Habib, Barandun Silvio, Cao Jinghao and Feppon Florian, "Edge Modes in Subwavelength Resonators in One Dimension", in: *Multiscale Modeling & Simulation* 21.3 (2023), pp. 964–992.

[3] Ammari Habib, Barandun Silvio, Davies Bryn, Hiltunen Erik Orvehed, Kosche Thea and Liu Ping, "Exponentially Localised Interface Eigenmodes in Finite Chains of Resonators", in: *Stud. Appl. Math.* (2024).

[4] Ammari Habib, Barandun Silvio, Davies Bryn, Hiltunen Erik Orvehed and Liu Ping, "Stability of the Non-Hermitian Skin Effect", in: *SIAM J. Appl. Math.* 84.4 (2024), pp. 1697–1717.

[5] Ammari Habib, Barandun Silvio, De Bruijn Yannick, Liu Ping and Thalhammer Clemens, *Spectra and Pseudo-Spectra of Tridiagonal k-Toeplitz Matrices and the Topological Origin of the Non-Hermitian Skin Effect*, 2024, arXiv: 2401.12626.

[6] Ammari Habib, Barandun Silvio and Liu Ping, *Perturbed Block Toeplitz Matrices and the Non-Hermitian Skin Effect in Dimer Systems of Subwavelength Resonators*, 2023, arXiv: 2307.13551.

[7] Ammari Habib, Barandun Silvio, Liu Ping and Uhlmann Alexander, *Generalised Brillouin Zone for Non-Reciprocal Systems*, 2024, arXiv: 2408.05073.

[8] Ammari Habib, Barandun Silvio, Liu Ping and Uhlmann Alexander, *Tunable Localisation in Parity-Time-Symmetric Resonator Arrays with Imaginary Gauge Potentials*, 2024, arXiv: 2405.05002.

[9] Ammari Habib, Davies Bryn and Hiltunen Erik Orvehed, "Functional Analytic Methods for Discrete Approximations of Subwavelength Resonator Systems", in: *Pure and Applied Analysis* (2024).

[10] Ammari Habib, Davies Bryn and Hiltunen Erik Orvehed, *Mathematical theories for metamaterials: From condensed matter theory to subwavelength physics*, NSF–CBMS Regional Conf. Ser. American Mathematical Society, Providence, to appear, 2024.

[11] Ammari Habib, Davies Bryn, Hiltunen Erik Orvehed, Lee Hyundae and Yu Sanghyeon, "Exceptional points in parity-time-symmetric subwavelength metamaterials", in: *SIAM J. Math. Anal.* 54.6 (2022), pp. 6223–6253.

[12] Ammari Habib, Davies Bryn, Hiltunen Erik Orvehed and Yu Sanghyeon, "Topologically Protected Edge Modes in One-Dimensional Chains of Subwavelength Resonators", in: *J. Math. Pures Appl. (9)* 144 (2020), pp. 17–49.

[13] Ammari Habib, Fiorani Francesco and Hiltunen Erik Orvehed, "On the validity of the tight-binding method for describing systems of subwavelength resonators", in: *SIAM J. Appl. Math.* 82.4 (2022), pp. 1611–1634.

[14] Ammari Habib and Hiltunen Erik Orvehed, *Edge Modes in Active Systems of Subwavelength Resonators*, 2020, arXiv: 2006.05719.

[15] Ammari Habib and Zhang Hai, "Super-Resolution in High-Contrast Media", in: *Proc. A.* 471.2178 (2015), pp. 20140946, 11.

[16] Borgnia Dan S., Kruchkov Alex Jura and Slager Robert-Jan, "Non-Hermitian Boundary Modes and Topology", in: *Phys. Rev. Lett.* 124.5 (Feb. 2020), p. 056802.

[17] Böttcher Albrecht and Silbermann Bernd, *Introduction to Large Truncated Toeplitz Matrices*, Springer New York, 1999.

[18] Coutant Antonin, Achilleos Vassos, Richoux Olivier, Theocharis Georgios and Pagneux Vincent, "Subwavelength Su-Schrieffer-Heeger Topological Modes in Acoustic Waveguides", in: *J. Acoust. Soc. Am.* 151.6 (2022), pp. 3626–3632.

[19] Craster Richard V. and Davies Bryn, "Asymptotic characterization of localized defect modes: Su-Schrieffer-Heeger and related models", in: *Multiscale Model. Simul.* 21.3 (2023), pp. 827–848.

[20] Da Fonseca C.M., "The Characteristic Polynomial of Some Perturbed Tridiagonal k-Toeplitz Matrices", in: *Appl. Math. Sci. (Ruse)* 1.1-4 (2007), pp. 59–67.
[21] Da Fonseca C.M. and Petronilho J., "Explicit Inverses of Some Tridiagonal Matrices", in: *Linear Algebra Appl.* 325.1–3 (2001), pp. 7–21.
[22] Davies Bryn and Lou Yiqi, "Landscape of Wave Focusing and Localization at Low Frequencies", in: *Stud. Appl. Math.* 152.2 (2023), pp. 760–777.
[23] Davis Chandler and Kahan W. M., "The rotation of eigenvectors by a perturbation. III", in: *SIAM J. Numer. Anal.* 7 (1970), pp. 1–46.
[24] Fefferman Charles L., Lee-Thorp James P. and Weinstein Michael I., "Honeycomb Schrödinger Operators in the Strong Binding Regime", in: *Comm. Pure Appl. Math.* 71.6 (2017), pp. 1178–1270.
[25] Fefferman Charles L., Lee-Thorp James P. and Weinstein Michael I., "Topologically Protected States in One-Dimensional Continuous Systems and Dirac Points", in: *Proc. Natl. Acad. Sci. USA* 111.24 (June 2014), pp. 8759–8763.
[26] Fefferman Charles L., Lee-Thorp James P. and Weinstein Michael I., "Topologically Protected States in One-Dimensional Systems", in: *Mem. Amer. Math. Soc.* 247.1173 (2017), pp. vii+118.
[27] Feppon F. and Ammari H., "Subwavelength resonant acoustic scattering in fast time-modulated media", in: *J. Math. Pures Appl. (9)* 187 (2024), pp. 233–293.
[28] Feppon Florian, Cheng Zijian and Ammari Habib, "Subwavelength Resonances in One-Dimensional High-Contrast Acoustic Media", in: *SIAM J. Appl. Math.* 83.2 (2023), pp. 625–665.
[29] Franca Selma, Könye Viktor, Hassler Fabian, van den Brink Jeroen and Fulga Cosma, "Non-Hermitian Physics without Gain or Loss: The Skin Effect of Reflected Waves", in: *Phys. Rev. Lett.* 129.8 (2022).
[30] Gaul André, *PseudoPy*, version 1.2.5.
[31] Ghatak Ananya, Brandenbourger Martin, van Wezel Jasper and Corentin Coulais, "Observation of Non-Hermitian Topology and Its Bulk-Edge Correspondence in an Active Mechanical Metamaterial", in: *Proc. Natl. Acad. Sci. USA* 117.47 (2020), pp. 29561–29568.
[32] Golub Gene H. and Van Loan Charles F., *Matrix Computations*, Fourth edition, Johns Hopkins Studies in the Mathematical Sciences, Baltimore: The Johns Hopkins University Press, 2013, 756 pp.
[33] Gover M.J.C., "The Eigenproblem of a Tridiagonal 2-Toeplitz Matrix", in: *Linear Algebra Appl.* 197–198 (1994), pp. 63–78.
[34] Hatano Naomichi and Nelson David R., "Localization Transitions in Non-Hermitian Quantum Mechanics", in: *Phys. Rev. Lett.* 77.3 (1996), pp. 570–573.
[35] Heiss W D, "The Physics of Exceptional Points", in: *J. Phys. A: Math. Theor.* 45.44 (2012), p. 444016.
[36] Hwang Suk-Geun, "Cauchy's interlace theorem for eigenvalues of Hermitian matrices", in: *Amer. Math. Monthly* 111.2 (2004), pp. 157–159.
[37] Kadic Muamer, Milton Graeme W, Hecke Martin van and Wegener Martin, "3D metamaterials", in: *Nat. Rev. Phys.* 1.3 (2019), pp. 198–210.
[38] Leykam Daniel, Bliokh Konstantin Y., Huang Chunli, Chong Y. D. and Nori Franco, "Edge Modes, Degeneracies, and Topological Numbers in Non-Hermitian Systems", in: *Phys. Rev. Lett.* 118.4 (2017), p. 040401.
[39] Lin Junshan and Zhang Hai, "Mathematical Theory for Topological Photonic Materials in One Dimension", in: *J. Phys. A: Math. Theor.* 55.49 (8th Dec. 2022), p. 495203.
[40] Lin Rijia, Tai Tommy, Li Linhu and Lee Ching Hua, "Topological Non-Hermitian Skin Effect", in: *Frontiers of Physics* 18.5 (2023), p. 53605.
[41] Longhi Stefano, Gatti Davide and Valle Giuseppe Della, "Robust Light Transport in Non-Hermitian Photonic Lattices", in: *Sci. Rep.* 5.1 (2015).

[42] Lyra M. L., Mayboroda S. and Filoche M., "Dual Landscapes in Anderson Localization on Discrete Lattices", in: *EPL (Europhysics Lett.)* 109.4 (2015), p. 47001.
[43] Marcellán F. and Van Assche W., eds., *Orthogonal polynomials and special functions*, vol. 1883, Lecture Notes in Mathematics, Springer-Verlag, Berlin, 2006.
[44] Margetis Dionisios, Watson Alexander B. and Luskin Mitchell, "On the Su–Schrieffer–Heeger Model of Electron Transport: Low-temperature Optical Conductivity by the Mellin Transform", in: *Stud. Appl. Math.* 151.2 (2023), pp. 555–584.
[45] Maxwell James Clerk, *A Treatise on Electricity and Magnetism*, vol. 1, Oxford Classic Texts in the Physical Sciences, New York: The Clarendon Press, Oxford University Press, 1873.
[46] Miri Mohammad-Ali and Alù Andrea, "Exceptional Points in Optics and Photonics", in: *Science* 363.6422 (2019), eaar7709.
[47] Mironov A. L. and Oleinik V. L., "Limits of Applicability of the Tight Binding Approximation", in: *Theoretical and Mathematical Physics* 99.1 (1994), pp. 457–469.
[48] Mironov A. L. and Oleinik V. L., "On the Limits of Applicability of the Tight Binding Approximation Method for a Complex-Valued Potential", in: *Rossíiskaya Akademiya Nauk* 112.3 (1997), pp. 448–466.
[49] Murphy N. C., Wortis R. and Atkinson W. A., "Generalized Inverse Participation Ratio as a Possible Measure of Localization for Interacting Systems", in: *Phys. Rev. B* 83.18 (2011).
[50] Okuma Nobuyuki, Kawabata Kohei, Shiozaki Ken and Sato Masatoshi, "Topological Origin of Non-Hermitian Skin Effects", in: *Phys. Rev. Lett.* 124.8 (2020), pp. 086801, 7.
[51] Okuma Nobuyuki and Sato Masatoshi, "Non-Hermitian Topological Phenomena: A Review", in: *Annual Rev. Cond. Matt. Phys.* 14.1 (2023), pp. 83–107.
[52] Parlett Beresford N., *The Symmetric Eigenvalue Problem*, Classics in Applied Mathematics 20, Philadelphia, Pa: Society for Industrial and Applied Mathematics, 1998, 398 pp.
[53] Qiu Jiayu, Lin Junshan, Xie Peng and Zhang Hai, *Mathematical Theory for the Interface Mode in a Waveguide Bifurcated from a Dirac Point*, 2023, arXiv: 2304.10843.
[54] Reichel Lothar and Trefethen Lloyd N., "Eigenvalues and Pseudo-Eigenvalues of Toeplitz Matrices", in: *Linear Algebra Appl.* 162–164 (1992), pp. 153–185.
[55] Rivero Jose H. D., Feng Liang and Ge Li, "Imaginary Gauge Transformation in Momentum Space and Dirac Exceptional Point", in: *Phys. Rev. Lett.* 129.24 (2022), p. 243901.
[56] Silva Ricardo Reis da, *Matrix Perturbations: Bounding and Computing Eigenvalues*, Oisterwijk: BOXPress, 2011.
[57] Su W. P., Schrieffer J. R. and Heeger A. J., "Solitons in Polyacetylene", in: *Phys. Rev. Lett.* 42.25 (1979), pp. 1698–1701.
[58] Thiang Guo Chuan, "Topological Edge States of 1D Chains and Index Theory", in: *J. Math. Phys.* 64.6 (2023).
[59] Thiang Guo Chuan and Zhang Hai, "Bulk-Interface Correspondences for One-Dimensional Topological Materials with Inversion Symmetry", in: *Proc. R. Soc. A.* 479.2270 (2023), p. 20220675.
[60] Thouless D.J., "Electrons in Disordered Systems and the Theory of Localization", in: *Phys. Rep.* 13.3 (1974), pp. 93–142.
[61] Trefethen Lloyd N. and Embree Mark, *Spectra and Pseudospectra*, Princeton University Press, Princeton, NJ, 2005.
[62] Wang Qiang and Chong Y. D., "Non-Hermitian Photonic Lattices: Tutorial", in: *J. Opt. Soc. Am. B* 40.6 (2023), pp. 1443–1466.
[63] Wang Wei, Wang Xulong and Ma Guancong, "Non-Hermitian Morphing of Topological Modes", in: *Nature* 608.7921 (2022), pp. 50–55.
[64] Yao Shunyu and Wang Zhong, "Edge States and Topological Invariants of Non-Hermitian Systems", in: *Phys. Rev. Lett.* 121.8 (2018).

[65] Yokomizo Kazuki, Yoda Taiki and Murakami Shuichi, "Non-Hermitian Waves in a Continuous Periodic Model and Application to Photonic Crystals", in: *Phys. Rev. Res.* 4.2 (2022), p. 023089.

[66] Yueh Wen-Chyuan, "Eigenvalues of Several Tridiagonal Matrices.", in: *Appl. Math.* 5 (2005), pp. 66–74.

[67] Yueh Wen-Chyuan and Cheng Sui Sun, "Explicit Eigenvalues and Inverses of Tridiagonal Toeplitz Matrices with Four Perturbed Corners", in: *ANZIAM J.* 49.3 (2008), pp. 361–387.

[68] Zhang Xiujuan, Zhang Tian, Lu Ming-Hui and Chen Yan-Feng, "A Review on Non-Hermitian Skin Effect", in: *Adv. Phys.: X* 7.1 (2022), p. 2109431.

[69] Zheng Li-Yang, Achilleos Vassos, Richoux Olivier, Theocharis Georgios and Pagneux Vincent, "Observation of Edge Waves in a Two-Dimensional Su-Schrieffer-Heeger Acoustic Network", in: *Phys. Rev. Appl.* 12.3 (2019).

Habib Ammari
ETH Zürich, Department of Mathematics, Rämistrasse 101, 8092 Zürich, Switzerland.
Email address: habib.ammari@math.ethz.ch

Silvio Barandun
ETH Zürich, Department of Mathematics, Rämistrasse 101, 8092 Zürich, Switzerland.
Email address: silvio.barandun@sam.math.ethz.ch

Ping Liu
School of Mathematical Sciences, Zhejiang University, No. 866, Yuhangtang Road, Hangzhou, 310058, China.
Email address: pingliu@zju.edu.cn